BIOLOGICAL AND CHEMICAL TRANSFORMATION OF HEXAMETHOXYMETHYL MELAMINE

by
Tuna Sürmeli Bilir
B.S., Chemistry, Boğaziçi University, 2020

Submitted to the Institute for Graduate Studies in
Science and Engineering in partial fulfillment of
the requirements for the degree
Master of Science

Graduate Program in Chemistry
Boğaziçi University
2024

To all victims of Hatay earthquake, to my uncle Kemal Sürmeli, my cousin Güneş Sürmeli and my aunt Delal Avcı, who left us too early this year.

ACKNOWLEDGEMENTS

First, I would like to thank my co-advisors, Assoc. Prof. Ulaş Tezel and Assist. Prof. Mehmet Fırat İlker. I am grateful to Assoc. Prof. Ulas Tezel for giving me an opportunity to work on this exciting project that later became a part of my thesis, trusting me with an instrument as delicate as LC-MS/MS, allowing me to take the lead on my research, and letting me be a part of his research group that helped me learn so many experimental techniques and instruments. I will always admire and respect him for his expertise, passion for science and approach to research. I am very grateful to Assist. Prof. Mehmet Fırat İlker for accepting me as a graduate student, allowing me to collaborate with different projects, being supportive and understanding, and trusting me to take charge of my work. His humane approach to all his students, his helpfulness and kindness are virtues that I will always cherish. I would like to thank my thesis committee members Assoc. Prof. Oktay Demircan, Prof. Ferhan Çeçen and Prof. Elif Pehlivanoğlu Mantaş for evaluating my thesis, their kind comments and helpful suggestions.

I would like to thank Assist. Prof. Mehmet Tahir Sandıkkaya for allowing me to collaborate on CHIST-ERA SWAIN Project. I am grateful to Prof. Ferhan Çeçen, my friends Başak Kılıç and Gökçin Gül for helping me get activated sludge samples, to Prof. Neren Ökte and Dr. Duygu Tuncel for lending me TiO_2. I am thankful to Asst. Prof. Berat Zeki Haznedaroğlu for treating me as a member of Imbiyotab family.

I would like to thank my dear friends individually. I am very grateful to Dr. Fahri Koray Sakarya for being so kind and comforting, making me laugh in most depressing times, I loved every conversation we've had and always felt understood. I am very thankful to Zeynep Şahin, who was my lab mate, neighbor, bridesmaid and sister, for uplifting me in tough times, sharing so many good memories, always being solution-oriented and strong. I am deeply grateful to Recep Can Altınbağ, working with him, making music with him, getting to know his genius mind has been a blessing, and his serenity brought comfort when experiments were failing. I am thankful to Ezgi Helvacıoğlu, for being the catalyst in my life, her joyfulness and kindness. I would like to especially thank Dr. Engin Bayram for

sharing his endless wisdom on analytical chemistry, giving me a chance to put my skills in use in exciting opportunities, his friendship and mentorship. I am thankful to Aslıhan Yesir, it was lovely to work in the same lab, cook, clean and laugh together, her positive attitude towards life has been a fresh breath of air. I would like to thank Duygu Özçelik Yılmaz for sharing her knowledge on LC-MS/MS, for her wit and friendship. I am thankful to Beyza Yılmaz for her friendship and support, sharing her knowledge about academia and thesis writing process. I am grateful to Damla Demirkol for her kindness, support and answering all my questions about thesis writing process. I am thankful to Fatma Erkoç for the warmth and laughter she brought to the Kilyos lab. I am thankful to my lab fellows Dila Hocaoğlu, Dr. İrem Karamollaoğlu, Dr. Emine Ertekin, Emren Borhan and Arca Yılmaz.

I would like to thank Assoc. Prof. Rana Özbal, Dr. Ayla Türkekul Bıyık, Dr. Emre Kuruçayırlı and Prof. Hadi Özbal. My research journey started in the archaeometry lab with their guidance, I am thankful for their support and mentorship.

I would like to thank my family, we have lost a lot of people this year, and still managed to be there for each other. I am grateful to my father Fehim Sürmeli and his wife Meryem Sürmeli for their endless love and support and fighting through my father's bypass together. I am grateful beyond words to my mother Mine Yalçın, who raised me, loved and supported me endlessly, for being incredibly selfless, strong and good-hearted even in the most difficult times. I am so lucky to have her as my mother. I am thankful to my family in Antakya, for surviving the earthquake, grieving and healing from our losses together. They are the strongest people I know.

There are no words to describe my gratefulness to my husband Taha Bilir. He has been my best friend and my family for the last eight years, he was incredibly supportive, loving, patient and helpful during my studies and each obstacle I came across. I am so blessed to have him as a life partner.

This study was partially supported by Scientific and Technological Research Council of Turkey (TÜBİTAK) (Grant No: 120N679), CHIST-ERA (Grant No: CHIST-ERA-19-CES-005) and TÜBİTAK National MSc Scholarship Program for Former Undergraduate Scholars (2210-E).

ABSTRACT

BIOLOGICAL AND CHEMICAL TRANSFORMATION OF HEXAMETHOXYMETHYL MELAMINE

Hexamethoxymethyl melamine (HMMM) is an emerging micropollutant. It has recently gained attention due to its widespread occurrence across the world, in surface water, seas, lake, road runoff, stormwater, soil and even crops like lettuce. The primary point source of this pollutant is industrial wastewater, while another significant contributor to its release into the environment is tire wear leachate, constituting a diffuse source. This compound is also abundant in Ergene River, Türkiye. Its structural similarity to currently banned triazine pesticides such as atrazine and its world-wide presence in various ecological systems prompts studies that can provide further insight into its source, fate in the environment and its transformation mechanisms via biotic and abiotic degradation. Although HMMM was detected in various matrices, literature regarding its biotransformation, chemical oxidation, and the mechanism by which these transformations occur remains limited. In this study, persistence of HMMM was confirmed along Ergene River. Further, its biotransformation was studied both with a single strain of bacterium, *Pseudomonas sp.* BIOMIG1^{BAC}, and activated sludge. Both inocula achieved over 80% removal of HMMM within 45 to 100 days. However, complete mineralization of HMMM was not observed, rather, transformation products accumulated. Melamine was found to be a possible dead-end product. A biotransformation pathway was proposed using the detected metabolites. Additionally, advanced oxidation of HMMM via UV- TiO_2 photocatalysis was studied and rapid removals ranging between 50-100% were achieved. Similar transformation products were observed during advanced oxidation and biological treatments, suggesting that degradation likely proceeds through similar mechanisms dominated by oxidation and hydrolysis reactions leading to sequential loss of methoxy- methyl groups. This study contributes to a better understanding of biological and chemical degradation mechanisms of HMMM. Furthermore, it is the first ever report in the literature to assess its degradation via UV-TiO_2 photocatalysis and to identify its oxidation byproducts.

ÖZET

HEKZAMETOKSİMETİL MELAMİNİN BİYOLOJİK VE KİMYASAL DÖNÜŞÜMÜ

Hekzametoksimetil melamin (HMMM), dünya çapında sıklıkla görülmeye başlaması sebebiyle son zamanlarda dikkat çekmeye başlamış olan bir mikrokirleticidir. Görüldüğü bölgeler, yüzey sularından, denizler ve göllerden, yollardan akan sulara, yağmur suyuna, toprağa, hatta marul gibi ekinlere kadar büyük bir alanı kapsamaktadır. Ana noktasal kaynağının endüstriyel atık suyu olmakla beraber araba lastiklerinden çevreye salındığı da bilinmektedir. Şu anda yasaklanmış olan atrazin gibi triazin türü pestisitlere kimyasal benzerliği ve dünya çapında çeşitli ekolojik sistemlerde tespit edilmiş olması, bu kimyasalın kaynağı, çevredeki akıbeti ve biyotik/abiyotik bozunum mekanizmalarını aydınlatacak çalışmalara gerekçe sağlamaktadır. HMMM'in çeşitli matrislerde tayini literatürde mevcut olsa da bu kimyasalın biyo-bozunumu, kimyasal oksidasyonu ve bu dönüşümlerin mekanizmalarıyla ilgili çalışmalar çok azınlıktadır. Bu çalışmada HMMM'in Ergene Nehri'ndeki süregelen varlığı doğrulanmıştır. Dahası, *Pseudomonas sp.* BIOMIG1^{BAC} bakteri türü ve aktif çamur ile biyo-bozunumu incelenmiştir. Her iki çalışmada da 45 ile 100 gün arasında %80'den fazla HMMM giderimi, sağlanmıştır, ancak tamamen mineralizasyon sağlanamamış, çeşitli dönüşüm ürünlerinin oluştuğu görülmüştür. Melaminin HMMM'in muhtemel bir kalıcı dönüşüm ürünü olduğu tespit edilmiştir. Ayrıca, HMMM'in UV-TiO_2 fotokatalizi ile ileri oksidasyonu çalışılmış ve %50-100 arasında hızlı giderim değerleri elde edilmiştir. İleri oksidasyon ve biyobozunum deneylerinde benzer dönüşüm ürünleri gözlemlenmiştir, bu da bozunmanın oksidasyon ve hidroliz reaksiyonları sonucu aşamalı olarak metoksi- metil gruplarının kırılmasından oluşan benzer mekanizmalar aracılığıyla ilerlediğine işaret etmektedir. Bu çalışma HMMM'in biyolojik ve kimyasal bozunumunun daha iyi anlaşılmasına katkıda bulunmaktadır. Ayrıca bu çalışmayla ilk kez HMMM'in UV-TiO_2 fotokatalizi ile giderimi ve oksidasyon yan ürünlerinin belirlenmesi başarılmıştır.

TABLE OF CONTENTS

ACKNOWLEDGEMENTS iv
ABSTRACT vi
ÖZET vii
LIST OF FIGURES xi
LIST OF TABLES xvii
LIST OF SYMBOLS xx
LIST OF ACRONYMS/ ABBREVIATIONS xxi
1. INTRODUCTION 1
2. LITERATURE REVIEW 5
2.1. HMMM as a Micropollutant 5
2.1.1. Chemistry and Industrial Applications of HMMM 5
2.1.2. Occurrence, Toxicity and Fate in the Environment 7
2.1.3. Biotic and Abiotic Degradation of HMMM 10
3. MATERIALS AND METHODS 15
3.1. LC-MS/MS Principle of Operation 15
3.2. Chemicals 18
3.3. Growth Media and Solutions 19
3.3.1. M63B1 Medium 19
3.3.2. M9 Medium 20
3.3.3. LB Broth and LB Agar 21
3.3.4. Stock Solutions and Plates 21
3.4. Detection and Quantitation of HMMM, Melamine and Cyanuric Acid via LC-MS/MS 23
3.5. Targeted Screening and Semi-quantitation of HMMM Transformation Products via LC-MS/MS 27
3.6. Detection and Quantitation of HMMM with HPLC-DAD 30
3.7. Detection and Quantitation of Organic Acids and Glucose via HPLC 31
3.8. Software 33
4. DETECTION AND QUANTITATION OF HMMM IN ERGENE RIVER 34
4.1. Introduction 34

4.2. Materials and Methods 35
4.2.1. Sampling Locations and Sampling Process 35
4.2.2. Sample Preparation and Analysis 38
4.3. Results and Discussion 38
5. BIOTRANSFORMATION OF HMMM BY PSEUDOMONAS SP. BIOMIG1^{BAC} 40
5.1. Introduction 40
5.1.1. Biotransformation of HMMM 40
5.2. Materials and Methods 41
5.2.1. Culture Preparation 41
5.2.2. Biotransformation Assays 42
5.2.3. Sampling, Sample Preparation and Analysis 43
5.3. Results and Discussion 44
5.3.1. Biotransformation of HMMM by *Pseudomonas sp.* BIOMIG1^{BAC} 44
5.3.2. Transformation Products of HMMM 47
5.3.3. Comments on Biotransformation Mechanism 54
5.3.3. Summary 58
6. BIOTRANSFORMATION OF HMMM BY ACTIVATED SLUDGE 59
6.1. Introduction 59
6.2. Materials and Methods 59
6.2.1. Culture Preparation 59
6.2.2. Biotransformation Assays 60
6.2.3. Sampling, Sample Preparation and Analysis 61
6.2.4. Activated Sludge Dry Weight 61
6.3. Results and Discussion 62
6.3.1. Biotransformation of HMMM by Activated Sludge 62
6.3.2. Transformation Products of HMMM 64
6.3.3. Summary 70
7. ENRICHMENT AND ISOLATION OF MELAMINE-DEGRADING SPECIES ... 72
7.1. Introduction 72
7.1.1. Melamine Biotransformation 74
7.1.2. Enrichment Culturing 76
7.2. Materials and Methods 77
7.2.1. Enrichment and Biotransformation Media 77

7.2.2. Enrichment of Melamine Degrading Species 78
7.2.3. Isolation of Melamine Degrading Species 79
7.2.4. Biotransformation Assay 79
7.2.5. Sampling, Sample Preparation and Analysis 80
7.3. Results and Discussion 80
7.3.1. Enrichment and Isolation of Melamine Degrading Species 80
7.3.2. Biotransformation of Melamine by Isolated Degrader 81
7.3.4. Summary 84
8. PHOTOCATALYTIC OXIDATION OF HMMM VIA UV/TiO_2 86
8.1. Introduction 86
8.2. Materials and Methods 88
8.2.1. Chemicals and Experimental Setup 88
8.2.2. Kinetic Model 90
8.2.3. Sampling and Analysis 91
8.3. Results and Discussion 91
8.3.1. Photocatalytic Activity 91
8.3.2. Effect of TiO_2 Dose in Photocatalytic Degradation of HMMM 92
8.3.3. Effect of pH 94
8.3.4. Effect of Matrix: Synthetic Wastewater Effluent 96
8.3.5. Transformation Products of Photocatalytic Degradation of HMMM 98
8.3.6. Summary 103
9. CONCLUSIONS 105
REFERENCES 109
APPENDIX A: HMMM DEGRADATION PATHWAY 122
APPENDIX B: PARENT AND FRAGMENT IONS OF TRANSFORMATION PRODUCTS 123

LIST OF FIGURES

Figure 1.1. Structure of HMMM. 2

Figure 1.2. Graphical abstract depicting the studies conducted within the scope of this thesis. 4

Figure 2.1. Pathway of HMMM synthesis from melamine. 6

Figure 2.2. Molecular structures of HMMM, atrazine and cyromazine. 10

Figure 2.3. Proposed generalized degradation mechanism of HMMM. 13

Figure 3.1. Illustration depicting the processes throughout LC-MS/MS analysis. 17

Figure 3.2. Schematic representation of compound optimization process prior to LC-MS/MS analyses. 18

Figure 3.3. Example extracted chromatograms of a QC standard containing melamine, HMMM, IS and cyanuric acid. 26

Figure 3.4. Calibration curves of a) HMMM and b) melamine and c) cyanuric acid. Trend line equations and R^2 values are displayed on the graphs. 27

Figure 3.5. An example of overlayed extracted ion chromatograms of selected TPs. 29

Figure 3.6. a) Calibration curve of HMMM generated by HPLC-DAD analysis, b) UV-Visible range spectrum of HMMM. 30

Figure 3.7. Calibration curves of a) glucose and b) acetic acid, detected by HPLC-RID and HPLC-DAD, respectively. 32

Figure 4.1. Map illustration of locations where samples were collected. 36

Figure 4.2. Photos from sampling locations. 37

Figure 5.1. Illustration of the experimental workflow followed throughout the studies described in the Chapter 5. 44

Figure 5.2. Concentrations of HMMM and melamine in a) N-free, b) C-free media inoculated with BIOMIG1 and c) abiotic control media during 100 days of incubation. 46

Figure 5.3 Optical density of N-free and C-free biological treatments throughout the experiment. 47

Figure 5.4. Glucose and acetate concentration in N-free flasks inoculated with BIOMIG1 during the course of 12 days. 47

Figure 5.5. Proposed structures for commonly observed fragment ions of HMMM and its TPs. 48

Figure 5.6. Concentration of Group-1 TPs in N-free flasks inoculated with BIOMIG1 during 100 days of incubation.. 49

Figure 5.7. Concentration of Group-2 TPs (as HMMM) in N-free flasks inoculated with BIOMIG1 during 100 days of incubation. 49

Figure 5.8. Concentration of Group-3 TPs (as HMMM) in N-free flasks inoculated with BIOMIG1 during 100 days of incubation. 50

Figure 5.9. Concentration of Group-4 TPs (as HMMM) in N-free flasks inoculated with BIOMIG1 during 100 days of incubation. 50

Figure 5.10. Concentration of Group-5 TPs (as HMMM) in N-free flasks inoculated with BIOMIG1 during 100 days of incubation. 51

Figure 5.11. Concentrations of HMMM, melamine, all TPs (excluding melamine) and all analytes (HMMM, melamine, TPs) in N-free flasks inoculated with BIOMIG1 during the course of incubation. 52

Figure 5.12. Chromatograms of a) TP314 and b) TP300, along with depictions of proposed isomeric structures. 53

Figure 5.13. Depiction of fundamental reactions that take place during degradation of HMMM..... 55

Figure 5.14. Depiction of common functional groups shared by HMMM and alachlor, and designation of bonds that cleave during the initial steps of degradation. 56

Figure 5.15. Molecular structures of HMMM and two s-triazine herbicides. 58

Figure 6.1. Illustration of the experimental workflow followed throughout the studies described in Section 6..... 62

Figure 6.2. Concentration of HMMM in selective media inoculated by activated sludge during 43 days of incubation..... 63

Figure 6.3. Concentrations of HMMM, melamine, all TPs (excluding melamine) and all analytes (HMMM, melamine, TPs) in flasks with HMMM as the sole C source inoculated by activated sludge during 55 days of incubation. ... 66

Figure 6.4. Concentration of Group-1 TPs in C-free flasks inoculated with activated sludge during 55 days of incubation..... 68

Figure 6.5. Concentration of Group-2 TPs in C-free flasks inoculated with activated sludge during 55 days of incubation. 68

Figure 6.6. Concentration of Group-3 TPs in C-free flasks inoculated with activated sludge during 55 days of incubation. 69

Figure 6.7. Concentration of Group-4 TPs in C-free flasks inoculated with activated sludge during 55 days of incubation. 69

Figure 6.8. Concentration of Group-5 TPs in C-free flasks inoculated with activated sludge during 55 days of incubation at 25°C (mean ±one STDV, *n*=2).... 70

Figure 7.1. Structure of melamine-cyanurate complex. 73

Figure 7.2. Biotransformation pathway of melamine. 75

Figure 7.3. Illustration of enrichment culturing, isolation of the degrader and biotransformation experiments workflow. 76

Figure 7.4. Concentrations of melamine and cyanuric acid in, flasks amended with a) glucose and nitrogen (full), and b) only glucose without nitrogen (N-free) inoculated with the isolated degrader during 28 hours of incubation at 25°C. 82

Figure 7.5. Concentrations of melamine and cyanuric acid in a) N-free, b) full, c) C-free and d) C/N-free selective media inoculated with the isolated degrader during 7 days of incubation at 25°C. 83

Figure 7.6. Optical density values of all biological treatments during biotransformation experiments with the isolated melamine degrader. 84

Figure 8.1. Illustration of TiO_2 photocatalysis mechanism. 86

Figure 8.2. HMMM concentrations displayed as percentage of initial concentration in only TiO_2, only UV and UV-TiO_2 combined treatments. 92

Figure 8.3. Effect of TiO_2 dose on HMMM degradation in dark adsorption and UV irradiation treatments. 93

Figure 8.4. Pseudo-first order kinetic model fitting of the HMMM degradation profiles at various TiO_2 doses. 93

Figure 8.5. Structures of HMMM and alachlor depicting the shared methoxy-methyl moiety. 94

Figure 8.6. Effect of pH on HMMM degradation in dark adsorption and UV irradiation treatments. 95

Figure 8.7. Pseudo-first order kinetic model fitting of the HMMM degradation profiles at various pH values (4, 7.5, 11). 96

Figure 8.8. HMMM degradation via dark adsorption and UV irradiation treatments in ultrapure water and synthetic wastewater effluent matrices. 97

Figure 8.9. Pseudo-first order kinetic model fitting of the HMMM degradation profiles in synthetic wastewater and ultrapure water matrices. 98

Figure 8.10. Concentrations of Group-1 TPs during 60 minutes of UV-TiO_2 treatment (initial HMMM=25.6 µM, TiO_2=1 g/L, pH= 7.5). 100

Figure 8.11. Concentrations of Group-2 TPs during 60 minutes of UV-TiO_2 treatment (initial HMMM=25.6 µM, TiO_2=1 g/L, pH= 7.5). 100

Figure 8.12. Concentrations of Group-3 TPs during 60 minutes of UV-TiO_2 treatment (initial HMMM=25.6 µM, TiO_2=1 g/L, pH= 7.5). 101

Figure 8.13. Concentrations of Group-4 TPs during 60 minutes of UV-TiO_2 treatment (initial HMMM=25.6 µM, TiO_2=1 g/L, pH= 7.5)..... 101

Figure 8.14. Concentrations of Group-5 TPs during 60 minutes of UV-TiO_2 treatment (initial HMMM=25.6 µM, TiO_2=1 g/L, pH= 7.5)..... 102

Figure 8.15. Concentrations of HMMM, melamine, all TPs (excluding melamine) and all analytes (HMMM, melamine, TPs) in UV-TiO_2 treatments. 102

Figure A. 1. Proposed degradation pathway of HMMM. 122

LIST OF TABLES

Table 2.1. The occurrence of HMMM in the environment, wastewaters and road runoff water. 8

Table 2.2. List of HMMM transformation products observed in the literature presented with their molecular weight and proposed molecular formula. 14

Table 3.1. Specifications of chemicals used throughout the experiments. 19

Table 3.2. Content of the M63B1 medium. 20

Table 3.3. Contents of M9 medium. 20

Table 3.4. Contents of trace metal solution used in the M9 medium. 21

Table 3.5. Ion source parameters employed during the LC-MS/MS analyses. 24

Table 3.6. MRM transitions and compound parameters used in screening of HMMM, melamine and cyanuric acid..... 24

Table 3.7. Summary of HPLC parameters employed in the LC-MS/MS screening of HMMM, melamine and cyanuric acid..... 24

Table 3.8. HPLC gradient timetable employed in the LC-MS/MS screening of HMMM, melamine and cyanuric acid..... 25

Table 3.9. Summary of HPLC parameters used in targeted LC-MS/MS screening of HMMM transformation products. 28

Table 3.10. Summary of HPLC parameters applied during detection of HMMM via HPLC-DAD. 31

Table 3.11. HPLC parameters used for detection of glucose and organic acids via HPLC-DAD and HPLC-RID. 32

Table 4.1. Description of sampling points, including coordinates, province, classification of the location and the river on which the point is located.. 37

Table 4.2. Concentration of HMMM detected in the collected samples. 39

Table 5.1. Contents of the flasks prepared for the HMMM biotransformation experiments with *Pseudomonas sp.* BIOMIG1^{BAC} 43

Table 5.2. Concentrations of HMMM, melamine, all TPs (excluding melamine) and all analytes (HMMM, melamine, TPs) in N-free flasks inoculated with BIOMIG1 during the course of incubation. 53

Table 5.3. Literature examples of the enzymes that can degrade relevant ether groups and their amino acid sequence similarity match within the genome of *Pseudomonas sp*. BIOMIG1^{BAC}. 57

Table 6.1. Contents of the media prepared for the HMMM biotransformation experiments with activated sludge..... 61

Table 6.2. Concentrations of HMMM, melamine, all TPs (excluding melamine) and all analytes (HMMM, melamine, TPs) in flasks HMMM as the sole C source inoculated by activated sludge during 55 days of incubation. 65

Table 7.1. Biotransformation of melamine as observed in the literature. 75

Table 7.2. Contents of the media prepared for the enrichment culturing and biotransformation experiments involving isolated melamine degrader. ... 78

Table 7.3. Concentration of melamine in each flask on the 3rd day of the activity tests. 81

Table 8.1. Recipe used to prepare synthetic textile wastewater effluent..... 89

Table 8.2. Trace metal stock solution recipe that is used in preparation of synthetic textile wastewater effluent..... 90

Table 8.3. Summary of the experimental conditions tested in the study..... 90

Table 8.4. R^2 values for the kinetic model linear regression lines and calculated rate constants (k) for the TiO_2 doses assessed (10-1000 mg/L). 94

Table 8.5. R^2 values for the kinetic model linear regression lines and calculated rate constants (k) for the pH values assessed (4, 7.5, 11)..... 95

Table 8.6. R^2 values for the kinetic model linear regression lines and calculated rate constants (k) for photocatalysis experiments in synthetic wastewater and ultrapure water..... 98

Table 8.7. Concentrations of HMMM, melamine, all TPs (excluding melamine) and all analytes (HMMM, melamine, TPs) in UV-TiO_2 treatments. 103

Table B.1. MRM method parameters for the targeted screening of TPs with LC-MS-MS. 123

Table B.2. Proposed structures and molecular formula of the detected transformation products and their fragment ions, their relative retention times with respect to HMMM and the type of treatments they were observed in..... 127

LIST OF SYMBOLS

e^-	electron
h^+	hole
λ_{max}	Maximum absorbance wavelength
μ	Micro-
ν	Frequency of electromagnetic wave

LIST OF ACRONYMS/ ABBREVIATIONS

6-PPD	N1-(4-Methylpentan-2-yl)-N4-phenylbenzene-1,4-diamine
6-PPD-quinone	N1-(4-Methylpentan-2-yl)-N4-phenylbenzene-1,4-diamine quinone
BAC	Benzalkonium chloride
CAD	Collision assisted dissociation
CUR	Curtain gas
CYA	Cyanuric acid
DDE	Dichlorodiphenyldichloroethylene
DDT	Dichlorodiphenyltrichloroethane
DOC	Dissolved organic carbon
DPG	Diphenyl guanidine
ESI	Electrospray ionization
GS1	Nebulizer gas
GS2	Auxiliary gas
HMMM	Hexamethoxymethyl melamine
HPLC	High-performance liquid chromatography
HRMS	High resolution mass spectrometer
IS	Internal standard
IS Voltage	Ion source voltage
LB	Luria Bertani
LC- MS/MS	Liquid chromatography tandem mass spectrometry
M63B1	A mineral medium used in biotransformation experiments
M63B1-BAC	Mineral medium with BAC
M9	A mineral medium used in biotransformation experiments
M9 BAC	Mineral medium with BAC
MRM	Multiple reaction monitoring
MS	Mass spectrometer
OD	Optical density
PTFE	Polytetrafluoroethylene
RPM	Revolutions per minute
S-WW	Synthetic wastewater

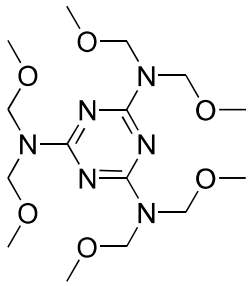
STDV	Standard Deviation
TEM	Temperature
TOC	Total organic carbon
TP	Transformation product
UHPLC	Ultra high-performance liquid chromatography
UPW	Ultrapure water
WWTP	Wastewater treatment plant

1. INTRODUCTION

Pollution of natural systems with micropollutants is one of the major environmental issues of 21st century. They are very diverse in terms of structure and are released into environmental systems from a range of point and diffuse sources. Particularly, persistent and mobile micropollutants pose a great threat to both overall environmental health and human health, since they can easily enter various environmental domains including seas, rivers, ground water, soil and crops, by means of hydrological transport (Hale et al., 2020). Their fate in the environment doesn't always end in mineralization, in fact, more often they can be transformed into more persistent and mobile pollutants via biotic and/or abiotic degradation, while the effects of these transformation products are often unpredictable. For instance, a known transformation product of dichlorodiphenyltrichloroethylene (DDT) is dichlorodiphenyldichloroethylene (DDE), which is associated with environmental catastrophes such as the eggshell thinning, which nearly drove bird of prey species, particularly bald eagle and peregrine falcon, into extinction (Baird and Cann, 2012). Over the years following the original discovery of it, both DDT and its transformation product, DDE have been shown to unforeseen hazards, from ecological disruption to carcinogenicity (Baird and Cann, 2012). Considering the profound variety of synthetic chemicals currently produced by human activity, it is now clear that the case of DDT is just one example and there is a large range of chemicals released into the environment without full knowledge of their fate and effects. Therefore, understanding the fate of micropollutants bears vital importance.

Hexamethoxymethyl melamine (HMMM) is a symmetrical triazine (s-triazine) compound that has six methoxy-methyl branches attached to a melamine core (Figure 1.1). It shares the same s-triazine structure with the pesticides atrazine and cyromazine, which are currently banned in EU (Bethsass and Colangelo, 2006). It is a member of chemicals known as melamine-formaldehyde compounds, which are heavily used for coating applications in textile, wood, automobile, metal and plastic industries. It has gained increasing attention over the years due to its detection in surface waters (rivers, seas, lakes, dams and road runoff water) across the world at concentrations 1 ng/L to 6.89 µg/L. Consequently, it has been included in NORMAN network emerging substances list. In a recent study, it was identified

as one of the core micropollutants of heavily polluted Ergene River in Türkiye(Emadian et al., 2021). At some sampling points, its concentration (max. 329.17 µg/L) exceeded other reported concentrations of HMMM worldwide by more than 40 times.



$C_{15}H_{30}N_6O_6$
Exact Mass: 390.22

N^2,N^2,N^4,N^4,N^6,N^6-
hexakis(methoxymethyl)-
1,3,5-triazine-2,4,6-triamine
(HMMM)

Figure 1.1. Structure of HMMM.

A scientific focus towards this chemical has recently increased due to latest findings regarding the tire additives and their toxicity. Recent studies showed that road runoff water constitutes micropollutants which are mainly derived from tire-wear particles (Peter et al., 2018). Those micropollutants include certain tire rubber additives such as HMMM, N1-(4-Methylpentan-2-yl)-N4-phenylbenzene-1,4-diamine (6PPD), diphenyl guanidine (DPG), and their transformation products (Du et al., 2020; Peter et al., 2018; Tian et al., 2021). Prior to these studies, the source of HMMM in the environment was only thought to be industrial wastewater, which is a point source. This was confirmed by reports of high concentrations of HMMM discovered in the vicinity of industrial wastewater discharge points. For instance, HMMM was detected at concentrations between 116.12-254.71 µg/L near the discharge point of an industrial zone located on Ergene River in all seasons, which harbors textile, dye, metal and automotive industries (Emadian et al., 2021). Current knowledge indicates that HMMM and several other tire wear additives are released into the water streams continuously by road runoff, which is a diffuse source that requires further attention.

There is currently no information about its hazards, however, considering its structural homology to triazine pesticides such as atrazine and cyromazine, it appears to have a

potential for toxicity. It has been discovered in a fraction of river water that caused mortality in Coho salmon, accompanying 6-PPD-quinone, a toxic transformation product of tire additive 6-PPD (Tian et al., 2021). The toxicity was attributed to 6-PPD- quinone, but later studies suggested that the toxicity could have arisen from possible synergistic effects (Hiki et al., 2021). In another study, it was detected in a river water sample that caused toxicity alarms in a Daphnia biomonitor, along with 3-cyclohexyl-1,1-dimethylurea (De Hoogh et al., 2006). These findings have strong implications that HMMM might be associated with toxicity, directly or indirectly.

There are only four studies on its biotransformation in the literature (Alhelou et al., 2019; Castan et al., 2023; Saifur and Gardner, 2023; Wiener and LeFevre, 2022). Those studies indicate that its mineralization is a challenge in the water environment. In all these studies, it has been demonstrated that biotransformation mainly yields transformation products which are more polar and mobile. One prominent transformation product is found to be melamine, which is also a micropollutant associated with various health hazards (Bolden et al., 2017).

Furthermore, there is no literature on advanced oxidation of HMMM. Considering its widespread occurrence, its potential toxicity related to its structural similarities to hazardous compounds and lack of adequate knowledge on its fate and removal, it is evident that more research regarding HMMM is necessary. Therefore, the main objective of this study was to evaluate biological and chemical transformation potential of HMMM in water environment and identify transformation mechanisms. The specific objectives included: (1) Detection and quantification of HMMM in possible source and monitoring zones along Ergene River as well as in influent and effluents of an industrial WWTP; (2) biotransformation of HMMM by a single strain of bacteria, *Pseudomonas sp.* BIOMIG1^{BAC}, and semi-quantification of its transformation products; (3) biotransformation of HMMM by a microbial consortium provided by activated sludge, and semi-quantification of its transformation products; (4) enrichment and isolation of a strain capable of degrading melamine, a known persistent transformation product of HMMM; and (5) degradation of HMMM by UV-TiO_2 based photocatalytic process and semi-quantification of its transformation products. Overall, the aim of the current work is to study HMMM through a holistic approach (Figure 1.2); from its detection in the environment and its biotransformation in various conditions, to its abiotic

oxidation, its fate and transformation products, thus providing comprehensive information about this emerging micropollutant.

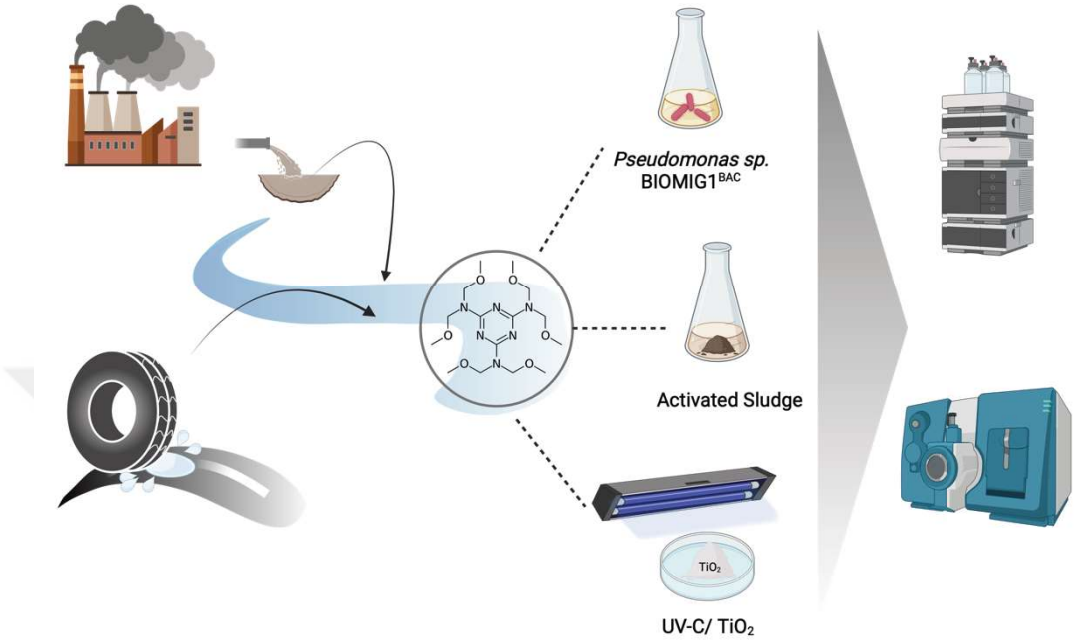


Figure 1.2. Graphical abstract depicting the studies conducted within the scope of this thesis.

2. LITERATURE REVIEW

2.1. HMMM as a Micropollutant

2.1.1. Chemistry and Industrial Applications of HMMM

HMMM is an s-triazine compound that has been utilized in industrial applications for several decades. It is a member of melamine-formaldehyde compounds, which are a diverse group of functionalized triazines. HMMM is synthesized from melamine in two major steps. The first step is referred as “methylolation”, where melamine is reacted with formaldehyde under basic conditions, while formaldehyde is added in minimum in six times stochiometric excess for complete formylation of amine branches (Rätzsch et al., 2004). The resulting compound is called “hexamethylol melamine”. In the second step, this is further reacted with excess methanol under slightly acidic conditions through a condensation reaction, which essentially results in etherification of each methylol end (Rätzsch et al., 2004) (Figure 2.1.). The end product is hexamethoxymethyl melamine (HMMM).

There is a plethora of melamine-formaldehyde compounds with varying physicochemical properties and application areas. For instance, some members are formylated and alkylated partially, thus leaving some of the O-H and N-H bonds intact and open for further reaction. These partially formylated and partially alkylated melamine-formaldehyde compounds can undergo self-condensation reactions at slightly increased temperature (or even at ambient temperatures), resulting in what is called “melamine-formaldehyde resins” (Rätzsch et al., 2004). Resinous property results from the uncontrolled condensation reactions occurring between O-H and N-H ends, yielding methylene or methyl ether linkages. The alcohol used for alkylation of methylol ends may be a higher alcohol, such as ethanol or butanol. The reaction duration, degree of formylation and alkylation all have different impacts, therefore this family of chemicals is quite diverse. HMMM is a stable member of this family since it is fully alkylated and therefore the only melamine-formaldehyde chemical that can be obtained as a pure compound, while all other members undergo spontaneous condensation reactions and contain higher molecular weight impurities

(Pizzi and Ibeh, 2014). Due to its stability, it provides better control over reactions in which it is involved. The main chemical role it carries in most industrial applications is cross-linking. HMMM itself or similar highly alkylated melamine formaldehyde resins have been reported to be a cross linker for coating formulations applied on textile, metal surfaces and wood, in the form of adhesive, paint or flame-retardant additives (Fink, 2013). However, one particular area HMMM has been exclusively used is worth mentioning in detail: tire additives. HMMM and highly alkylated melamine formaldehyde resins are reported to be used as reinforcing resin networks in rubber formulations and also as adhesion promoters in coating formulations of steel chords in tires (Rodgers, 2004). Regarding industrial formulations, patent and rights are effective and industries are generally reluctant to share trade secrets. Therefore, the mechanisms, the exact formulations and reactions are not fully explained in such sources. The number of academic publications that provide insight about industrially applied reactions of HMMM is very limited. The most definitive evidence of HMMM being used in tire formulations is provided by environmental research publications, where leaching of HMMM from tires into road runoff has been proven repeatedly (Peter et al., 2018).

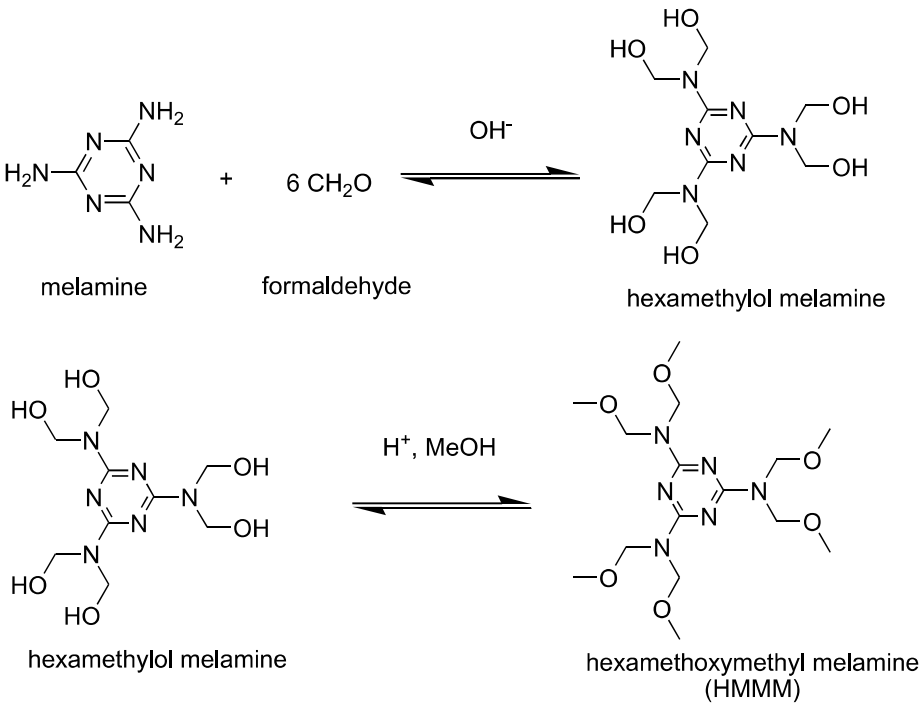


Figure 2.1. Pathway of HMMM synthesis from melamine.

2.1.2. Occurrence, Toxicity and Fate in the Environment

The literature on the occurrence of HMMM and its TPs in the environment goes back at least two decades. It has been first reported in the samples collected from surface waters used for drinking water production in Netherlands, where HMMM was found at an estimated concentration of 0.5 µg/L, along with two structurally related compounds, which are tentatively identified as demethylated and diformylated forms of HMMM (Bobeldijk et al., 2002). From then on, it has been reported in surface waters across the world at concentrations ranging between 1 ng/L and 6.89 µg/L (Table 2.1). It was recently classified as one of the core micropollutants in Ergene River (Emadian et al., 2021). HMMM was detected in all sampling points across Ergene River during all seasons at concentrations between 0.01-329.17 µg/L. This maximum concentration is at least 40 times higher than any of the reported maximum concentrations of HMMM in other surface waters (Table 2.1). Due to consistently high concentrations of HMMM (116.12-254.71 µg/L) near a discharge point, its primary source was identified to be an industrial zone situated upstream along the river, which is dominated by textile, dye, automotive, metal and electronics industries (Emadian et al., 2021). Indeed, most of the available reports designate industrial wastewater as a major point source of HMMM. Krauss et al. reported presence of HMMM, seven likely TPs (with m/z ratios of 359, 377, 347, 333, 271, 331 and 299) and four likely precursors (with m/z ratios of 530, 484, 519, 421) in a tributary of River Elbe that receives wastewater discharge from automotive manufacturers (Krauss et al., 2019). In this work, they screened for site-specific pollutants via untargeted high resolution mass spectrometry (HRMS) and established relationships between possible industrial sources and characteristic pollutant families. HMMM was detected at a concentration of 87.4 µg/L in the effluent of a wastewater treatment plant (WWTP) located in Germany (Hug et al., 2014), indicating that despite treatment, HMMM still persisted in industrial discharge. In fact, in four WWTPs in Germany, its concentration was found to be 2-4 times higher in effluents than influents (max. 60.8 µg/L) (Alhelou et al., 2019). The authors attributed this to possible ongoing formation of HMMM from its higher molecular weight precursors, such as formylated and diformylated derivatives, which were also detected in the samples (Alhelou et al., 2019). Across 52 WWTP effluents in Europe, HMMM was found to reach concentrations as high as 461 µg/L (Finckh et al., 2022).

Table 2.1. The occurrence of HMMM in the environment, wastewaters and road runoff water.

Domain	HMMM Concentration	Country	Reference
Surface waters	0.5 µg/L	Netherlands	(Bobeldijk et al., 2002)
Wastewater effluent	87.4 µg/L	Germany	(Hug et al., 2014)
River	0.01-0.80 µg/L	Germany	(Dsikowitzky and Schwarzbauer, 2015)
Road runoff, rivers, wastewater effluent	25 ng/L- 76 µg/L	Germany	(Seitz and Winzenbacher, 2017)
River	0.55 ng/L-6.89 µg/L	China	(Peng et al., 2018)
Road runoff	2.0-6.5 µg/L	USA	(Peter et al., 2018)
Surface waters	60-530 ng/L	Germany	(Alhelou et al., 2019)
Wastewater	0.1-60.8 µg/L	Germany	(Alhelou et al., 2019)
Surface waters	0.48-46 ng/L	Australia	(Rauert et al., 2020)
Sea	1-28 ng/L	USA	(Tian et al., 2020)
River	0.01-329.17 µg/L	Türkiye	(Emadian et al., 2021)
Sea	0.3-3 µg/L	USA	(Petras et al., 2021)
River	0.4-2.1 µg/L	Canada	(Johannessen et al., 2022)
Drinking water	1.6-3.9 ng/L	Canada	(Johannessen and Metcalfe, 2022)
Runoff sediment	4.6-92.9 µg/kg dry weight	Germany	(Fuchte et al., 2022)
Wastewater effluent	89.1 ng/L-461 µg/L	Europe	(Finckh et al., 2022)
River	36.6-53.7 ng/L	China	(Wu et al., 2023)
Snow melt	1.1-8.4 µg/L	Germany	(Maurer et al., 2023)

Aside from wastewater, there have also been reports of HMMM occurrences in road runoff samples and tire wear leachate. For instance, in a study by Peter et al., prominent chemicals in road runoff water and tire wear leachate were determined via untargeted HRMS screening, and the resulting chemical profile included HMMM along with three of its de-methoxymethylated TPs, bicyclic amines such as DPG and 1,3-dicyclohexylurea, and poly-ether glycols (Peter et al., 2018). In another study, untargeted HRMS screening of wastewater effluent and road runoff samples revealed signature pollutants specific to each source, which included previously described road runoff indicators such as HMMM and DPG (Du et al., 2020). Fuchte et al. identified 187 micropollutants associated with road runoff waters and sediment particles (Fuchte et al., 2022). HMMM was found at

concentrations between 4.6-92.9 µg/kg-dry weight in the runoff sediment samples, which are dominated by tire wear particles (Fuchte et al., 2022). It was later demonstrated that HMMM concentrations increased in the Don River, Canada during storm events, since road runoff reaches receiving waters via rain or snow melt (Johannessen et al., 2022). It is evident that another major contributor of HMMM and its derivatives in the environment is leaching from tire wear particles, which are transported into surface waters via road runoff. The available literature clearly indicates that HMMM and its TPs are continuously released into the environment via industrial discharge and road runoff, which constitute point and diffuse sources respectively.

There is limited knowledge regarding toxicity of HMMM. Upon reports of increased mortality in Coho salmon exposed to urban stormwater, a study was conducted to compare the chemical profiles of urban stormwater and tire wear leachate (Peter et al., 2018). The untargeted HRMS screening yielded candidate toxicants, some of which were identified by library matching as HMMM, its derivatives, DPG and various poly-ether glycol compounds (Peter et al., 2018). In a follow-up study, they attributed the mortality to 6PPD-quinone, an oxidation byproduct of tire additive 6PPD (Tian et al., 2021), however, a later work disputed this by demonstrating that the chemical is not acutely toxic when applied alone (Hiki et al., 2021). In a separate study, it was illustrated that HMMM, in the presence of 3-cyclohexyl-1,1-dimethylurea, likely exhibited a synergistic toxic effect to *Daphnia magna* biomonitors operated in River Meuse (De Hoogh et al., 2006). HMMM was detected along with rubber related metals Zn, Pb, Cr and other amines such as N-cyclohexyl- N-cyclohexanamine in crumb rubber leachate, at a high concentration of 1.7 mg/L (Xu et al., 2019). The leachate was shown to cause mild to severe malfunctions in brain and cardiovascular development, when applied to chicken embryos. Crumb rubber, derived from shredded tires, is a widely used component of floor materials in playgrounds and fitness saloons. Therefore, characteristic compounds present in crumb rubber, such as HMMM, requires assessment for potential toxic effects, since human exposure is inevitable. In a study by Dumont et al., tire wear particles were generated and separated into three fractions, the leachate of each were applied to *Chlorella vulgaris* (microalgae), *Daphnia magna* (plankton) and *Lemna minor* (aquatic plant) for acute toxicity assessment (Roubeau Dumont et al., 2023). Untargeted screening revealed that the major components in all three fractions were HMMM (11.6-15 mg/L) followed by benzotriazole (0.58-0.69 mg/L), with various other tire-related metals

and compounds. All fractions exerted acute toxicity in *D. magna* and decreased photosynthetic efficiency in *L. minor* (Roubeau Dumont et al., 2023). Although no current studies report direct toxic action of HMMM on any of the conventionally tested organisms, the available literature demonstrates that tire wear leachate poses toxicity risks and HMMM is a likely synergistic contributor. Aside from the studies that hint synergistic toxic effects of HMMM, its structural similarity to a variety of triazine herbicides is also an implication of possible toxicity (Figure 2.2). Evidently, further work is required on this aspect.

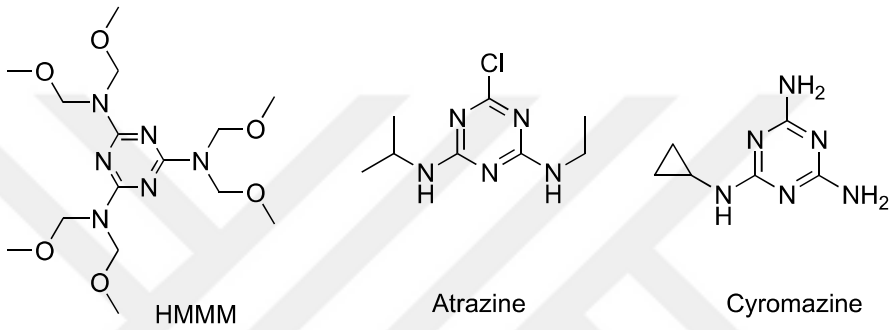


Figure 2.2. Molecular structures of HMMM, atrazine and cyromazine.

2.1.3. Biotic and Abiotic Degradation of HMMM

HMMM is a polar compound with high water solubility (9.85 g/L) (Alhelou et al., 2019) and relatively low octanol to water partition coefficient ($\log K_{ow} = 1.61$) (Dsikowitzky and Schwarzbauer, 2015), therefore, it is expected to be mobile through hydrological systems. The fact that HMMM is shown to readily leach from tire wear particles into water is a confirmation of this expectation (Castan et al., 2023; Peter et al., 2018). Indeed, in a study that focused on modelling of HMMM and its reported TPs via COSMO-RS solvation theory, it was shown that this family of compounds would readily partition into water systems (Johannessen and Parnis, 2021). It was demonstrated that with the higher number of lost methoxy-methyl groups, the polarity and mobility of TPs increased. This can be verified by the previously discussed reports of HMMM and its TPs in surface waters and wastewater effluents (Bobeldijk et al., 2002; Krauss et al., 2019; Seiwert et al., 2020). These studies reveal that HMMM can degrade into TPs in the environment and the family of HMMM related compounds persist in surface waters. This suggests that further investigation of its biotic and abiotic degradation mechanisms is necessary.

Literature regarding biotransformation and fate of HMMM is also scarce. To date, only four studies assessed the biotransformation of HMMM (Alhelou et al., 2019; Castan et al., 2023; Saifur and Gardner, 2023; Wiener and LeFevre, 2022) and three of them provided information about its transformation products (Alhelou et al., 2019; Castan et al., 2023; Wiener and LeFevre, 2022). In the study by Alhelou et al., it was shown that activated sludge could degrade 77.4% of HMMM supplied as the sole carbon source in 29 days, while 25% of HMMM was degraded abiotically in the control samples (Alhelou et al., 2019). Through untargeted HRMS screening, 21 TPs of HMMM were tentatively identified and quantified. It was shown via TOC analysis that HMMM was not mineralized. Melamine did not form to considerable extent, while a TP that has a single -CH_2-OH branch attached to the melamine core was found to accumulate (Alhelou et al., 2019).

In another study, it was shown that *Trametes versicolor* could degrade 69.6% of HMMM in 14 days, while 10 previously unreported TPs were detected (Wiener and LeFevre, 2022). Melamine was designated as a dead-end metabolite; however, TPs were not quantified. These two studies are the only examples in the literature to propose a degradation pathway for HMMM. Uptake and metabolism of HMMM and three other tire wear compounds (benzotriazole, DPG and 6PPD) by lettuce plant was demonstrated in a recent study (Castan et al., 2023). Aquaponic cultures of lettuce were exposed to both real tire wear leachate and solutions of individual chemicals. HMMM and 10 TPs, 3 of which previously unreported, were detected and semi-quantified in root, stem and leaf systems. It was shown that TPs accumulated over the course of 14 days and metabolism did not proceed to mineralization (Castan et al., 2023). This is the only evidence in literature that HMMM can be incorporated to crops.

In a recent study it was shown that stormwater microbiomes may harbor species that can tolerate and/ or degrade HMMM (Saifur and Gardner, 2023). Stormwater samples were used to inoculate liquid media containing environmentally relevant concentrations of HMMM (18-1800 ng/L), either alone or in the presence of external carbon source. The liquid cultures that exhibit growth were inoculated on selective solid media that contains HMMM as the sole carbon source and the isolates that grow were found to belong to *Bacillus* and *Pseudomonas* genera. Further, it was shown that when HMMM was spiked in carbon supplied media, growths of *Bacillus cereus* and *Pseudomonas putida* species were enhanced,

in comparison to growth in media that were not spiked with HMMM. This is the only work in literature that demonstrates a relationship between stormwater microbiomes and possible co-metabolism of HMMM and DPG. However, interpretations were made based on cell growth and degradation of both chemicals were not monitored. The bottom line of the limited literature regarding biotransformation is that HMMM can be biotransformed by various organisms into a multitude of transformation products.

A good understanding of fate and removal of pollutants rely on elucidation of biotic and abiotic degradation mechanisms. Based on the literature available, it appears that degradation of HMMM to melamine proceeds through sequential hydrolysis and oxidation reactions that result in sequential de-methoxymethylation. Types of TPs that can be formed during degradation of HMMM can be visualized via a generic pathway (Figure 2.3). During degradation, while the melamine core remains intact, methoxy-methyl (MM) groups are oxidatively or hydrolytically cleaved in intermediate steps, yielding aldehyde (M=O) or alcohol (M-OH) end groups on the triazine core. Each such step proceeds through loss of either a formaldehyde or methanol, thus leading to an overall decrease in intact MM branches (n-1). Once the remaining M=O and M-OH groups are cleaved as well, a complete MM group is lost from the initial structure. Hence, the families of possible TP structures can be imagined in 6 groups based on the number of intact MM branches they have. Each group harbors various combinations of M-OH and M=O end groups. For instance a TP that has 4 intact MM groups, one aldehyde and one methanol end group can be formulated as 4MM(M=O)(M-OH).

This formula abbreviation methodology is proposed in order to visualize the changes on the main structure of HMMM during its degradation better. Here, a list of TPs is compiled from the literature, in which reported molecular weights, proposed molecular formula and formula abbreviations are presented (Table 2.2). Through the course of this thesis, TPs were named according to their molecular weight (e.g., TP156 has a molecular weight of 156 g/mol), and further structural information is described with the aid of the proposed formula abbreviations.

Aside from the biotransformation studies, there is no literature about chemical transformation of HMMM by any of the known advanced oxidation processes. The limited

literature on its biotic and abiotic degradation, its fate and its relation to toxic chemicals, provide sufficient motivation for further work focusing on HMMM. It is aimed in this study to contribute to the growing literature on HMMM, shed light upon its transformation in biological and chemical contexts and better understand the effects of the presence of this chemical in our environment.

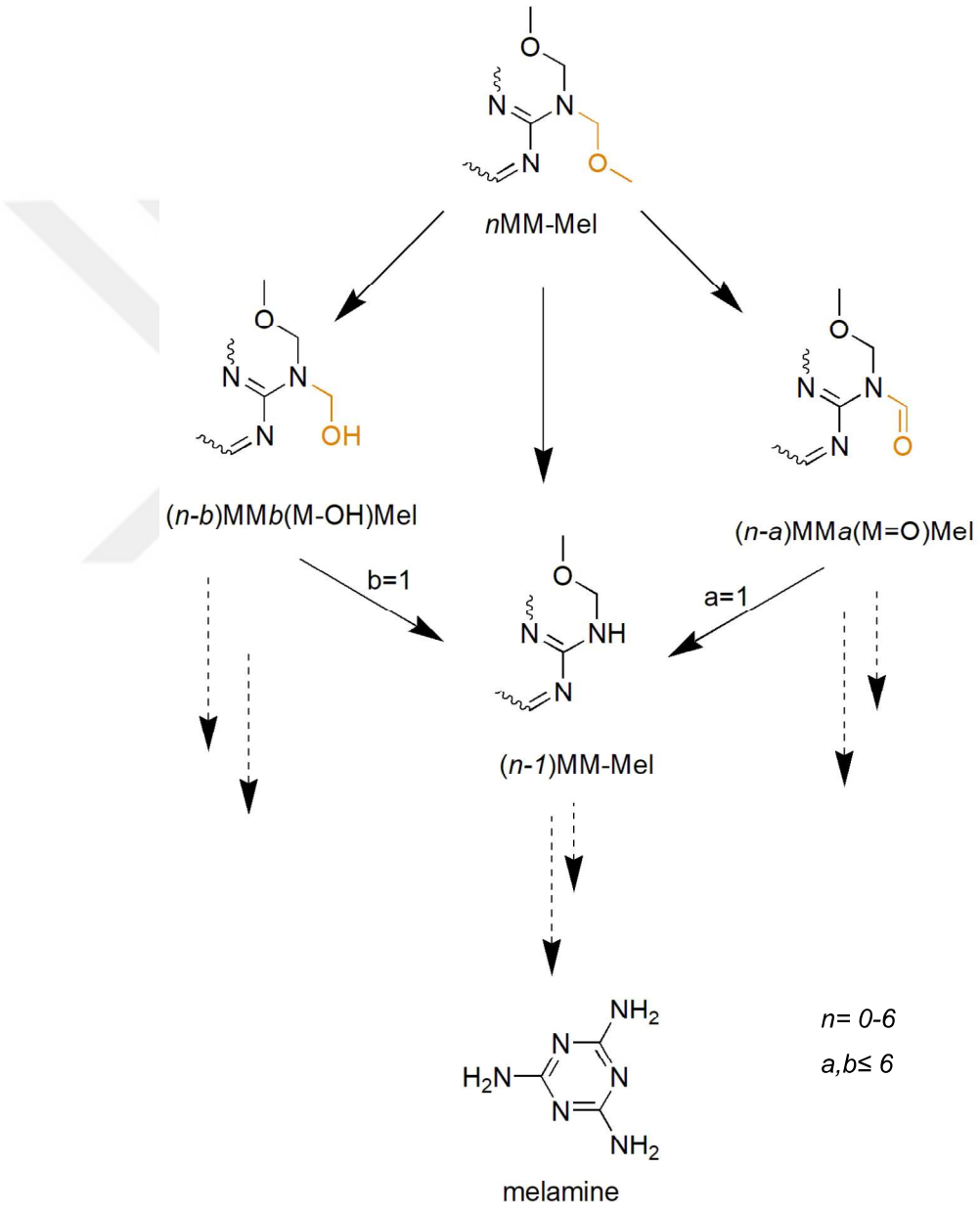


Figure 2.3. Proposed generalized degradation mechanism of HMMM. "*n*" refers to the number of methoxymethyl groups attached to the triazine ring, "a" and "b" refer to the number of alcohol and aldehyde end groups.

Table 2.2. List of HMMM transformation products observed in the literature presented with their molecular weights and proposed molecular formula. TPs are referred in the thesis with the nomenclature and proposed formula abbreviations provided in this table.

Formula Abbreviation	Molecular Formula	Molecular Weight (g/mol)	TP Nomenclature
HMMM (6MM-Mel)	$C_{15}H_{30}N_6O_6$	390.22	HMMM
5MM(M-OH)-Mel	$C_{14}H_{27}N_6O_6$	376.22	TP376
5MM(M=O)-Mel	$C_{14}H_{25}N_6O_6$	374.22	TP374
4MM2(M-OH)-Mel	$C_{13}H_{26}N_6O_6$	362.20	TP362
4MM(M-OH)(M=O)-Mel	$C_{13}H_{23}N_6O_6$	360.20	TP360
3MM3(M-OH)-Mel	$C_{12}H_{24}N_6O_6$	348.20	TP348
5MM-Mel	$C_{13}H_{26}N_6O_5$	346.20	TP346
2MM4(M-OH)-Mel	$C_{11}H_{22}O_6N_6$	334.17	TP334
4MM(M-OH)-Mel	$C_{12}H_{24}N_6O_5$	332.15	TP332
4MM(M=O)-Mel	$C_{12}H_{22}N_6O_5$	330.15	TP330
3MM(M-OH)(M=O)-Mel	$C_{11}H_{20}N_6O_5$	316.20	TP316
3MM2(M=O)-Mel	$C_{11}H_{18}N_6O_5$	314.20	TP314
4MM-Mel	$C_{11}H_{22}N_6O_4$	302.20	TP302
2MM(M-OH)2(M=O)-Mel	$C_{10}H_{16}N_6O_5$	300.15	TP300
3MM(M-OH)-Mel	$C_{10}H_{20}N_6O_4$	288.16	TP288
3MM(M=O)-Mel	$C_{10}H_{18}N_6O_4$	286.15	TP286
2MM2(M=O)-Mel	$C_9H_{14}N_6O_4$	270.15	TP270
3MM-Mel	$C_9H_{18}N_6O_3$	258.15	TP258
2MM(M-OH)-Mel	$C_8H_{16}N_6O_3$	244.14	TP244
2MM(M=O)-Mel	$C_8H_{14}N_6O_3$	242.12	TP242
1MM2(M-OH)-Mel	$C_7H_{14}N_6O_3$	230.12	TP230
2MM-Mel	$C_7H_{14}N_6O_2$	214.13	TP214
0MM2(M-OH)(M=O)	$C_6H_8N_6O_3$	212.11	TP212
1MM(M-OH)-Mel	$C_6H_{12}N_6O_2$	200.10	TP200
0MM2(M-OH)-Mel	$C_5H_{10}N_6O_2$	186.10	TP186
1MM-Mel	$C_5H_{10}N_6O$	170.10	TP170
0MM(M-OH)-Mel	$C_4H_8N_6O$	156.08	TP156
0MM(M=O)-Mel	$C_4H_6N_6O$	154.08	TP154
Melamine	$C_3H_6N_6$	126.99	Melamine

3. MATERIALS AND METHODS

Since the instrumental analysis methods are shared by the experiments described in the following chapters, the details regarding the instrumental analysis methods are explained in this chapter as a compilation. Further methodological details specific to the experiments are described under “Materials and Methods” sections of each chapter.

3.1. LC-MS/MS Principle of Operation

Micropollutants are by definition pollutants of anthropogenic origin that occur at concentrations within the ng/L to µg/L ranges in receiving waters (Emadian et al., 2021). As opposed to macropollutants which correspond to organic molecules with complex structures that can be released into the environment at higher loads, micropollutants have known structures and are found in lower concentrations (Emadian et al., 2021). They are diverse and once they are subject to various environmental processes, they can be converted into a variety of even more diverse family of structures. Since in the case of micropollutants both the parent molecule and the transformation products are found in ng/L to µg/L levels, their detection and quantitation requires equipment with high sensitivity and accuracy.

Instrumental analyses conducted with liquid or gas chromatography (LC and GC, respectively) coupled with mass spectrometers (MS) are possibly the most commonly employed methods for detection and identification of micropollutants and their transformation products. While liquid and gas chromatography provide separation of variety of chemicals, mass spectrometers are essentially the detectors that yield signals as indicators of the mass and quantity of the chemicals. This type of coupled instrumental assemblies are referred as hyphenated techniques, since they combine two or more instrumental components (e.g. LC-MS, GC-MS, etc.) (Ekman, 2009). There are numerous chromatography and mass spectrometry instruments and instrument components that operate on different principles, each providing distinct advantages based on need. Liquid chromatographs coupled with tandem mass spectrometer systems (LC-MS/MS) are one of the most common instrument combinations used in detection and quantification micropollutants. Considering most micropollutants have low molecular weights (compared

to biomolecules and polymers) and majority of them are non-ionic, they can be separated based on their polarity by reversed-phased chromatography and can be screened based on their mass-to-charge ratios (m/z) via mass spectrometry.

The instrument assembly used within the scope of this thesis is a high-performance liquid chromatography unit coupled to a mass spectrometer composed of an electrospray ion source, a tandem quadrupole mass analyzer with a linear ion trap, and an electron multiplier ion detector. The principle of operation is as follows: mixture of analytes in a pressurized liquid mobile phase are passed through a reversed phased (non-polar) chromatography column and are separated based on their polarity and the extent of their retention in the stationary phase (the column packing material). The separated analytes exit the column and are delivered to ion source of the mass spectrometer. Here, the mobile phase is vaporized, and the analytes are ionized into their parent ion form by either being protonated ($[MH]^+$, M= molecular weight) or deprotonated ($[M-H]^-$) with application of high temperature and high positive or negative voltage. Among a variety of ion sources utilized in mass spectrometers, electrospray ionization is a highly favored technique since it offers a mild form of ionization in comparison to other techniques such as electron impact ionization, it is applicable to non-volatile analytes and requires minimal sample preparation, unlike matrix assisted laser desorption/ ionization (MALDI). The molecular ions are transferred into the first quadrupole mass analyzer in vacuum, where application of radiofrequency (RF) and direct current (DC) potentials that affect each molecular ion to behave differently in the created electromagnetic field, since each have a different m/z ratio (Ekman, 2009). With the application of RF and DC potentials, it is ensured that only desired range of ions complete the trajectory of the quadrupole, while the others deviate. Thus, single parent ions or a range of them can be selected from a variety of analytes. After the first quadrupole, the selected ions enter the collision cell, where a potential and an inert gas (N_2) is employed to initiate collision assisted dissociation. In this compartment, parent ions are fragmented into daughter ions. The mass spectrometer used in this work possesses a collision cell which can also serve as a linear ion trap. A linear ion trap essentially collects selected parent or daughter ions of specified m/z values by application of a potential that is suitable to keep the selected ions stable in the cell and filter out the remaining ions. After fragment ions exit the collision cell, they enter the second quadrupole mass analyzer. Here the principle of operation is the same as the first quadrupole, with the distinction that the ions selected in this compartment are

fragments of a parent ion. Finally, the selected parent and/or daughter ions enter the electron multiplier detector, where a signal is generated based on their abundance and m/z ratio. Entire process is depicted in Figure 3.1. Tandem MS provides a very selective and sensitive screening method since it simultaneously selects parent and fragment ions of an analyte, which renders it a highly favored tool in screening of micropollutants and their transformation products.

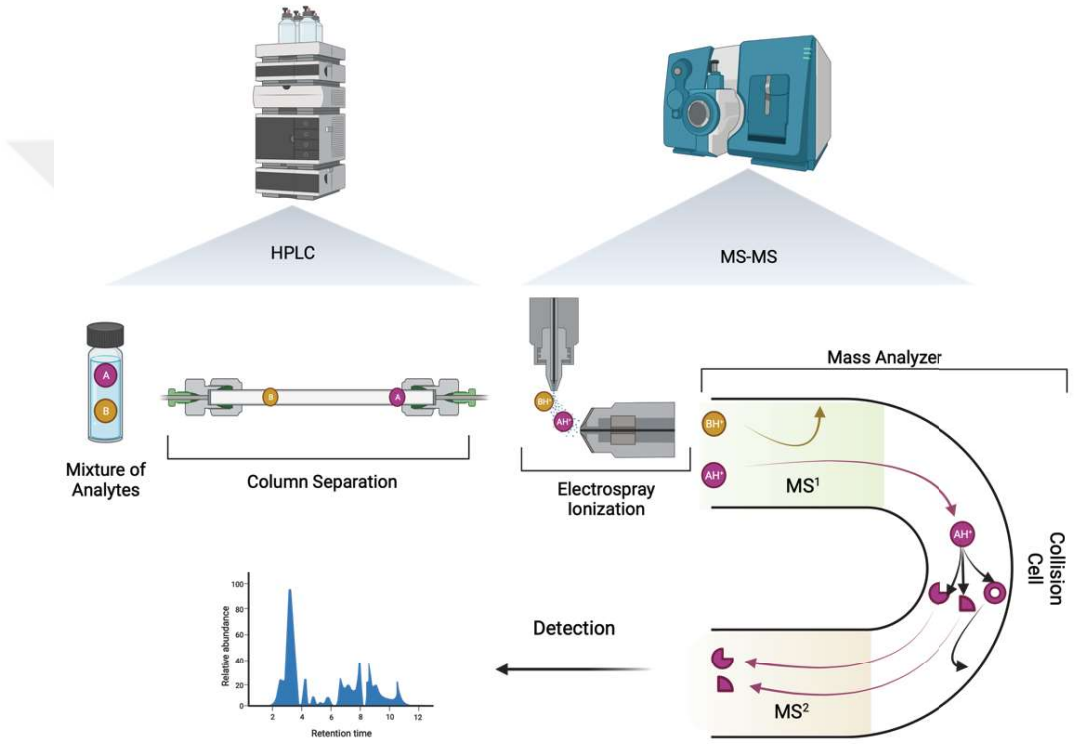


Figure 3.1. Illustration depicting the processes throughout LC-MS/MS analysis.

For each compound that is screened via LC-MS/MS, device parameters should be optimized as a first step of analytical method development. For the mass spectrometer used throughout this study (AB Sciex QTRAP 4500, Framingham, USA), optimization is performed via direct infusion of a dilute solution of the reference material at known concentrations into MS. The parameters optimized include declustering potential (DP), collision energy (CE) and collision cell exit potential (CXP). As the name suggests, DP is applied in order to avoid clustering of molecular ions, therefore its optimization is essential for the correct filtration of desired parent ions (Q1). CE is the energy applied in the collision cell, which determines the extent of fragmentation. CXP is the potential applied to the

fragment ions (Q2) as they exit the collision cell, which determines how well they are detected (Figure 3.2).

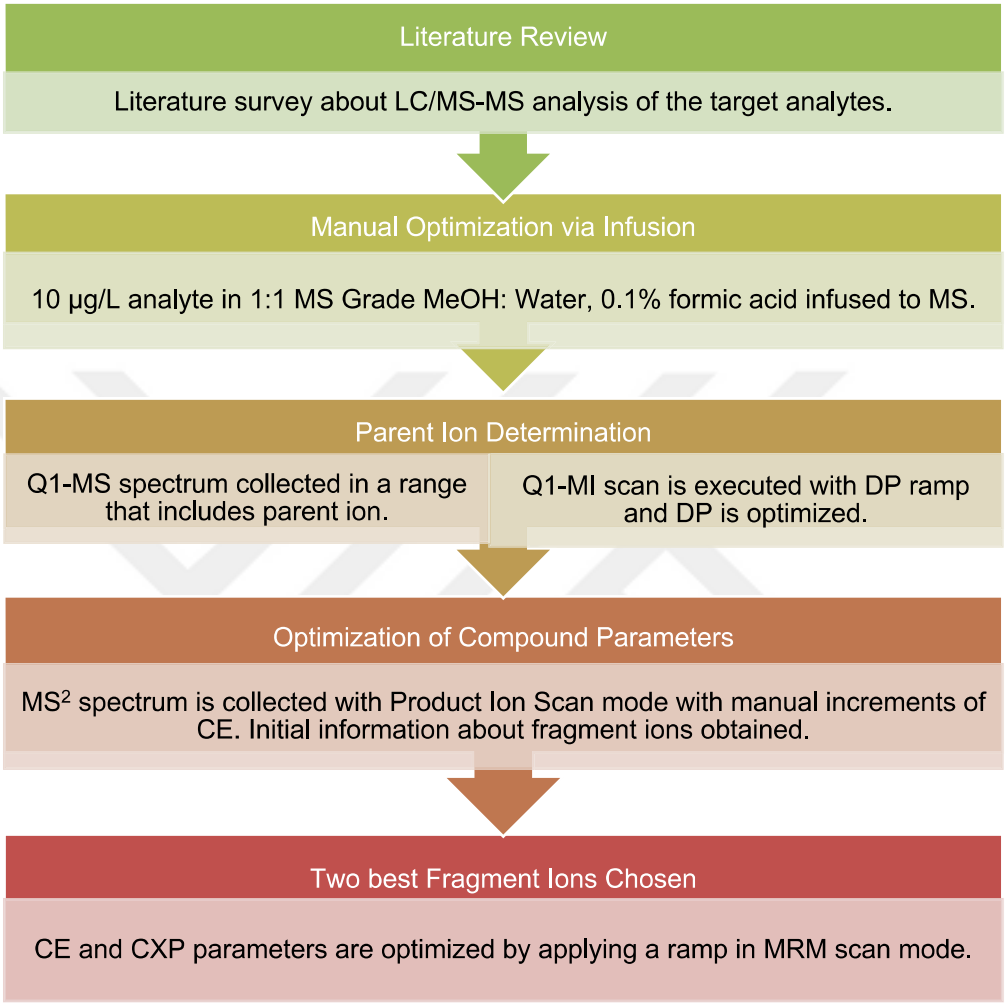


Figure 3.2. Schematic representation of compound optimization process prior to LC-MS/MS analyses.

3.2. Chemicals

MS grade methanol and water purchased from Isolab Inc. (Germany) were used as HPLC mobile phases, sample diluents and solvents in stock solution preparation. HMMM (>99%) was purchased from TCI (Japan). Melamine (>99%) and the internal standard methyl-d_3-triphenylphosphonium iodide (95%) were purchased from Sigma Aldrich (Germany). Information about the chemicals used during detection and quantitation process can be found in Table 3.1.

Table 3.1. Specifications of chemicals used throughout the experiments.

Chemical	CAS	Molecular Weight (g/mol)	Formula	Purpose of Use	Purity	Company
2,4,6-tris[bis(methoxy methyl)amino]-1,3,5-triazine (HMMM)	3089-11-0	390.44	$C_{15}H_{30}N_6O_6$	Target analyte, standard	>98%	TCI Japan
MS grade MeOH	67-56-1	32.04	CH_3OH	Mobile phase, solvent	MS Grade	ISOLAB
MS grade H_2O	7732-18-5	18.02	H_2O	Mobile phase, solvent	MS Grade	ISOLAB
Formic acid	64-18-6	46.025	CH_2O_2	Mobile phase modifier	MS Grade	Sigma Aldrich
Melamine	108-78-1	126.123	$C_3H_6N_6$	Target analyte, standard	99%	Sigma Aldrich
Cyanuric acid	108-80-5	129.07	$C_3H_3N_3O_3$	Target analyte, standard	99%	Sigma Aldrich
Methyl-d_3-triphenylphosph onium iodide (INT44)	1560-56-1	407.24	$CD_3P(C_6H_5)_3I$	Internal standard	95 Atom %D	Sigma Aldrich
Acetonitrile	75-05-8	41.05	C_2H_3N	Mobile phase	Gradient Grade	ISOLAB

3.3. Growth Media and Solutions

3.3.1. M63B1 Medium

M63B1 medium was one of the minimal media used throughout the experiments. The medium composition is listed in Table 3.2. All solutions are prepared in ultrapure water (Milliapore, MilliQ). Stock solutions for $(NH_4)_2SO_4$, $MgSO_4 \cdot 7H_2O$, $FeSO_4 \cdot 7H_2O$ and Thiamine solutions were prepared in designated concentrations (w/v) and stored at 4°C. When needed, media were prepared based on the specified recipe at desired volume, autoclaved at 121°C for 15 minutes and stored at ambient temperature until use.

Table 3.2. Content of the M63B1 medium.

Compound/ Solution	Concentration
K_2HPO_4	7.40 g/L
KH_2PO_4	3.00 g/L
$(NH_4)_2SO_4$ (20%)	10 mL/L
$MgSO_4 \cdot 7H_2O$ (10%)	1 mL/L
$FeSO_4 \cdot 7H_2O$ (1‰)	0.5 mL/L
Thiamine (vitamin B1) (0.5‰)	2 mL/L

3.3.2. M9 Medium

M9 medium was another mineral medium used in the course of the experiments. Trace metal solution, $MgSO_4.7H_2O$, $CaCl_2$ and $FeCl_2.4H_2O$ solutions were prepared separately following the described recipe and specified concentrations.

M9 medium was prepared excluding the $MgSO_4.7H_2O$, $CaCl_2$ and $FeCl_2.4H_2O$ solutions and was autoclaved at 121°C for 15 minutes. $MgSO_4.7H_2O$, $CaCl_2$ and $FeCl_2.4H_2O$ were autoclaved separately under the same conditions separately and mixed with the rest of the medium under aseptic conditions. This approach is adopted in order to avoid calcium sulfate precipitation.

Table 3.3. Contents of M9 medium.

Compound/ Solution	Concentration
K_2HPO_4	7.40 g/L
KH_2PO_4	3.00 g/L
NaCl	0.50 g/L
NH_4Cl	1.00 g/L
Trace Metal Solution	1.00 mL/L
0.1M $MgSO_4.7H_2O$ sol.	10 mL/L
0.01M $CaCl_2$ sol.	10 mL/L
0.005M $FeCl_2.4H_2O$ sol.	1 mL/L

Table 3.4. Contents of trace metal solution used in the M9 medium.

Compound	Concentration (mg/L)
$ZnCl_2$	0.5
$MnCl_2 \cdot 4H_2O$	0.3
H_3BO_3	3.0
$CoCl_2 \cdot 6H_2O$	2.0
$CuCl_2 \cdot 2H_2O$	0.1
$NiSO_4 \cdot 6H_2O$	0.2
$Na_2MoO_4 \cdot 2H_2O$	0.3

3.3.3. LB Broth and LB Agar

Luria Bertani (LB) broth contained 10 g/L tryptone, 5 g/L yeast extract and 5 g/L NaCl in ultrapure water. The solution was autoclaved at 121˚C for 15 minutes and stored at ambient temperature.

LB agar plates were prepared by adding 1.5% (w/v) agar into an LB broth solution and autoclaving at 121˚C for 15 minutes. The LB agar solution was poured into plates aseptically, after cooling to approximately 60^0C post-autoclave.

3.3.4. Stock Solutions and Plates

3.3.5.1. Glucose (5%). 5 g of anhydrous glucose was dissolved in 100 mL ultrapure water. The mixture was autoclaved at 121˚C for 15 minutes. For experiments where glucose was used as a carbon source, this was used as a 10-fold concentrated stock solution and glucose concentration in the flasks was 5 g/L.

3.3.5.2. Glucose, sodium acetate and sodium succinate (2%). Separately, 2 g of each anhydrous glucose, sodium acetate and sodium succinate were dissolved in 100 mL ultrapure water and the solutions were autoclaved at 121˚C for 15 minutes. For experiments where all three carbon sources were used, these 2% stock solutions were used and the concentration of each carbon source in the flasks were set to 2 g/L.

3.3.5.3. HMMM (1 g/L). 0.01 g of HMMM was dissolved in 10 mL ultrapure water and the solution was filtered through 0.22 µm sterile hydrophilic PTFE filters into sterile 12 mL amber glass under aseptic conditions. This filter-sterilized solution was used in biotransformation assays.

3.3.5.4. Melamine (1 g/L). 0.01 g of melamine was dissolved in 10 mL ultrapure water and the solution was filtered through 0.22 µm sterile hydrophilic PTFE filters into sterile 12 mL amber glass under aseptic conditions. This filter-sterilized solution was used in biotransformation assays.

3.3.5.5. NaCl (0.85%). 0.85 g of anhydrous NaCl was dissolved in 100 mL ultrapure water and the solution was autoclaved at 121°C for 15 minutes. This solution was used to rinse and suspend biomasses throughout the experiment.

3.3.5.6. BAC (10 g/L). 2 g of BAC (50%, w/w) was dissolved in 100 mL ultrapure water and the solution was filtered through 0.22 µm sterile hydrophilic PTFE filter into a sterile autoclave bottle under aseptic conditions. This filter-sterilized stock solution was used to prepare media spiked with BAC throughout experiments involving BAC-degrading *Pseudomonas sp.* BIOMIG1^{BAC}.

3.3.4.7. M63B1-200BAC. This solution refers to M63B1 medium that contains 200 mg/L BAC as the sole carbon source. Sterile M63B1 and 10 g/L BAC solutions are used to prepare this medium at desired volumes, under aseptic conditions.

3.3.4.8. N-free M9-10 Melamine Plates. These plates were used during the isolation process of melamine degraders (Chapter 7). M9 medium was prepared excluding the NH_4Cl from the recipe. 1.5% (w/v) agar and 0.5% glucose (w/v) were added to the medium prior to autoclave at 121°C for 15 minutes. After autoclave, the solution was allowed to cool to around 60°C. Sterile solutions of $MgSO_4$, $CaCl_2$ and $FeCl_2$ were added at concentrations described in Section 3.3.2, aseptically. Sterile 1 g/L melamine stock solution was added to adjust the melamine concentration in the medium to 10 mg/L, aseptically. The final agar medium was poured inside the sterile laminar flow biosafety cabinet.

3.4. Detection and Quantitation of HMMM, Melamine and Cyanuric Acid via LC-MS/MS

HMMM, melamine and cyanuric acid in the samples collected during the experiments were measured by using AB Sciex QTRAP 4500 linear ion trap tandem mass spectrometer equipped with TurboV IonSpray electrospray ionization probe, while separation was achieved via Eksigent Ekspert Ultra LC 110 ultra high-performance liquid chromatography unit (AB Sciex, Framingham, MA, USA) or Agilent 1260 Series HPLC (Agilent Technologies, Palo Alto, CA, USA).

Prior to measurements, optimum parameters for detection of HMMM and melamine were determined via direct infusion to mass spectrometer. The compound parameters optimized through infusion involve collision energy (CE), declustering potential (DP) and collision cell exit potential (CXP).

For separation, Thermo Accucore C18 (150x 2.1 mm, 2.6μm) was used. Mobile phase consisted of a binary solvent system involving MS grade methanol (Eluent A) and MS grade water (Eluent B), both fortified with 0.1% formic acid. Flow rate was 0.4 mL/min, and column temperature was 40°C. Injection volume was 10 μL and autosampler was maintained at 4^{0}°C Gradient elution started with 5% Eluent A (0-2 minutes), increased to 95% Eluent A (2-8 minutes), maintained at 95% Eluent A (8-17 minutes), and returned to starting condition for 4 minutes of non-acquired pre-equilibration. Total analysis time was 21 minutes (including the 4-minute pre-equilibration). Details about the HPLC method can be found in Table 3.7 and Table 3.8.

The parameters for electrospray ion source were set to the following values: polarity of electrospray ionization, positive/negative; curtain gas (CUR), 30; collision gas (CAD), medium; ion spray voltage (IS), 5500/ -4500 V; source temperature (TEM), 550°C; nebulizer gas (GS1), 50; auxiliary gas (GS2), 60. Sample acquisition was conducted with unscheduled multiple reaction monitoring (MRM) mode. Analyst 1.6 Software (AB Sciex) was used to control the instrument and data acquisition. MultiQuant 3.0.1 (AB Sciex) software was used for peak annotation and quantitative data processing. Information about the overall MS parameters can be found in Table 3.5 and Table 3.6.

Table 3.5. Ion source parameters employed during the LC-MS/MS analyses.

Source Parameters	
Curtain Gas (psi)	30
Collision Gas	Medium
Ion Spray Voltage (V)	5500/ -4500
Temperature (°C)	550
Ion Source Gas 1 (psi)	50
Ion Source Gas 2 (psi)	60

Table 3.6. MRM transitions and compound parameters used in screening of HMMM, melamine and cyanuric acid.

Q1 (m/z)	**Q3 (m/z)**	**Dwell Time (msec)**	**ID**	**DP (volts)**	**EP (volts)**	**CE (volts)**	**CXP (volts)**
391.0	177.1	50	HMMM-1	26	10	39	6
391.0	283.1	50	HMMM-2	26	10	19	8
126.9	84.9	50	Melamine-1	56	10	25	8
126.9	67.9	50	Melamine-2	56	10	41	6
280.1	183.0	50	IS-1	96	10	61	10
280.1	152.0	50	IS-2	96	10	91	8
128.0	42.0	25	Cyanuric Acid-1	-50	-10	-30	-5
128.0	85.0	25	Cyanuric Acid-2	-50	-10	-14	-15

Table 3.7. Summary of HPLC parameters employed in the LC-MS/MS screening of HMMM, melamine and cyanuric acid.

HPLC PARAMETERS			
General Parameters		**Column Properties**	
Injection Volume	10 µL	**Column Brand**	Accucore RP-MS
Column Temperature	40°C	**Length (mm)**	150
Autosampler Temperature	4°C	**Inner Diameter (mm)**	2.1
Pre-equilibration	4 minutes	**Particle Size (um)**	2.6
Flow Rate	0.4 mL/min	**Packing Material**	C18

Table 3.8. HPLC gradient timetable employed in the LC-MS/MS screening of HMMM, melamine and cyanuric acid.

Gradient Program		
Time	**MeOH 0.1% FA (Eluent A)**	**Water 0.1% FA (Eluent B)**
00:00:01	5	95
00:02:00	5	95
00:08:00	95	5
00:17:00	95	5

For quantitation, calibration standards composed of known concentrations of cyanuric acid, melamine and HMMM reference standard materials were used. All standards were dissolved in 1:1 MS grade methanol: MS grade water solvent mixture. At least 6-point calibration curves between concentrations of 0.4 µg/L and 400 µg/L were constructed. It was ensured that all calibration curves had linear regression lines with R^2 coefficients greater than 0.99 (Figure 3.4). Regression line of the calibration curve was forced to pass through the origin. Each calibration standard and every unknown sample were spiked with either 10 µg/L or 100 µg/L of methyl-d_3-triphenylphosphonium iodide as an internal standard (IS). An internal standard is a pure chemical that is similar to the group of analytes in terms of instrumental response, but unlikely to be found in the samples analyzed or interact with any of the analytes (Tan et al., 2009). Use of internal standards and relative responses is a widespread approach to minimize effect of instrumental errors and to ensure the reproducibility of the analysis.

Calibration curves were constructed as plots of analyte peak area- to- IS peak area versus analyte concentration- to- IS concentration. Therefore, quantitation of unknown samples was achieved in the same manner. Analyte concentration is calculated using expressed concentration and peak area relationship expressed as

$$\frac{A_{analyte}}{A_{IS}} = s \times \frac{C_{analyte}}{C_{IS}}, \tag{3.1}$$

where $A_{analyte}$ is analyte peak area, A_{IS} is IS peak area, s is slope of the calibration curve, $C_{analyte}$ is concentration of the analyte and C_{IS} is the concentration of the IS in the sample.

Quality assurance and quality control (QA/QC) measures employed for these analyses involve:

- Use of relative response of analytes to internal standard for quantitation.
- Analysis of blanks consisting of 1:1 MS grade methanol: MS grade water solution every 10-12 samples to check for carryover throughout the analysis.
- Analysis of quality control (QC) standards composed of HMMM, melamine, cyanuric acid and IS at known concentrations every 10-12 samples to monitor peak reproducibility (Figure 3.3).
- Maintaining the autosampler at 4˚C for the duration of the analysis.

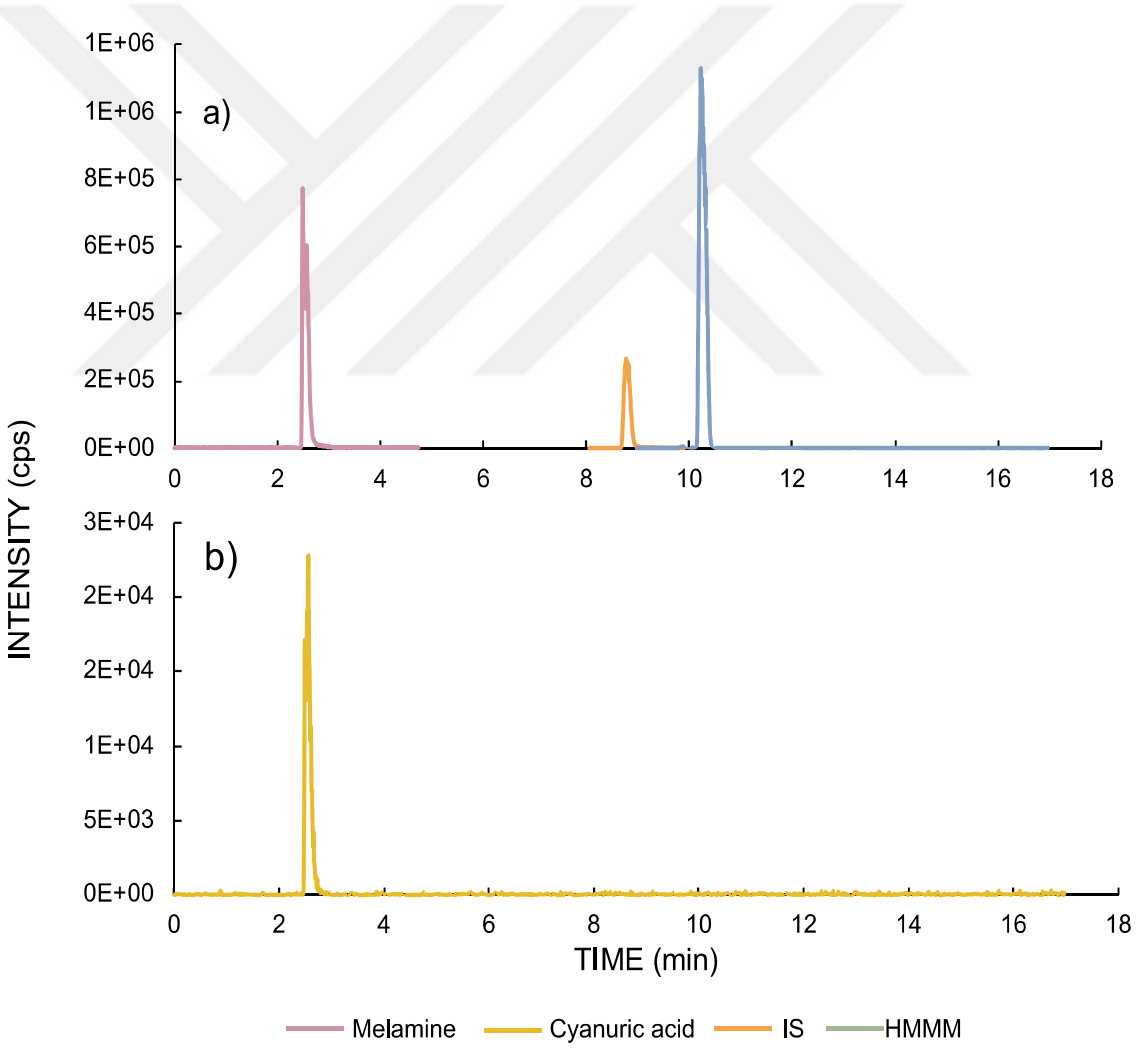


Figure 3.3. Example extracted chromatograms of a QC standard containing a) 40 µg/L melamine, 40 µg/L HMMM, 100 µg/L IS and b) 40 µg/L cyanuric acid.

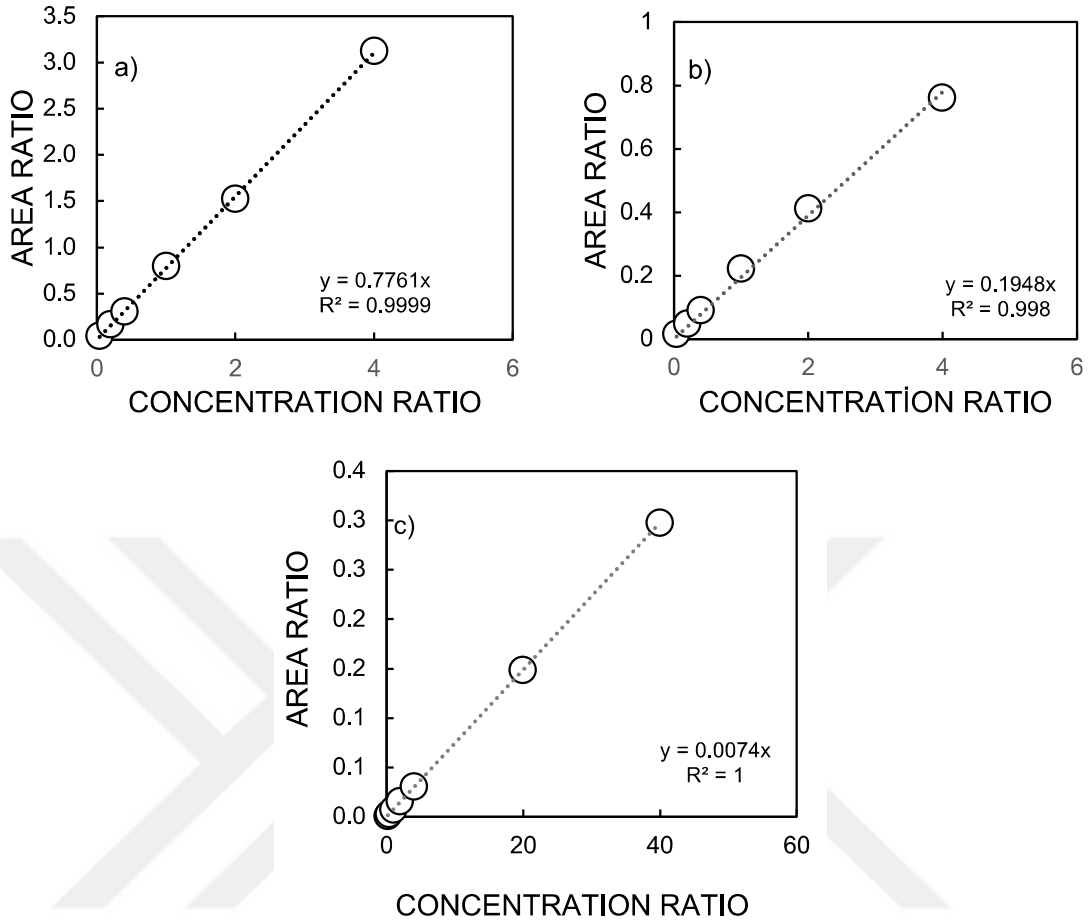


Figure 3.4. Calibration curves of a) HMMM and b) melamine and c) cyanuric acid. Trend line equations and R^2 values are displayed on the graphs.

3.5. Targeted Screening and Semi-quantitation of HMMM Transformation Products via LC-MS/MS

HMMM and its TPs in the samples collected during the experiments were measured by using AB Sciex QTRAP 4500 linear ion trap tandem mass spectrometer equipped with TurboV IonSpray electrospray ionization probe, while separation was achieved via Agilent1260 Series high performance liquid chromatography unit (Agilent Technologies, Palo Alto, CA, USA). For separation, Thermo Accucore C18 (100x 2.1 mm, 2.6µm) was used. Mobile phase consisted of a binary solvent system involving MS grade water (Eluent B) and MS grade methanol (Eluent A), both fortified with 0.1% formic acid. Flow rate was 0.4 mL/min, and column temperature was 40˚C. Injection volume was 10 µL. Gradient elution started with 5% Eluent A (0-2 minutes), increased to 95% Eluent A (2-8 minutes), maintained at 95% Eluent A (8-20 minutes), returned to 5% Eluent A and held for

equilibration (20.1-25 minutes). Total analysis time was 25 minutes. Details about the HPLC method can be found in Table 3.9. TPs screened in our samples were selected from the literature on the biotransformation of HMMM (Alhelou et al., 2019; Castan et al., 2023; Wiener and LeFevre, 2022). Initially, all information regarding the TPs appearing in the literature, including their detected parent and fragment ions were compiled in a list (Table 2.2). TPs that were only detected by their parent ions in the literature were paired with commonly observed fragment ions of other TPs. TPs that were only detected by their Na-adducts were also screened for their H-adduct parent and fragment ions.

Table 3.9. Summary of HPLC parameters used in targeted LC-MS/MS screening of HMMM transformation products.

HPLC PARAMETERS			
General Parameters		**Column Properties**	
Injection Volume	10 µL	**Column Brand**	Accucore RP-MS
Column Temperature	40^0C	**Length (mm)**	100
Autosampler Temperature	-	**Inner Diameter (mm)**	2.1
Pre-equilibration	-	**Particle Size (um)**	2.6
Flow Rate	0.4 mL/min	**Packing Material**	C18
Gradient Program			
Time (min)	**MeOH 0.1% FA (Eluent A)**	**Water 0.1% FA (Eluent B)**	
00.00	5	95	
02.00	5	95	
08.00	95	5	
20.00	95	5	
20.10	5	95	
25.00	5	95	

For all TPs compound parameters were set at the same value, where CE is 25, DP is 40, CXP is 8 and EP is 10. The final screening method consisted of 109 MRM transitions, including those for HMMM, melamine and IS. The method targeted 27 TPs, excluding HMMM and melamine. The same electrospray ion source parameters explained in Section 3.2. were employed. The entire list of MRM transitions is included in Appendix B. TPs were named based on their molecular weight. HMMM and melamine were quantified following

the same calibration process described in Section 3.2. Given the fact that there are no reference materials for the targeted TPs, a semi-quantitation approach was adopted to have estimates of TP concentrations. As previously explained, samples prepared for analysis and all calibration standards were fortified with 100 µg/L of methyl-d_3-triphenylphosphonium iodide as an internal standard (IS).

For semi-quantitation of TPs, relative response of each TP (to IS) and slope of the HMMM calibration curve was used in the equation (3.1) to calculate TP concentration "as HMMM" or "HMMM-equivalent". This approach has been employed in numerous instances in xenobiotic degradation literature, in cases when it was impossible to obtain reference materials for transformation products of a given parent molecule (Johannessen et al., 2021). A pooled sample composed of mixture of biological treatment samples collected on separate days was used as a quality control standard during method optimization. An example chromatogram from the designated QC standard is shown in Figure 3.5.

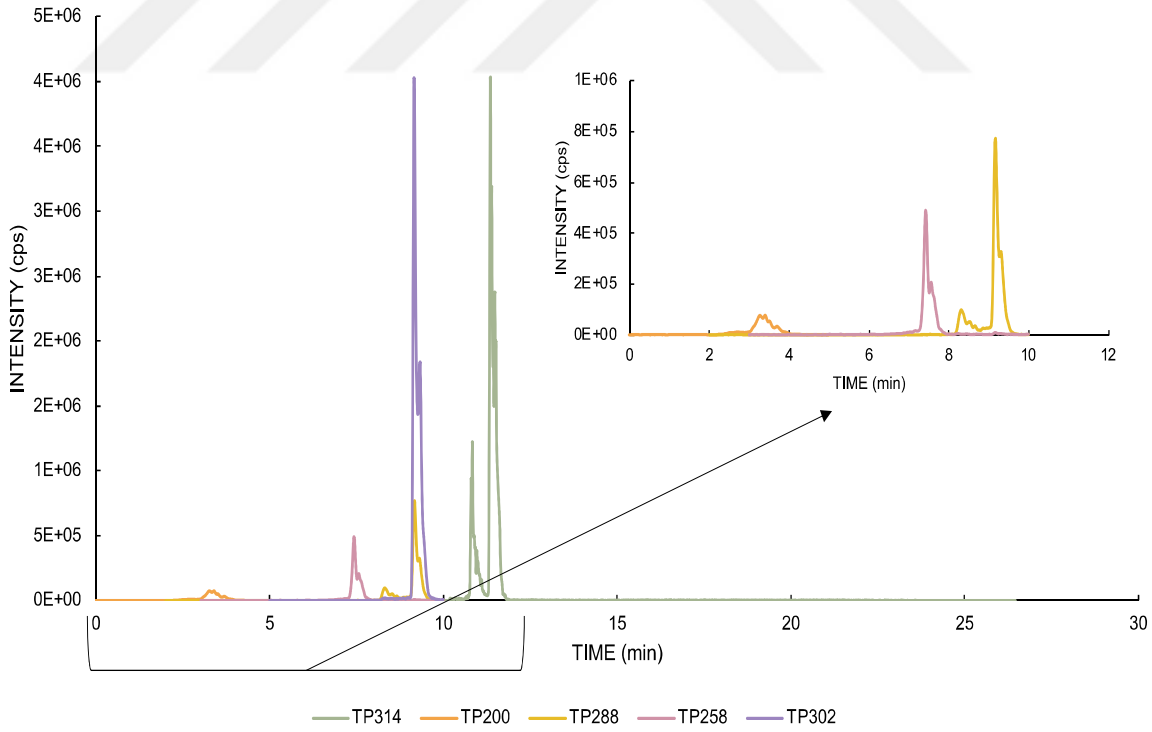


Figure 3.5. An example of overlayed extracted ion chromatograms of selected TPs (TP314, TP200, TP288, TP258 and TP302). The chromatograms of TP200, TP288 and TP258 are given in zoomed insert for better display.

3.6. Detection and Quantitation of HMMM with HPLC-DAD

In the course of biotransformation of HMMM by activated sludge experiments explained in the Chapter 6, the HMMM concentration was monitored via Agilent 1260 Series HPLC (Agilent Technologies, Palo Alto, CA, USA) coupled to a UV/ Visible diode array detector (DAD). The stationary phase was Agilent Zorbax Eclipse Plus C18 (100x 4.6 mm, 3.5µm). A binary mobile phase system consisting of MS grade acetonitrile (Isolab, Germany) and ultrapure water (Millipore, MilliQ) was used.

The gradient elution started at 10% acetonitrile (0-5 minutes), increased to 90% acetonitrile (5-10 minutes), maintained at 90% acetonitrile (10-17 minutes), returned to initial conditions and held at 10% acetonitrile (17.1-20 minutes). Flow rate was 1 mL/min, the column temperature was 35˚C and the injection volume was 50 µL. Detection was performed at a wavelength of 217 nm, which is the wavelength at which maximum absorbance of HMMM occurs. Information about the instrumental parameters is summarized in Table 3.10. An example of the calibration curve and the UV-Visible absorbance spectrum of HMMM are given in Figure 3.6.

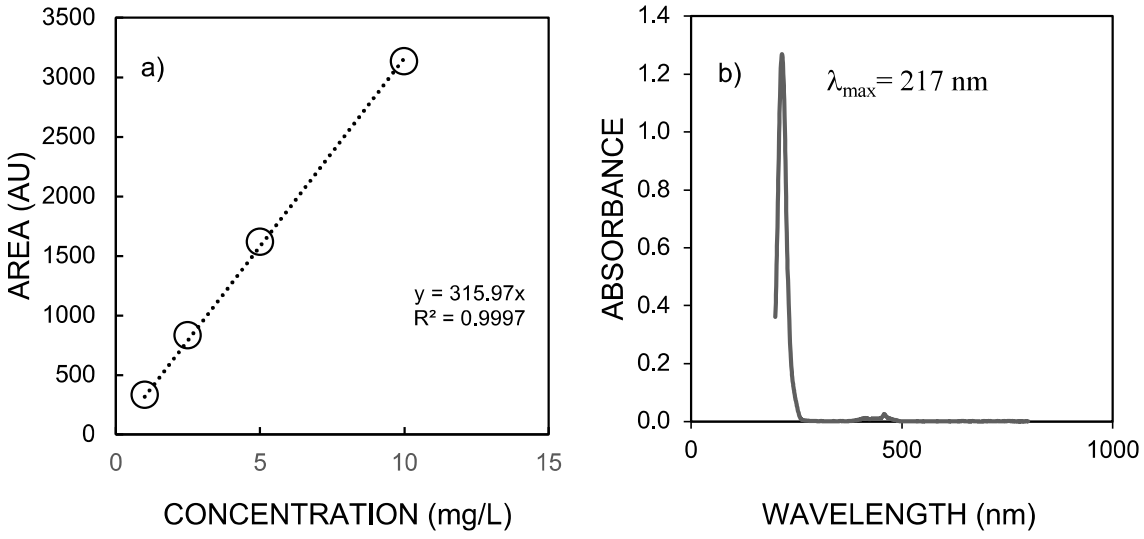


Figure 3.6. a) Calibration curve of HMMM generated by HPLC-DAD analysis with trend line equation and R^2 value displayed on the graph, b) UV-Visible range spectrum of HMMM within 200-780 nm wavelengths, where the wavelength at maximum absorbance occurs is indicated on the graph.

Table 3.10. Summary of HPLC parameters applied during detection of HMMM via HPLC-DAD.

HPLC PARAMETERS			
Injection Volume	50 µL	**Column Properties**	
Detector	DAD	**Column Brand**	Agilent Zorbax Eclipse Plus C18
Wavelength	217 nm	**Length (mm)**	100
Back Pressure	39-81 bar	**Inner Diameter (mm)**	4,6
Column Oven	35°C	**Particle Size (um)**	3,5
Flow Rate (mL/min)	1	**Packing Material**	C18 alkyl chain
Gradient Program			
Time (min)	**Flow (mL/min)**	**Ultrapure Water (Eluent C)**	**Acetonitrile (Eluent D)**
00.00	1	10	90
05.00	1	10	90
10.00	1	90	10
17.00	1	90	10
17.10	1	10	90
20.00	1	10	90

3.7. Detection and Quantitation of Organic Acids and Glucose via HPLC

In the experiments set up with glucose, acetic acid and succinic acid, these analytes were monitored via Agilent 1260 Series HPLC (Agilent Technologies, Palo Alto, CA, USA) coupled serially to both a UV/Visible DAD and a refractive index detector (RID). Glucose detection was achieved via RID whereas organic acids were detected via DAD operated at 210 nm. The separation was achieved via Agilent Hi-Plex H ion exclusion column (300x 7.8 mm, 8µm), maintained at 65°C.

An isocratic elution was used with 0.01 N H_2SO_4 as the mobile phase. Mobile phase was prepared by diluting necessary amount of H_2SO_4 (95-98%, Sigma Aldrich, Germany) in ultrapure water (Milliapore, MilliQ) to a final concentration of 0.01 N. The flow rate was 0.6 mL/min, and the injection volume was 20 µL. Details regarding the instrumental parameters are summarized in Table 3.11. Example calibration curves are shown in Figure 3.7.

Table 3.11. HPLC parameters used for detection of glucose and organic acids via HPLC-DAD and HPLC-RID.

HPLC PARAMETERS			
Analysis Parameters		**Column Properties**	
Mobile Phase	0.01N H_2SO_4	**Column Brand**	Agilent Hi-Plex H Ion Exclusion
Column Temperature	65°C	**Length (mm)**	300
Injection Volume	20 ul	**Inner Diameter (mm)**	7.8
UV Detector	210 nm	**Particle Size (um)**	8
RID Cell Temperature	35°C	**Packing Material**	H ion exchange column
Isocratic Program			
Duration	**Flow (mL/min)**	**Mobile Phase**	
60 min	0.60	100% 0.01N H_2SO_4	

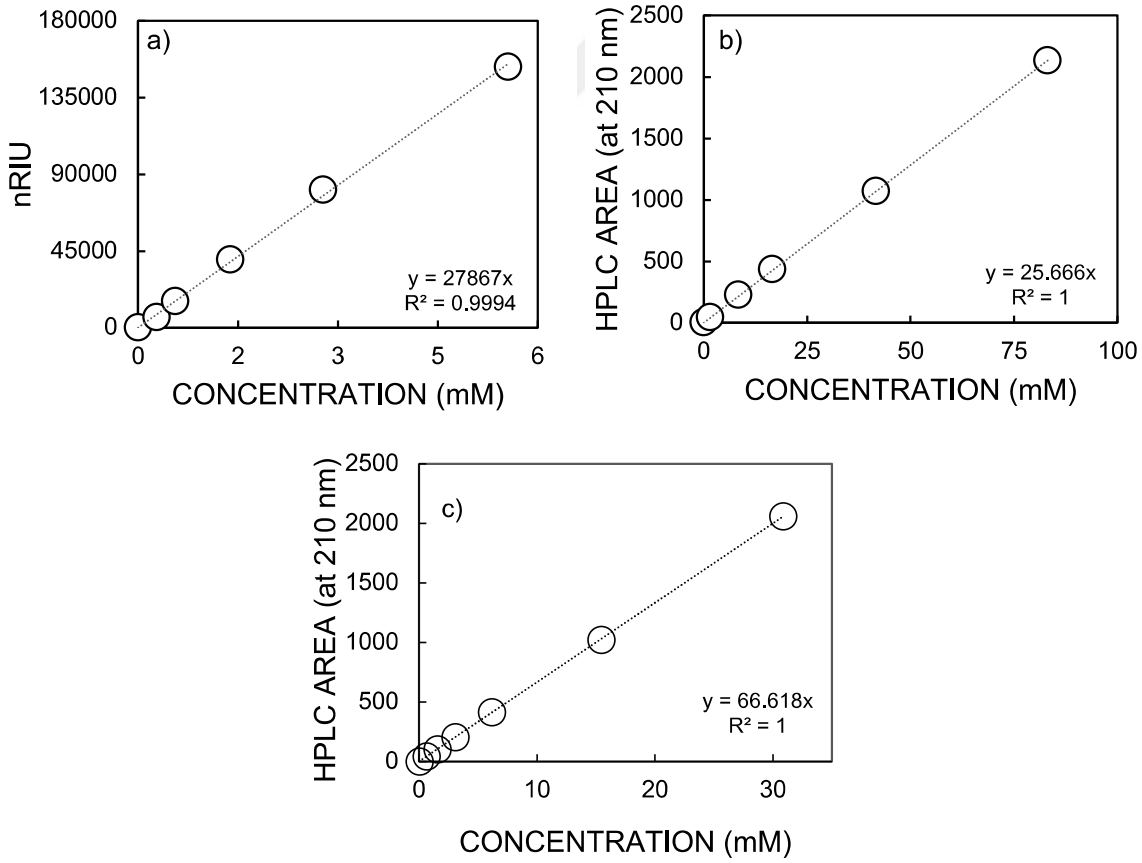


Figure 3.7. Calibration curves of a) glucose and b) acetic acid, detected by HPLC-RID and HPLC-DAD, respectively. Linear trend line equations and R^2 values are displayed on graphs.

3.8. Software

All quantitative data process was performed in Microsoft Office Excel for Mac version 16.80. Molecular structures are drawn in ChemDraw version 8.0. Illustrations were constructed in BioRender.

4. DETECTION AND QUANTITATION OF HMMM IN ERGENE RIVER

4.1. Introduction

Ergene River is a 283 km long water stream located in the northwest region of Turkey. The entire watershed spans three provinces in this region: Edirne, Kirklareli and Tekirdag. This region is highly composite, it hosts a variety of industrial zones with intense industrial activities, as well as large agricultural lands and dense urban areas. Unfortunately, the resulting industrial, agricultural and domestic waste has not been well mediated, and as of today Ergene River and its tributaries have class IV water quality (*Tekirdağ İli 2015 Yılı Çevre Durum Raporu*, 2015), which is the most polluted surface water quality class based on Turkey's surface water management regulations. Even more disappointingly, no concrete and productive actions are being taken against this issue, and it is very likely that the damage is irreparable. One action was Marmara Deep Sea Discharge, which very likely overloaded the already polluted sea, resulting in mucilage crisis a year later this plan's offset. Based on the annual Environmental Status Reports prepared by governorship of each province (since 2011), for years, most of the municipalities discharged domestic wastewater into Ergene River, without any prior treatment (*Tekirdağ İli 2015 Yılı Çevre Durum Raporu*, 2015). Even today, many municipalities do not perform a primary or secondary wastewater treatment, let alone advanced treatment. The information about industrial wastewater treatment and discharges is even more limited and will not be shared with public despite being officially requested. Despite the high pollution levels, Ergene River is widely utilized for irrigation, which facilitate transport of pollutants to soil and agricultural products. It is also noteworthy that Ergene River meets Maritsa River, which flows across several countries in Europe and into the Aegean Sea, rendering the pollution in Ergene an international problem.

Every day, thousands of industrial chemicals are being discharged into receiving waters, some with proper treatment and some without. The variety, the amount and the nature of these chemicals are becoming harder to keep up with, and the regulations are clearly falling behind. Current state of pollution is a call for more rigorous research and acknowledgement about ecotoxicity of industrial chemicals produced, their fate and effects

on the environment once they are discharged. Within this context, environmental chemistry research has been critical in the last decades.

In 2020, Emadian et al published a comprehensive study of pollution in Ergene River (Emadian et al., 2021). The study, completed within the scope of a TUBITAK project called "Development of a geographical information systems based decision-making tool for water quality management of Ergene watershed using pollutant fingerprints", comprised of quantitation of 222 micropollutants in 300 samples seasonally collected along 75 sampling points across Ergene River, from May 2017 to August 2018 (Emadian et al., 2021). The selection of targeted pollutants was based on priority substances and watch lists composed by European Commission. The quantitation was achieved by LC-MS/MS. In this study core micropollutants of Ergene River were identified using data driven clustering methods. Among these core micropollutants, HMMM was a noteworthy one. It was detected in almost all sampling points, in all seasons, at concentrations between 0.01µg/L and 329.17 µg/L (Emadian et al., 2021). Its main source in Ergene was identified to be Buyukkaristiran Industrial Zone, which is largely dominated by textile, dye, automotive, metal and electronics industries. In relation with the study by Emadian et al. described above, a TUBITAK and CHIST-ERA funded project named "Sustainable Watershed Management Through IoT-Driven Artificial Intelligence (SWAIN)" was initiated for better modelling of pollution in rivers and the development of an AI-driven pollution early warning system. Our research group has been a participant in SWAIN project and the work described in this chapter is done within its scope, constituting a portion of our contribution. With the work described in this chapter, the objective is to verify ongoing presence of HMMM in Ergene River at various source and monitoring points, as well as in a selected WWTP influent and effluent samples, to establish the environmental relevance of work on HMMM.

4.2. Materials and Methods

4.2.1. Sampling Locations and Sampling Process

Samples were collected from four selected locations, three of which were located on Ergene River and one of which was located on Maritsa River (Figure 4.1, Table 4.1). Points t1-2 and m3 are selected as potential source zones for HMMM, given their proximity to

wastewater discharge points of two large industrial zones. Point m8 and Mar1 are selected as monitoring points in order to assess how far along the river can HMMM be observed. Point m8 is a small city center and Mar1 is a rural area, and both points are located distant from industrial zones. Additionally, from a wastewater treatment plant located in Ergene-1 industrial zone, samples were collected from influent, and effluents of biological treatment and chemical treatment units. The treatment plant components include grit chamber, oil/sand interceptor, aeration tank, sedimentation tank, chemical sedimentation using alum. That treated wastewater effluent is discharged into Marmara Sea through deep sea discharge.

Sampling from points t1-2, m3 and Ergene-1 industrial zone wastewater treatment plant were made in January 2023. Sampling from Mar-1 were made in August 2022 and November 2022. Sampling from m8 were made in August 2022, November 2022 and January 2023.

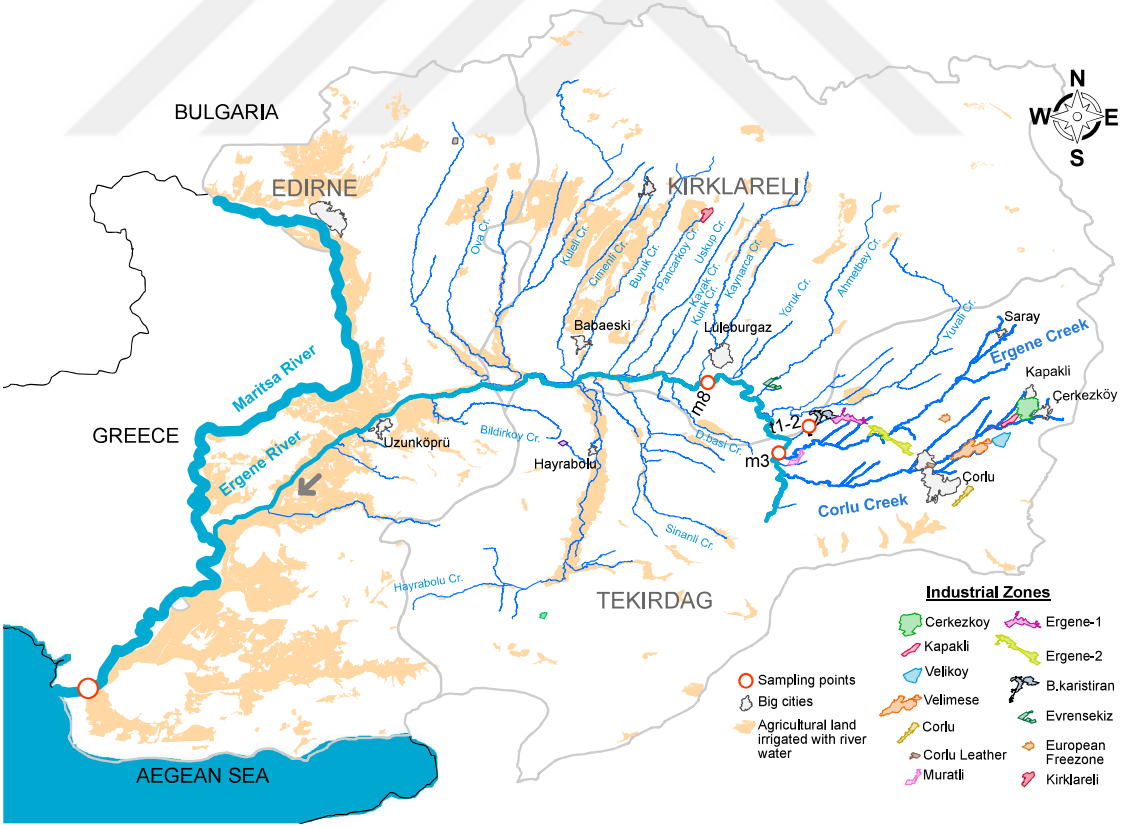


Figure 4.1. Map illustration of locations where samples were collected.

Samples were taken from the river using a custom-made PTFE sampling bucket. The vessel is attached with a handle and a 5-meter rope, in order to release the vessel into the

river water, in cases when access to the river by foot was not possible (Figure 4.2). The bucket was rinsed three times with the river water prior to sampling and the sample was collected from 30-40 cm below the water surface. 500 mL glass autoclave bottles were rinsed three times with the collected water sample and then were filled with the water sample leaving as minimal headspace as possible. The sample bottles were stored in a cool box containing ice batteries during transportation and stored at 4˚C in the laboratory until sample processing.

Table 4.1. Description of sampling points, including coordinates, province, classification of the location and the river on which the point is located.

Point	Latitude	Longitude	Province	Category	River
t1-2	41°15'39.99"N	27°32'51.32"E	Kırklareli	Source	Ergene
m3	41°12'8.35"N	27°28'35.78"E	Tekirdağ	Source	Ergene
m8	41°20'45.44"N	27°19'34.22"E	Kırklareli	Monitoring	Ergene
Mar-1	40°43'41.04"N	26°4'39.173"E	Edirne	Monitoring	Maritsa
Ergene-1	41°16'37.17"N	27° 35'23.67"E	Tekirdağ	-	-



Figure 4.2. Photos from sampling locations.

4.2.2. Sample Preparation and Analysis

Prior to analysis, 5 mL of samples were mixed with 5 mL MS grade methanol (Sigma Aldrich, Germany) in 15 mL conical polypropylene centrifuge tubes (Isolab, Germany), stirred by vortex mixer for 30 seconds and centrifuged at 4500 rpm for 10 minutes. The supernatants were filtered through 0.22 µm hydrophilic PTFE filters (Isolab, Germany) into 10 mL amber glass vials with PTFE lined screw caps.

For analysis in LC-MS/MS, 800 µL of the filtered sample was mixed with 200 µL of 50 µg/L IS in 1.5 mL amber chromatography vials screw capped with PTFE septa. The IS solution was prepared in 1:1 MS grade methanol: MS grade water solvent. The final sample volume was 1 mL, and the final IS concentration in the vial was 10 µg/L. Sample analysis and quantitation of HMMM was performed based on the procedure described in Section 3.2.

4.3. Results and Discussion

HMMM is detected in all samples above the limit of detection of the analytical method (Table 4.2). The highest concentration of HMMM on the river was observed in the designated source zone of HMMM (t1-2) at 32.0 $\pm$0.22 µg/L. In January, HMMM is detected at both source zones (t1-2, m3) and both monitoring zones (m8, Mar1) at concentrations between 0.21$\pm$0.02- 32.0$\pm$0.22 µg/L. In general, HMMM concentration levels were lower in Mar1 (0.21-0.45 µg/L) than in m8 (6.41-14.1 µg/L), which may be attributed to its higher distance from the source zone. It is also likely that, aside from industrial wastewater input, HMMM can be released into the river via road runoff in m8 (an urban center), which is expected to a lesser extent in Mar1 given that it is a rural area.

In Ergene-1 WWTP, HMMM is not efficiently removed by the wastewater treatment processes available at the treatment plant. Interestingly, HMMM concentration seems to increase from 1.27$\pm$ 0.03 µg/L to 14.7 $\pm$0.27 µg/L by the end of chemical treatment process (Table 4.2). This may be explained by the wastewater volume changes during the processes, also by the discussion provided by Alhelou et al. that ongoing formation of HMMM could take place from possible precursors (Alhelou et al., 2019). The latter discussion would require further investigation in order to determine the possible precursors and demonstrate

consistently that this in situ HMMM generation happens throughout wastewater treatment processes.

Table 4.2. Concentration of HMMM detected in the collected samples.

Sampling Point	**Sampling Time**	**HMMM Concentration (Mean±STDV,µg/L, *n*=2)**
t1-2	January	32.00±0.22
m3	January	12.4±0.03
m8	August	14.1±0.23
m8	November	6.41±0.02
m8	January	13.6±0.02
Mar1	August	0.21±0.02
Mar1	November	0.45±0.00
Influent	January	1.27±0.03
Biological Effluent	January	4.85±0.07
Chemical Effluent	January	14.7±0.27

In summary, HMMM continues to be detectable along the Ergene River, from candidate source zones to monitoring zones kilometers away. This suggests that its release into water occurs continuously and degradation through biotic and abiotic routes in the river matrix does not take place to large extent. Furthermore, analyses of the samples taken from an industrial zone wastewater treatment plant indicate that conventional treatment processes do not effectively alleviate HMMM.

5. BIOTRANSFORMATION OF HMMM BY PSEUDOMONAS SP. BIOMIG1^{BAC}

5.1. Introduction

5.1.1. Biotransformation of HMMM

Despite gaining popularity in environmental research within the last two decades, the literature on biotransformation of HMMM is very limited. Overall, there are currently only three published studies focusing on the biotransformation of HMMM and detection of its degradation mechanism (Alhelou et al., 2019; Castan et al., 2023; Wiener and LeFevre, 2022). Alhelou et al. assessed biotransformation of HMMM by activated sludge in a mineral medium that lacks any other carbon sources (Alhelou et al., 2019). In this work, they have discovered that 77.4% of HMMM is degraded in biological treatments, as opposed to 25% loss of HMMM in the abiotic controls in 29 days. They have identified and tentatively quantified 21 transformation products (TP) of HMMM via LC-HRMS. In this work, melamine was not found to be a significant metabolite, rather, other lower molecular weight TPs such as TP156, which is a melamine derivative with a single methylol branch, emerged (Alhelou et al., 2019). In another work by Wiener et al., 69.9% of HMMM was biotransformed by *Trametes versicolor*, a white rot fungus, in 14 days (Wiener and LeFevre, 2022). In this work, they have identified 10 novel TPs via HRMS and designated melamine as a possible dead-end metabolite, however, they didn't perform semi-quantitation or information about mass balance (Wiener and LeFevre, 2022). Both Alhelou et al. and Weiner et al. proposed biotransformation pathways for HMMM, compiling all TPs they have observed. Castan et al. studied uptake and metabolism of HMMM and several other tire-derived chemicals by lettuce (Castan et al., 2023). In this study, it was discovered that HMMM uptake occurs in lettuce plants and is transported through the roots into the leaves in hydroponic conditions (Castan et al., 2023). They have detected and semi-quantified 10 TPs of HMMM, three of which were novel to the literature. They did not detect melamine as a TP. Amounts of formed TPs peaked at day-10 and persisted until the end of the experiment (day-14) (Castan et al., 2023).

In addition, Karakaya (2019) studied the biotransformation of HMMM by *Pseudomonas sp.* BIOMIG1^{BAC} (Karakaya, 2019). This strain has unusually large genome occupied with diverse xenobiotic degradation genes (Altinbag et al., 2020). For instance, BIOMIG1 is capable of degrading quaternary ammonium disinfectants which are very hard-to-degrade chemical substances. They have found that this strain is able to transform HMMM into melamine in 45 days when a mixed carbon source composed of glucose, acetate and succinate were provided under nitrogen-deficient conditions, however, candidate TPs except melamine and cyanuric acid were not screened. They have found that HMMM degradation does not proceed any further than melamine and during its degradation, glucose is fermented to equivalent amount of acetate. They proposed that these nitrogen deficient conditions trigger a cascade of enzymatic pathways, which facilitates co-metabolic degradation of HMMM, since it was not consumed as a carbon or nitrogen source, and only glucose in the medium was consumed via fermentation to acetate (Karakaya, 2019).

Based on the limited literature it is evident that biotransformation of HMMM requires further work. Previously published works did not assess biodegradation activity of a single strain of bacteria, in fact, each studied a different source of biomass (activated sludge, fungus and lettuce) (Alhelou et al., 2019; Castan et al., 2023; Wiener and LeFevre, 2022). The only study utilizing a single strain bacteria required more in depth understanding of biotransformation of HMMM and did not screen for its TPs (Karakaya, 2019). This study aims to build up on the previous findings regarding biotransformation of HMMM by *Pseudomonas sp.* BIOMIG1^{BAC} by screening for the transformation products and contribute to the existing literature.

5.2. Materials and Methods

5.2.1. Culture Preparation

A pure strain of *Pseudomonas sp.* BIOMIG1^{BAC} was obtained from our laboratory inventory, in the form of a spread plate. Initially, in a sterile 50 mL polypropylene centrifuge tube, 10 mL M63B1-200BAC solution was prepared (see Section 3.3.4). A single colony from the plate was transferred aseptically into 10 mL of sterile M63B1-200BAC medium. This liquid culture was grown for 24 hours at 25°C on an orbital shaker operated at 100 rpm.

In six autoclaved 250 mL Erlenmeyer flasks, 50 mL sterile M63B1-200BAC solutions were prepared. Each flask was inoculated with 0.5 mL of the 24-hour grown culture. These constituted the upscaled seeds for the biotransformation assays. These liquid cultures were grown until their OD reached approximately 0.3. Then, content of each flask was divided into two 25 mL aliquots by transferring the liquid into sterile 50 mL polypropylene centrifuge tubes aseptically. The cultures were centrifuged at 4500 rpm for 10 minutes. The supernatants were discarded aseptically, and the pellets of the same cultures were combined by re-suspending them in 1 mL sterile 0.85% NaCl solution, yielding six 50 mL centrifuge tubes each containing 1 mL biomass suspension. These suspended cultures were transferred aseptically to 1.5 mL sterile microcentrifuge tubes and centrifuged at 10000 rpm for 10 minutes. The supernatants were discarded, and this re-suspension and rinse cycle was repeated twice under aseptic conditions. In the final step, each pellet was suspended once again in 1 mL sterile 0.85% NaCl and these were used to inoculate the prepared sterile selective media.

5.2.2. Biotransformation Assays

Biotransformation of HMMM was tested under two conditions which are summarized in Table 5.1. These test conditions are N-free (nitrogen-free but carbon source provided) and C-free (C source except HMMM is absent). The aim was to assess which conditions best facilitated biotransformation of HMMM, and if biotransformation occurred, whether HMMM was consumed as the sole carbon source or the sole nitrogen source. For N-free treatments, stock solution of sterile M63B1 medium that was prepared from the ingredients listed in Section 3.3.1 was used, omitting $(NH_4)_2SO_4$. For C-free treatments, the original M63B1 medium recipe described in Section 3.3.1. was followed. In preparation of N-free treatments, 5% (w/v) sterile glucose solution was added aseptically into the sterile media to obtain a 5 g/L glucose concentration in the flasks. Filter-sterilized 1 g/L HMMM stock solution was added aseptically to each flask at a final concentration of 10 mg/L (25.6 µM). The total volume of each treatment medium was 50 mL. M63B1 medium containing 10 mg/L HMMM was used as an abiotic control. All selective media were prepared in 250 mL screw capped Erlenmeyer flasks, with caps left loose in biological treatments to allow air entrance. All biological treatment flasks were in triplicate and the abiotic control flasks were in duplicate. All biological treatments were inoculated with biomass re-suspended in 1 mL

sterile 0.85% NaCl, which was prepared following the process described in Section 5.2.3. All flasks were placed on the orbital shaker operated at 100 rpm and grown at 25°C.

Table 5.1. Contents of the flasks prepared for the HMMM biotransformation experiments with *Pseudomonas sp.* BIOMIG1^{BAC}.

	N-free Medium	**C-free Medium**
Inoculum (mL)	1	1
Glucose (5%) (mL)	5	-
HMMM (1g/L)(mL)	0.5	0.5
N-free M63B1 Stock (mL)	43.5	
M63B1 Stock (mL)	-	48.5
Total Volume (mL)	50	50

5.2.3. Sampling, Sample Preparation and Analysis

For monitoring HMMM and its TPs, 1 mL samples were taken from all flasks aseptically, mixed with 1 mL MS grade water and 2 mL MS grade methanol in 15 mL centrifuge tubes. The mixture was vortexed for 10 seconds, centrifuged at 4500 rpm for 10 minutes and filtered through 0.22 µm hydrophilic PTFE filters into 10 mL amber glass vials. The samples were stored at 4°C until analysis. Prior to screening HMMM, 40 µL of these samples were mixed with 760 µL 1:1 MS grade methanol: MS grade water solution and 200 µL 50 µg/L IS solution in 2 mL amber chromatography vials, thus yielding 100-fold diluted samples spiked with 10 µg/L IS. Prior to screening for TPs, 400 µL of the filtered samples were combined with 100 µL 1 mg/L IS solution and 500 µL 1:1 MS grade methanol: MS grade water solution, which yields 10- fold diluted samples with 100 µg/L IS. Since the TPs are more diverse and possibly in smaller concentrations than HMMM, preparation of more concentrated samples was preferred. Then, samples were screened for HMMM and TPs following the procedures described in Section 3.4 and Section 3.5, respectively. Dilution factors were taken into account during quantitation.

For monitoring glucose in N-free treatments, 0.75 mL samples were taken from the flasks aseptically and mixed with 0.75 mL 0.01 N H_2SO_4 in 2 mL microcentrifuge tubes. The mixture was mixed by pipetting in and out, centrifuged at 10000 rpm for 5 minutes and

filtered through 0.22 µm hydrophilic PTFE filters into 2 mL amber chromatography vials. Prepared samples were analyzed for glucose and acetate based on the methods explained in Section 3.7. Dilution factors were taken into account during quantitation. Entire experimental process is summarized in Figure 5.1.

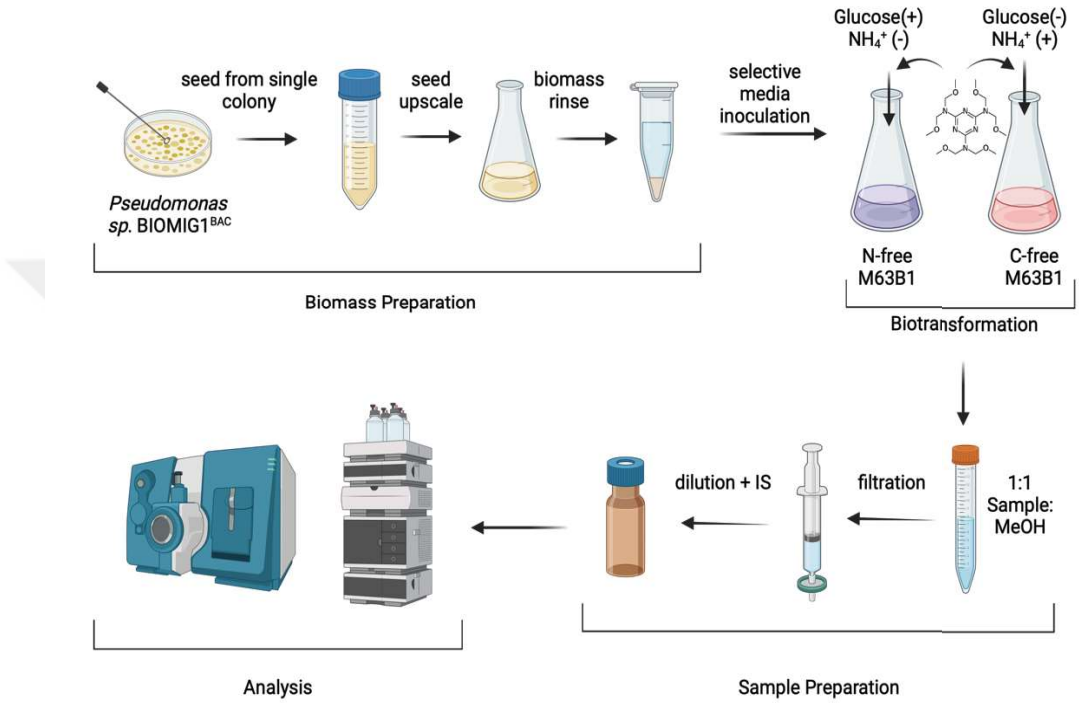


Figure 5.1. Illustration of the experimental workflow followed throughout the studies described in the Chapter 5.

5.3. Results and Discussion

5.3.1. Biotransformation of HMMM by *Pseudomonas sp.* BIOMIG1^{BAC}

By the end of 100th day, about 86% of initial HMMM in N-free biological treatments had disappeared, as opposed to 34% decrease in abiotic controls and 50% decrease in C-free biological treatments (Figure 5.2). On the other hand, a significant increase in melamine concentration was only observed in N-free treatments. While melamine concentration increased to 23.11 $\pm$ 0.90 µM in N-free treatments by the end of the experiment, it only reached up to 2.51 $\pm$ 0.29 µM and 3.51 $\pm$ 0.23 µM in abiotic controls and C-free treatments, respectively. Given the fact a 1:1 stochiometric ratio between HMMM and melamine is

expected as a result of degradation, the amount of melamine formed roughly corresponds to the amount of HMMM lost in N-free treatments.

Although degradation of HMMM to melamine appears to occur both biotically and abiotically, the significantly higher loss of HMMM and higher formation of melamine in N-free treatments as opposed to abiotic controls and C-free treatments, hints that presence of a biological activity in these conditions might accelerate this process. As it is apparent, even in the case of N-free treatments, the degradation rate is very low compared to biodegradability standards (OECD, 2006) and biotransformation does not seem to proceed to mineralization. Rather, as a result of degradation, accumulation of melamine as a dead-end product occurs. This is in accordance with the limited literature examples about biotransformation studies on HMMM (Wiener and LeFevre, 2022), and on other triazines similar to HMMM, where, for instance, transformation products with intact triazine cores as a result of incomplete atrazine degradation by *Rhodococcus sp.* Strain NI86/21 were reported (Nagy et al., 1995).

Throughout the experiment, OD of both type of biological treatments decreased continuously (Figure 5.3). This indicates that HMMM is not metabolized within a growth promoting process and it is not consumed as a sole nitrogen or carbon source. However, the fact that this biotransformation occurs to its highest extent in the condition where nitrogen is absent and glucose is present, presence of a carbon source might have helped sustain some biological activity through 100 days.

Similar to previous observations made in a study from our research group focusing on biotransformation of HMMM with *Pseudomonas sp.* BIOMIG1^{BAC} (Karakaya, 2019), the strain converted nearly all HMMM into melamine, while it consumed glucose completely. However, some outcomes of the experiments in this work contradict with those of the previous work by Karakaya (Karakaya, 2019). In that work, a transformation of HMMM into melamine happened in 45 days as opposed to 100 days in current experiments. Moreover, during that study, it was observed that glucose was fermented to acetate, whereas in this study, acetate was not detected during consumption of glucose (Figure 5.4). This inconsistency in results can be interpreted as biotransformation of HMMM by *Pseudomonas sp.* BIOMIG1^{BAC} not yet occurring readily and reproducibly under the studied conditions.

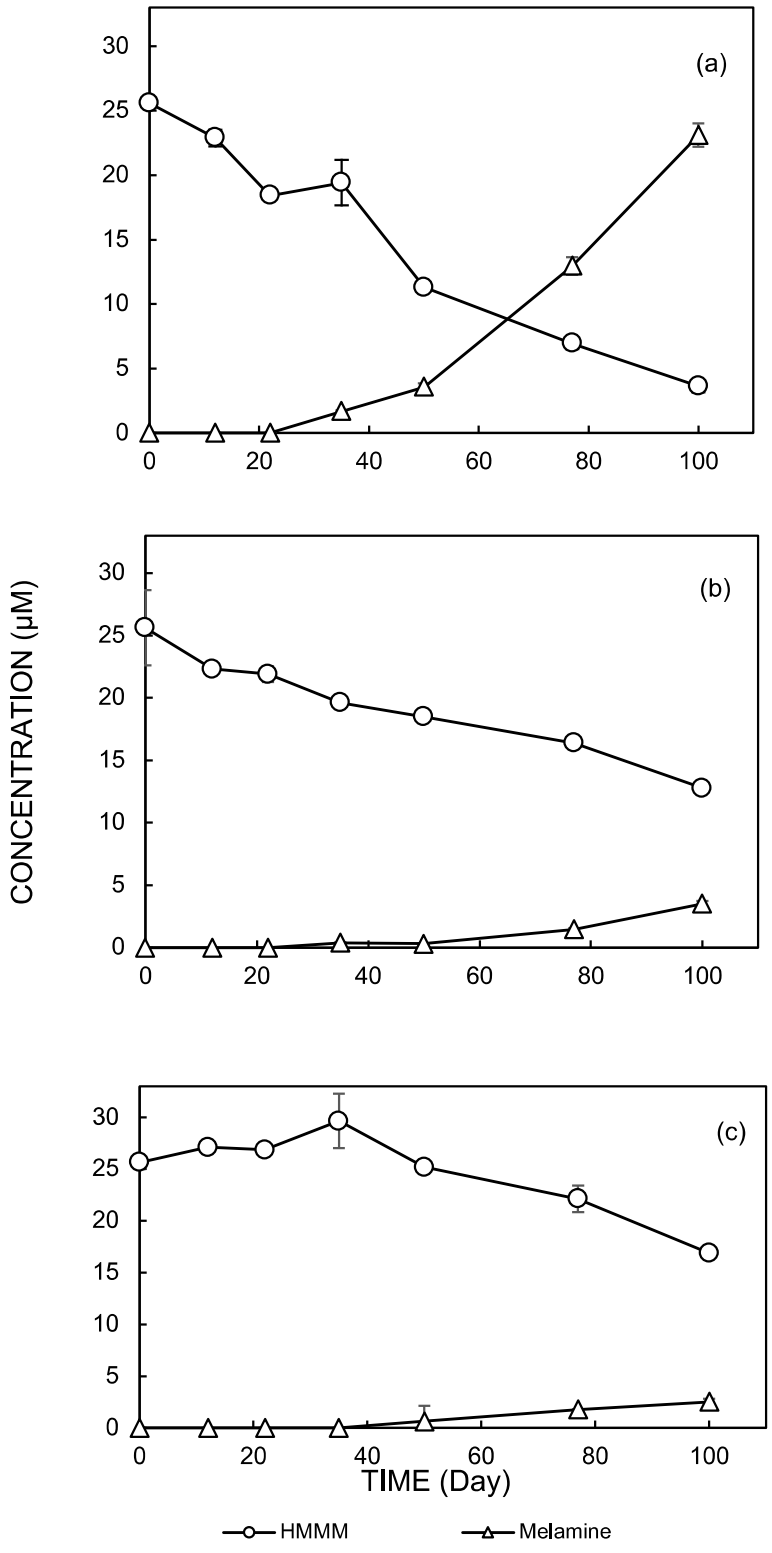


Figure 5.2. Concentrations of HMMM and melamine in a) N-free, b) C-free media inoculated with BIOMIG1 and c) abiotic control media during 100 days of incubation at 25°C (presented as mean ±one STDV, *n*=3)

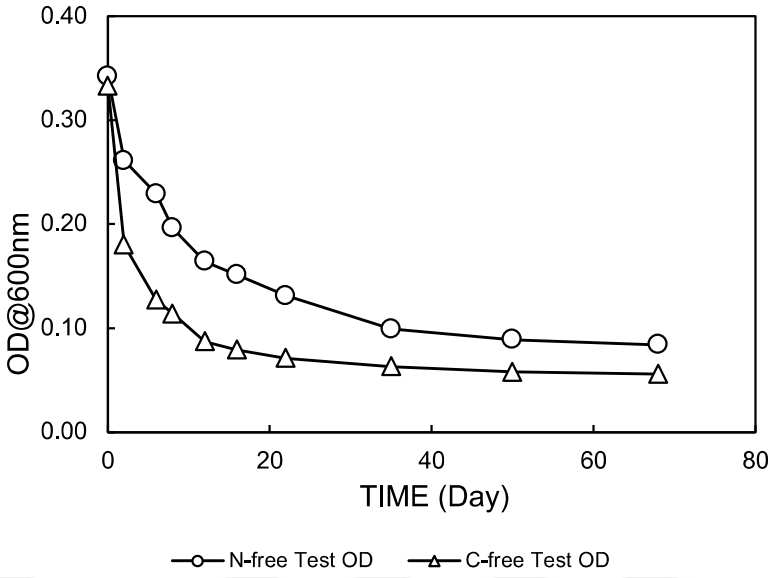


Figure 5.3 Optical density of N-free and C-free biological treatments throughout the experiment.

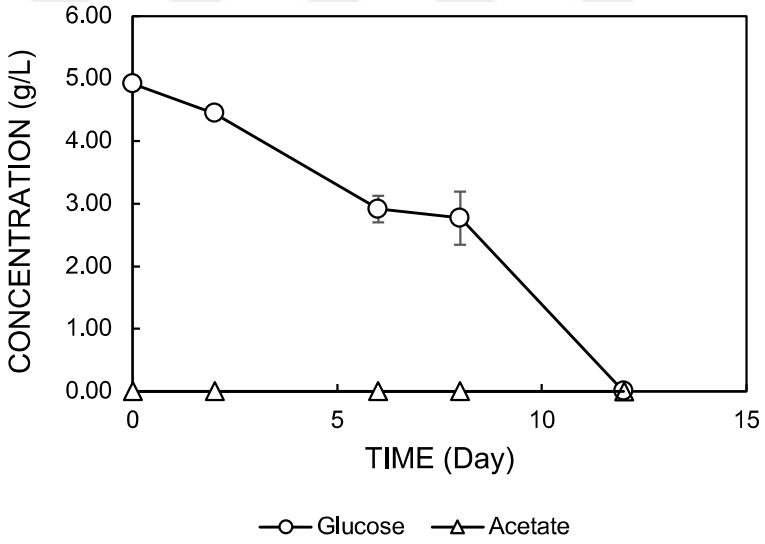


Figure 5.4. Glucose and acetate concentration in N-free flasks inoculated with BIOMIG1 during the course of 12 days at 25°C (presented as mean ±one STDV, *n*=3).

5.3.2. Transformation Products of HMMM

Potential HMMM transformation products (TPs) were compiled from the available literature as explained in Sections 3.5 and 5.1. Some TPs in the literature were only detected with their Na-adduct form (for instance TP360, TP330 and TP317), their H-adduct parent ions were added to the screening list as well. TPs that were detected in the literature using

only their parent ion exact mass were paired with common fragment ions shared by many TPs, such as fragments with m/z values 139, ,151, 163, 177 or 207 (Figure 5.5). The targeted method was optimized using a pooled sample composed of equal volumes of N-free treatment samples from days 0, 22, 50, 77 and 100. Several CE and DP values were tested for best observation of parent-fragment ion pairs and several gradient programs were tested for best separation. The final parameters are given in Section 3.5 and Appendix B.

TP screening was conducted at 5 time points (days 0, 22, 50, 77 and 100) on N-free biological treatment samples and at 3 time points on abiotic control samples (days 0, 50 and 100). Duplicate samples from N-free biological treatments and abiotic controls were analyzed. A total of 17 TPs were detected, excluding melamine. As explained in Section 3.5, TPs were semi-quantified by using their relative response to IS peak area and the slope of the HMMM calibration curve (Equation 3.1). Therefore, their concentrations are reported "as HMMM" or "HMMM equivalents".

Although their exact concentrations cannot be measured using this approach, increasing/ decreasing trends can be observed confidently, since changes in ion response of chemicals in LC-MS/MS are correlated with their abundance and can be measured very sensitively (Alhelou et al., 2019). Observed TPs are summarized in 5 groups (Figure 5.6, 5.7, 5.8, 5.9 and 5.10.). The grouping is done arbitrarily, in order to visualize each TP with best resolution.

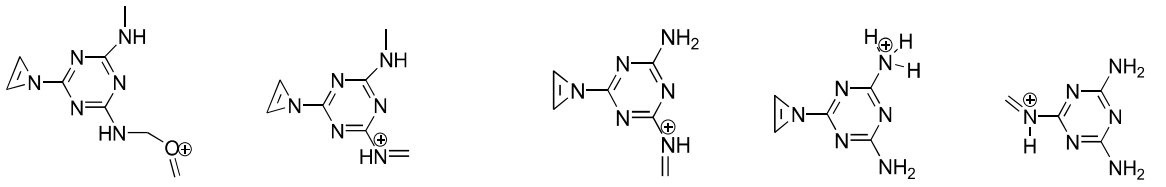


Figure 5.5. Proposed structures for commonly observed fragment ions of HMMM and its TPs.

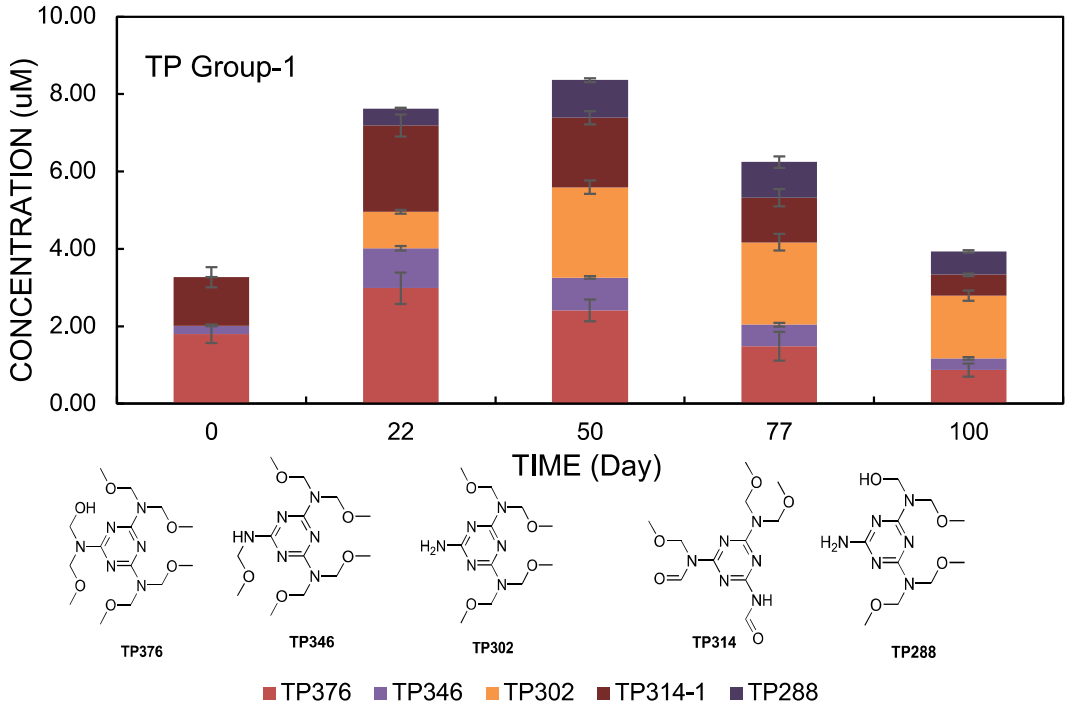


Figure 5.6. Concentration of Group-1 TPs in N-free flasks inoculated with BIOMIG1 during 100 days of incubation at 25°C (mean ±one STDV, *n*=2).

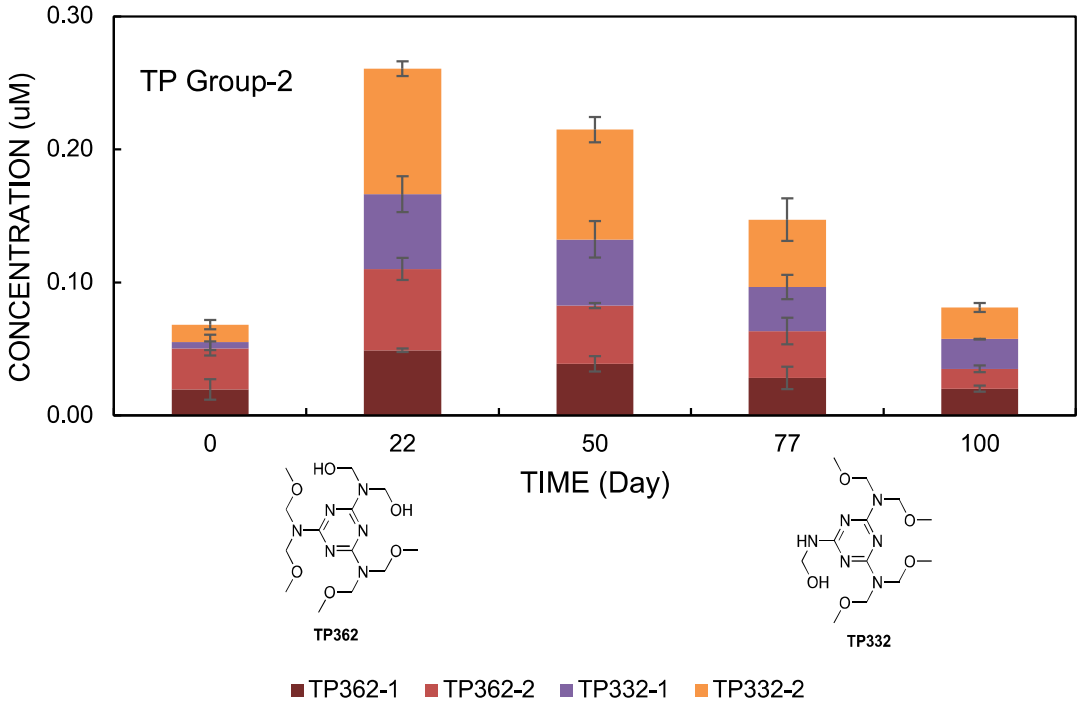


Figure 5.7. Concentration of Group-2 TPs (as HMMM) in N-free flasks inoculated with BIOMIG1 during 100 days of incubation at 25°C (mean ±one STDV, *n*=2).

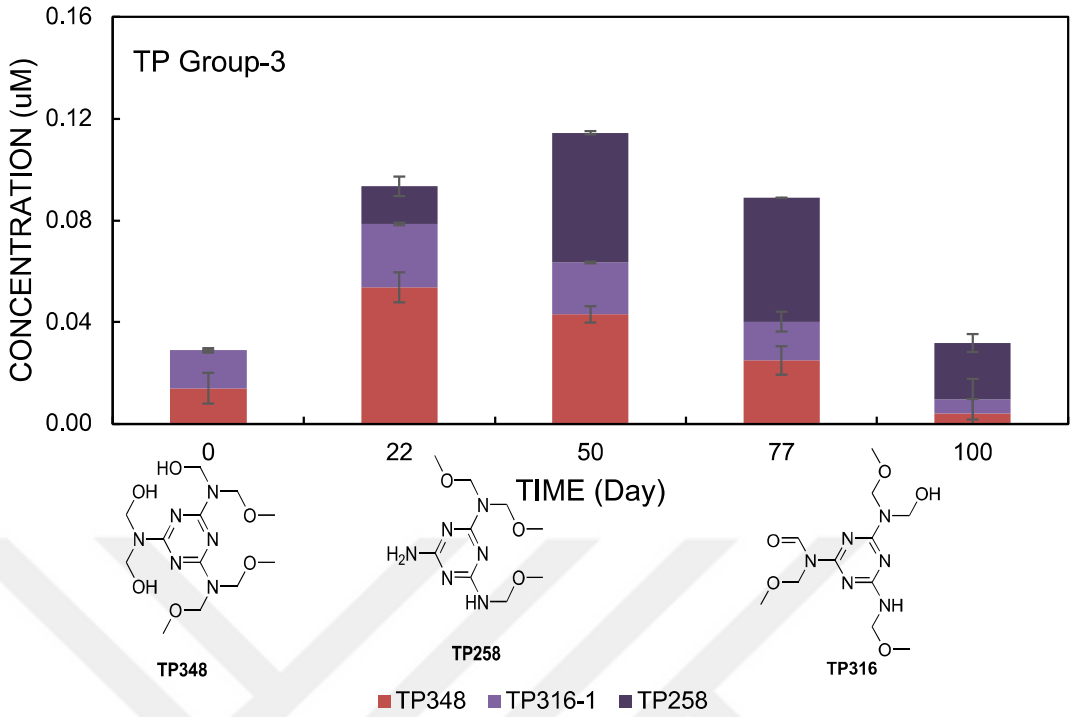


Figure 5.8. Concentration of Group-3 TPs (as HMMM) in N-free flasks inoculated with BIOMIG1 during 100 days of incubation at 25°C (mean ±one STDV, *n*=2).

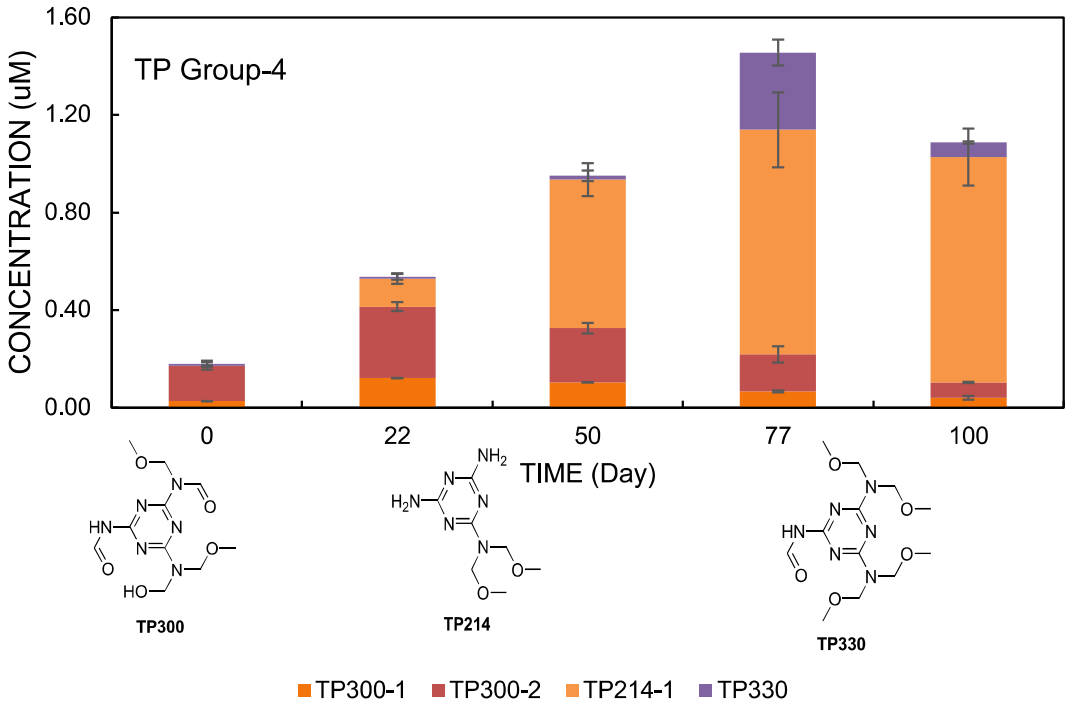


Figure 5.9. Concentration of Group-4 TPs (as HMMM) in N-free flasks inoculated with BIOMIG1 during 100 days of incubation at 25°C (mean ±one STDV, *n*=2).

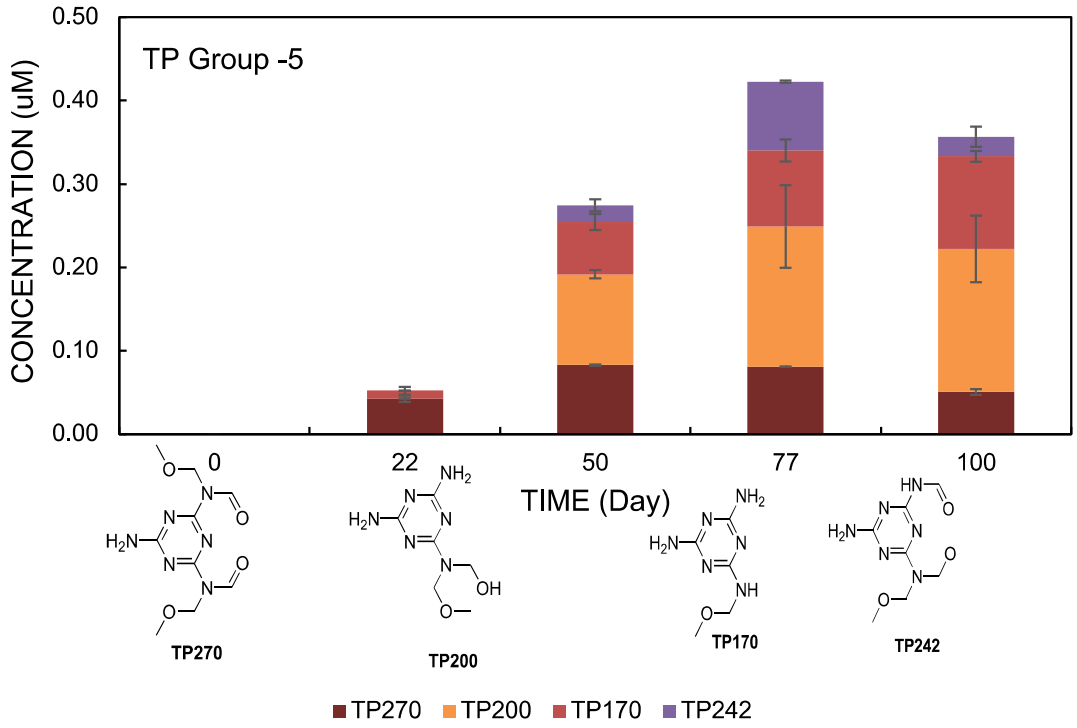


Figure 5.10. Concentration of Group-5 TPs (as HMMM) in N-free flasks inoculated with BIOMIG1 during 100 days of incubation at 25°C (mean ±one STDV, *n*=2).

Some high molecular weight structures that were present from the first day on, mainly TP376, TP362, TP346 and TP314, were previously reported as known impurities of HMMM (Alhelou et al., 2019) (Figure 5.6, Figure 5.8). Other TPs that were present from day-0 detected at much lower concentration, and it is possible that they were formed during the sample storage period prior to analysis. None of the TPs that were detected in day-0 samples had molecular weights higher than 300 g/mol, suggesting that mostly higher molecular weight TPs tended to exist as impurities or appear during sample storage. Following melamine, most abundant TPs were in the family of 5MM- and 4MM-Mel derivatives. Most TPs are common in both biological treatments and abiotic controls; only TP242, TP200 and TP170 appear exclusively in biological treatments, which may be explained by their relatively smaller molecular weight. However, the sum of TP concentrations and their trends are different between them. Overall concentration of TPs excluding melamine is lower in biological treatments and this sum has an increasing-then-decreasing trend, while melamine continuously increases (Figure 5.11). Only some small molecular weight TPs, namely, TP170, TP200 and TP214, have increasing trends in biological treatments. In abiotic controls, total concentration of TPs increases until day-50 and remain stable until day-100.

Melamine also increases in the abiotic controls, however, its concentration by day-100 is nearly 10% of melamine concentration in biological treatments, as discussed in Section 5.3.1. It is evident that in the biological treatments, a myriad of TPs of all sizes form and most of them degrade into melamine, whereas in the abiotic controls, degradation is slower and mostly results in accumulation of higher molecular weight TPs. Overall mass balance is conserved within ±15% of day-0 sum of HMMM, melamine and all TPs, in both biological treatments and abiotic controls (Table 5.2). This conservation might suggest that almost all TPs that formed during the degradation process were detected and no significant mineralization of HMMM occurred. Based on the TP screening results described in this chapter, as well as Chapter 6 and Chapter 8, a degradation pathway is constructed for HMMM (Appendix A). It was also observed that some TPs had isomers that weren't reported in the literature. TP362 isomers were already established in the literature but in this work, isomers of TP332, TP316, TP314, TP300 and TP214 were detected for the first time. Example chromatograms of TP314 and TP300 are presented in Figure 5.12. These isomers were detected with the same parent-fragment pairs; however, their peaks were consistently separated from each other by 0.5 minutes. The isomers of the TPs are named with number prefixes, such as TP362-1 and TP362-2.

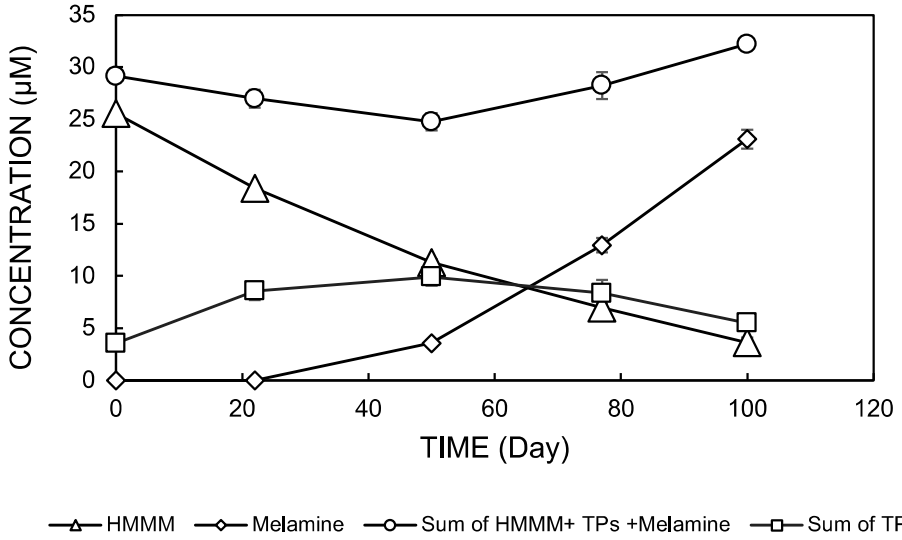


Figure 5.11. Concentrations of HMMM, melamine, all TPs (excluding melamine) and all analytes (HMMM, melamine, TPs) in N-free flasks inoculated with BIOMIG1 during the course of incubation at 25°C. Concentrations of TPs are reported as HMMM equivalents, melamine was quantified separately (mean ±one STDV, *n*=2).

Table 5.2. Concentrations of HMMM, melamine, all TPs (excluding melamine) and all analytes (HMMM, melamine, TPs) in N-free flasks inoculated with BIOMIG1 during the course of incubation at 25°C. Concentrations of TPs are reported as HMMM equivalents, melamine was quantified separately (mean ±one STDV, *n*=2). Mass balances as a percentage of sum of all analytes at day-0.

Treatment	Day	HMMM (µM)	Melamine (µM)	TPs (as HMMM µM)	HMMM lost (%)	HMMM+TPs+ Melamine (as HMMM µM)	Mass Balance
Test	0	25.59	0.00	3.55	0.00	29.13	100.00
	50	11.30	3.57	9.92	55.85	24.78	85.06
	100	3.63	23.11	5.49	85.83	32.23	110.62
Control	0	25.67	0.00	6.77	0.00	32.44	100.00
	50	25.19	0.62	11.25	1.88	37.05	114.22
	100	16.90	2.51	11.84	34.15	31.25	96.32

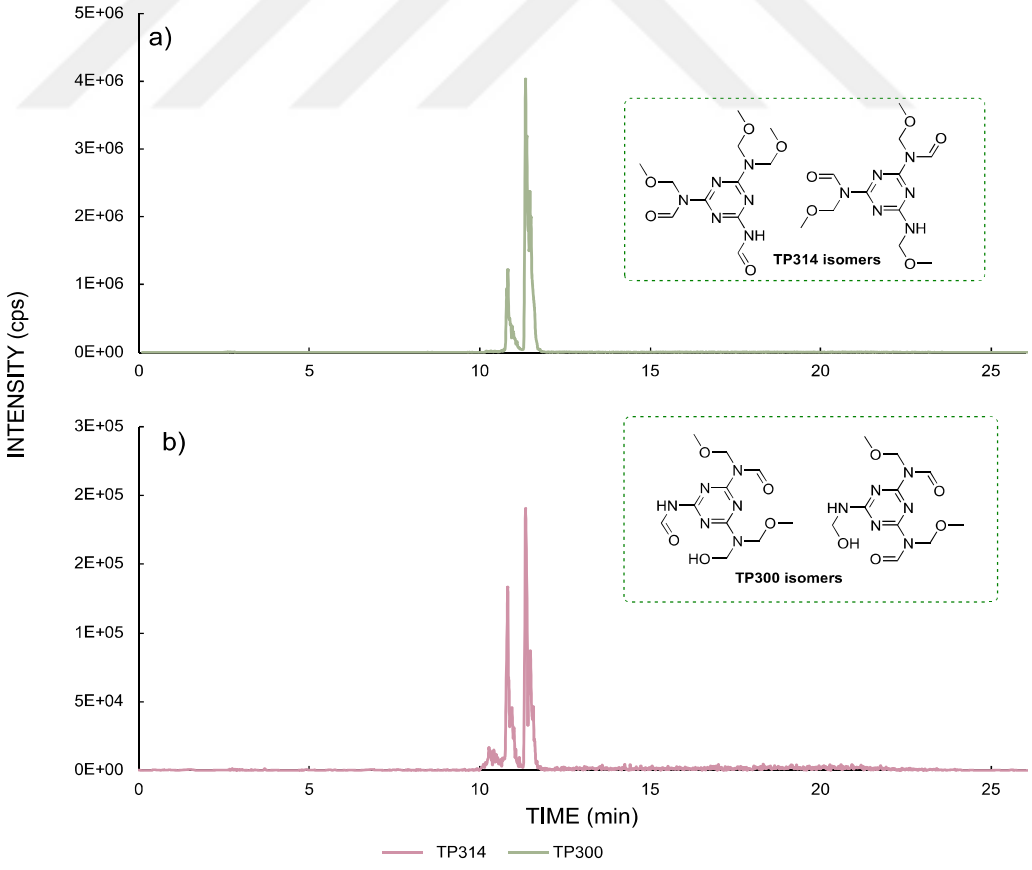


Figure 5.12. Chromatograms of a) TP314 and b) TP300, along with depictions of proposed isomeric structures.

5.3.3. Comments on Biotransformation Mechanism

HMMM, as a substituted s-triazine compound, essentially has three major functional groups: methyl- methoxy ether-, tertiary amine- and a symmetrical triazine. HMMM biotransformation to melamine progresses essentially through sequential oxidation and hydrolysis reactions of ether branches (Figure 5.13).

A possible challenge in biotransformation of HMMM might be attributed to the presence of methoxy methyl branches connected to each amine end of the triazine ring. These end groups are evidently ethers, which are known to be quite resistant towards degradation (McElroy and Hyman, 2019). In fact, these ethers on HMMM were designed to increase the shelf stability of the product, and to have better control over cross-linking reactions in which it is involved (Snyder and Vuk, 1992). Abiotic degradation of ether requires rather harsh conditions, since ethers are mostly unreactive towards many known reagents (McElroy and Hyman, 2019). It is this inertness that renders them suitable as solvents for organic reactions.

Their fate in the environment has been studied in the past decades and removal of ethers from the environment has been a challenge due to their chemical stability (McElroy and Hyman, 2019). There have been numerous studies in biodegradation of ethers, particularly various methyl ethers, and degradation all the way to mineralization is less frequently observed (Thornton et al., 2020). Usually, biodegradation leads to accumulation of transformation products. For instance, when a known gasoline additive methyl tertiary butyl ether (MTBE) was treated with *Pseudomonas mendocina* KR-1, in the presence of n-alkanes as carbon and energy source, MTBE was almost fully converted to tert-butyl alcohol (TBA) but did not become mineralized (Smith et al., 2003).

In most cases, ether biodegradation is found to occur as a co-metabolic process, rather than utilization of the ether compound as the sole carbon and energy source, and some transformation products persisted. Ether biotransformation is often attributed to non-specific oxygenases such as methane monooxygenase (McElroy and Hyman, 2019), propane monooxygenase (Steffan et al., 1997), ammonia monooxygenase (Hyman et al., 1994), and cytochrome P450 oxygenases (Fayolle et al., 2001).

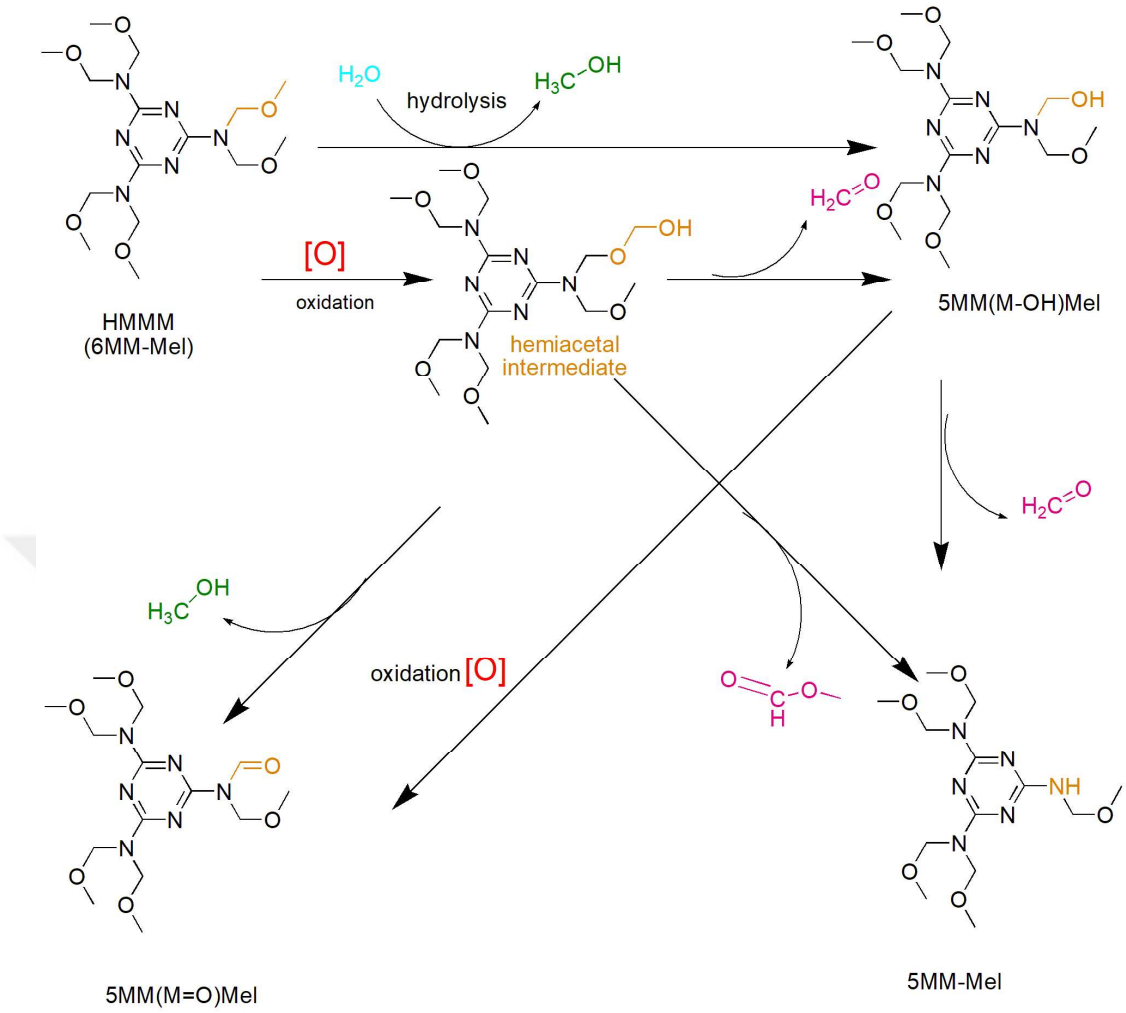


Figure 5.13. Depiction of fundamental reactions that take place during degradation of HMMM.

The transformation is believed to occur by a hemiacetal intermediate that is formed by oxidation of the terminal methyl of methyl ethers (Fayolle et al., 2001). This intermediate is later thought to decompose into formaldehyde and corresponding alcohol (very likely abiotically), since hemiacetal equilibrium often favors aldehyde state in water and in slightly acidic conditions, which may easily be the case in biological matrices. Another less likely route is that the hemiacetal could further be oxidized to an alkoxy-formate intermediate, which can further breakdown into formate and the corresponding alcohol. Evidence of both routes were reported in literature (Fayolle et al., 2001). Figure 5.13, which depicts the main reactions that likely take place during degradation, is constructed based on this literature. Ether functionality is present in various well studied persistent micropollutant groups. One such example is the group of pesticides known as chloroacetanilides. These pesticides do

not share the same triazine ring as HMMM, but they do share the amino-methoxy-alkyl feature bound to an aromatic cyclic structure with HMMM. They also have very infamous members which have been banned from use due to their hazards, such as alachlor which has been banned in EU (Tirmenstein and Mangipudy, 2014), therefore, their biotransformation has been studied more extensively than HMMM. In majority of these studies, biotransformation ended at various transformation products and full mineralization is not observed (Słaba et al., 2013). A critical step in degradation for these chemicals is cleavage of the bond between either nitrogen and methoxy-alkyl group or the oxygen and terminal alkyl group (Figure 5.14). This transformation is believed to proceed through N-dealkylation or O-demethylation, via either previously mentioned cytochrome P450, Rieske non-heme ion oxygenases (Chen, Wang, et al., 2014) or a carboxylesterase (Gao et al., 2015).

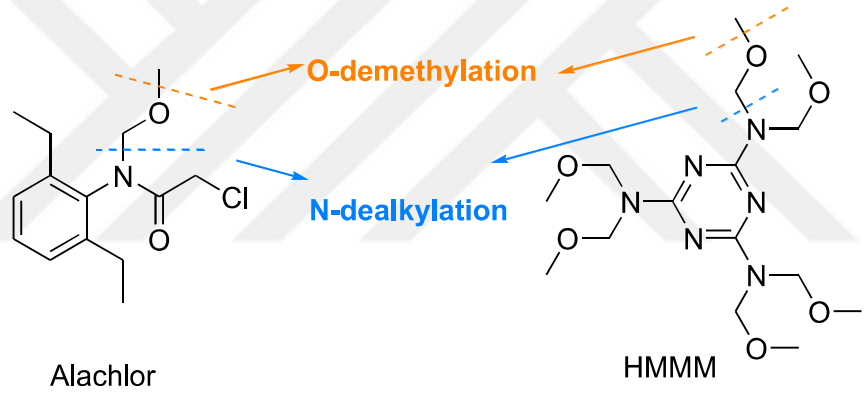


Figure 5.14. Depiction of common functional groups shared by HMMM and alachlor, and designation of bonds that cleave during the initial steps of degradation.

Amino acid sequences of several enzymes catalyzing the degradation of ethers and chloroacetanilide herbicides are found to have a degree of similarity in the whole genome of *Pseudomonas sp.* BIOMIG1^{BAC} (Altinbag et al., 2020) as seen in Table 5.3, which may also be relevant to degradation of HMMM to melamine through removal of ether branches.

Another challenge in biotransformation of HMMM can be attributed to the triazine ring it contains (Figure 5.15). Numerous reports of organisms capable of degrading triazine compounds have been published in the literature, however, a significantly smaller portion of these reports indicate complete removal (Wackett, M. Sadowsky, B. Martinez, 2002). Even degradation of melamine, which is the simplest triazine, results in accumulation of a

transformation product called cyanuric acid in many organisms (Wackett, M. Sadowsky, B. Martinez, 2002). Triazine degradation involves genes *TriA, TrzB, TrzC and TrzD* coding for various deaminases and amidohydrolases (Wackett, M. Sadowsky, B. Martinez, 2002).

Table 5.3. Literature examples of the enzymes that can degrade relevant ether groups and their amino acid sequence similarity match within the genome of *Pseudomonas sp.* BIOMIG1^{BAC}.

Organism	**Substrate**	**Enzyme**	**Protein Access Number**	**Query Cover**	**E value**	**Blast Type**
Pseudomonas aeruginosa (Smits et al., 2003)	n-alkanes	alkane-1 monooxygenase	NP_251264.1	86%	3E-75	tblastn
Rhodococcus ruber (Chauvaux et al., 2001)	Ethyl t-butyl ether	Cythochrome p-450 (ethB)	AAL25730.1	87%	2E-21	tblastn
Sphingomonad wittichii (Chen, Wang, et al., 2014)	Chloroacetanilide herbicides	Rieske non-heme iron oxygenase	AIA08943	48%	8E-16	tblastn

Based on the whole genome of *Pseudomonas sp.* BIOMIG1^{BAC} (Altinbag et al., 2020) it is evident that the species lacked some of the melamine degrading genes. For instance, the amino acid sequence coded by *TriA* gene which belongs to melamine deaminase was found in the genome of *Pseudomonas sp.* BIOMIG1^{BAC} (query cover: 91%, E value: 7E-36, tblastn), however *TrzD* gene encoding for cyanuric acid amidohydrolase was not present. In the absence of one or more enzymes within the cascade, it is likely that biotransformation of melamine would be hindered.

This was confirmed in a previous work in our research group, where it was observed that *Pseudomonas sp.* BIOMIG1^{BAC} could not degrade melamine alone (Karakaya, 2019). Therefore, mineralization of HMMM was not expected but degradation down to melamine was an expected outcome.

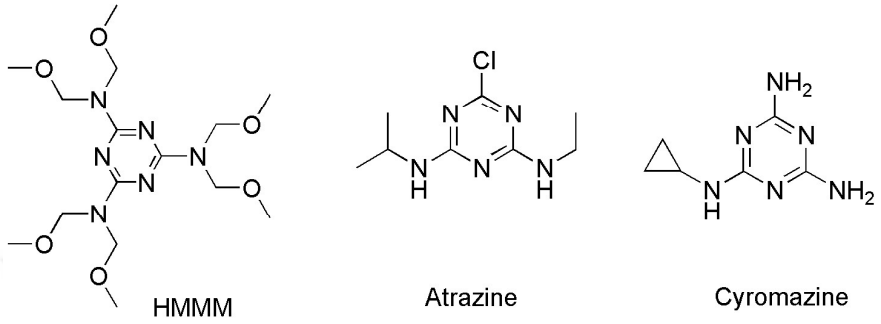


Figure 5.15. Molecular structures of HMMM and two s-triazine herbicides.

5.3.3. Summary

As evident from the experimental results, *Pseudomonas sp.* BIOMIG1^{BAC} did not mineralize HMMM in any of the tested conditions. HMMM degradation into melamine occurred considerably (in stochiometric ratio) only in N-free biological treatment conditions, however, even this spanned a long duration of 100 days. In both biological treatments and abiotic controls, many TPs have been detected until 100th day, suggesting that both HMMM and its TPs are resistant to biotic and abiotic degradation. Even though in the N-free biological treatments where 86% of HMMM is degraded, melamine is seen to accumulate, which is another hazardous micropollutant. Although complete removal is not achieved, this is the first study in the literature to illustrate nearly complete biotransformation of HMMM into melamine using a single strain of bacterium.

6. BIOTRANSFORMATION OF HMMM BY ACTIVATED SLUDGE

6.1. Introduction

Activated sludge has been a widely employed biological wastewater treatment process for decades (Haandel and Lubbe, 2012). It has been used in treatment of both domestic and industrial wastewater routinely. Since it harbors a diverse microbial community, it has also been a reliable source for interesting xenobiotic degrading species. As frequently referenced in this thesis, Alhelou et al. had used a sample of activated sludge to assess biotransformation of HMMM and had succeeded (Alhelou et al., 2019). There is a number of studies conducted with xenobiotic degrading species and microbial consortia isolated from activated sludge. For instance, several *Rhodococcus* strains capable of biodegrading various alkyl ethers, including diethyl ether, anisole and tetrahydrofuran (THF); were isolated from an activated sludge sample in Germany (Kim et al., 2008).

In another study, a strain of *Novosphingobium* genus was isolated from an industrial WWTP activated sludge, which could degrade several chloroacetanilide pesticides within 5 days (Chen, Zhang, et al., 2014). Numerous reports like these motivate research regarding utilization of activated sludge for degradation of xenobiotics. This is the case not only because activated sludge might harbor potential selective degraders, but also any xenobiotic biotransformation attempt started with the mixed community of an activated sludge sample would provide significant information about how these chemicals interact with real-life wastewater treatment applications.

6.2. Materials and Methods

6.2.1. Culture Preparation

Activated sludge used in these experiments was taken from İSKİ Paşaköy Advanced Biological Wastewater Treatment Plant (Paşaköy, İstanbul). A sample was collected from

the secondary clarifier sludge into a sterile 500 mL polypropylene bottles leaving as minimal headspace as possible.

Prior to inoculation, a 5 mL sludge sample was taken aseptically into sterile 50 mL polypropylene centrifuge tubes and centrifuged at 4500 rpm for 20 minutes for each flask (Figure 6.1). The pellet was rinsed twice with 5 mL sterile 0.85% NaCl solution, re-suspended in 5 mL sterile 0.85% NaCl and transferred in a flask under aseptic conditions.

6.2.2. Biotransformation Assays

Biotransformation of HMMM via activated sludge was tested under four different conditions which are summarized in Table 6.1. These test conditions are N-free (nitrogen-absent but carbon source present), C-free (nitrogen present but C source absent), full (both nitrogen and additional carbon present) and C/N-free (nitrogen and additional carbon source absent). For N-free and C/N-free treatments, stock solution of sterile M9 medium was prepared from the ingredients listed in Section 3.3.1, excluding NH_4Cl. was prepared and used. For C-free and full treatments, the original M9 medium recipe described in Section 3.3.1. was followed. In preparation of N-free and full treatments, sterile 2% glucose, 2% sodium acetate and 2% sodium succinate solutions (w/v, see Section 3.3.4.) were added aseptically into the sterile media to obtain a 2 g/L initial concentration of each carbon source in the flasks. Filter-sterilized 1 g/L HMMM stock solution was added aseptically to each flask at a final concentration of 10 mg/L (25.6 μM).

The total volume of each treatment medium was 40 mL, which includes the stock solutions of M9 or N-free M9 media, carbon sources, melamine and inoculum (Table 6.1). Abiotic controls were non-inoculated C/N-free and full treatment media that contained 10 mg/L HMMM. All selective media were prepared in 100 mL screw capped Erlenmeyer flasks, with caps left loose in biological treatments to allow air entrance. All biological treatment and control flasks were in duplicate. All biological treatments were inoculated with biomass re-suspended in 5 mL sterile 0.85% NaCl, which was prepared following the process described in Section 6.2.1. All flasks were placed on the orbital shaker operated at 100 rpm and cultivated at 25˚C.

Table 6.1. Contents of the media prepared for the HMMM biotransformation experiments with activated sludge.

	N-free Medium	C-free Medium	Full Medium	C/N-free Medium
Inoculum (mL)	5	5	5	5
Glucose (2%) (mL)	4	-	4	-
Na-Acetate (2%) (mL)	4	-	4	-
Na-Succinate (2%) (mL)	4	-	4	-
HMMM (1g/L) (mL)	0.4	0.4	0.4	0.4
N-free M9 Stock (mL)	22.6	-	-	34.6
M9 Stock (mL)	-	34.6	22.6	-
Total Volume (mL)	40	40	40	40

6.2.3. Sampling, Sample Preparation and Analysis

For screening HMMM and its TPs, samples of 0.75 mL volume were collected aseptically from each flask and mixed with 0.75 mL MS grade methanol in 2 mL microcentrifuge tubes. The solution was vortex-mixed for 30 seconds and centrifuged at 10000 rpm for 5 minutes. The supernatants were filtered through 0.22 µm hydrophilic PTFE filters into 2 mL amber chromatography vials. These samples were screened for HMMM via HPLC, following the procedure described in Section 3.6.

Prior to analysis of TPs, 100 µL of the filtered samples were combined with 100 µL IS and 800 µL 1:1 MS grade methanol: MS grade water solution, yielding 20-fold diluted samples spiked with 100 µg/L IS. These samples were analyzed based on the procedure explained in Section 3.5.

6.2.4. Activated Sludge Dry Weight

Dry weight of the activated sludge sample was determined based on the Standard Methods Total Solids Protocol (American public health association et al., 2012). Aluminum weighing dishes containing cut-out 0.45 µm polystyrene filter papers were ignited in the muffle furnace (Daihan Scientific, South Korea) for 1 hour at 550°C, they were later cooled down in the desiccator until use. Once they reach room temperature, their tare weight was

determined (aluminum weighing dish and filter paper together). 5 mL homogeneous aliquots of activated sludge suspensions were poured onto the filter papers while vacuum filtration was applied. Filters were placed back onto the weighing dishes and were dried in the oven for 2 hours at 105°C. After drying, samples were cooled down in the desiccator until they reach ambient temperature. The combined weight of the weighing dish, filter paper and dried activated sludge were measured. These treatments were made in four replicates. The resulting dry weight was found to be 4.90 ± 0.00 g/L.

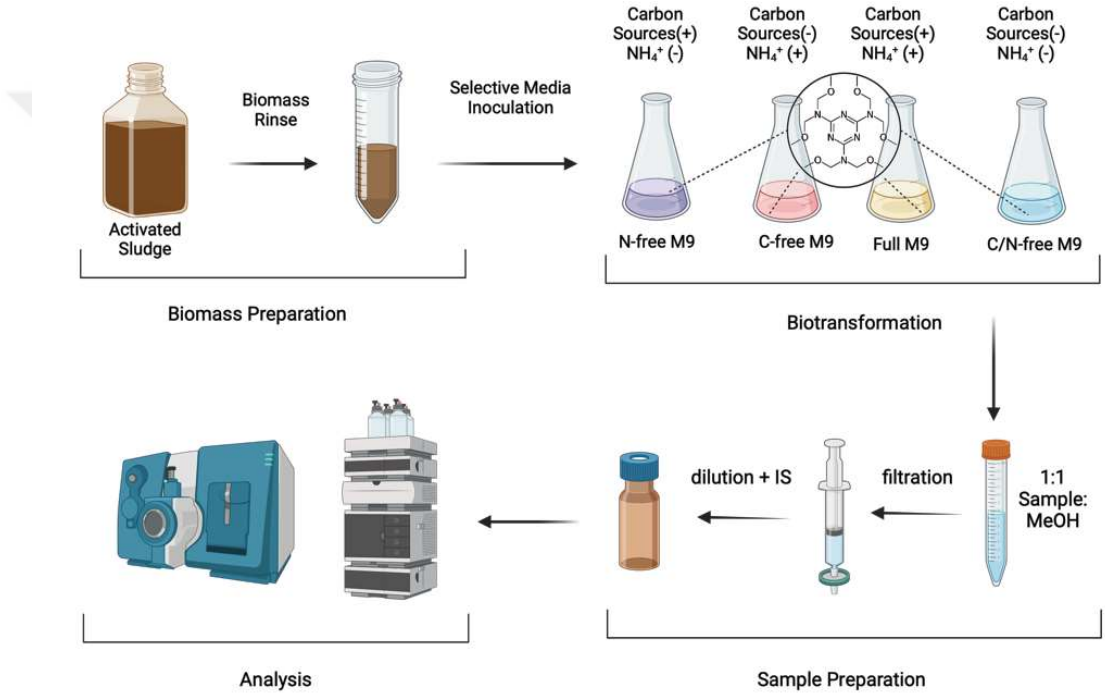


Figure 6.1. Illustration of the experimental workflow followed throughout the studies described in Section 6.

6.3. Results and Discussion

6.3.1. Biotransformation of HMMM by Activated Sludge

The incubation lasted for 55 days for C-free flasks, while it was discontinued for the remaining selective media after 43 days, since no significant change in HMMM concentration was observed (Figure 6.2). Among the four treatment conditions tested, a significant HMMM removal was only observed in C-free biological treatment. HMMM concentration in C-free treatments decreased from 24.4 ± 0.98 µM to 3.16 ± 1.48 µM by

day-55, corresponding to 87.0% loss of initial concentration, as opposed to 20.0% loss of HMMM in abiotic controls within the same duration (Figure 6.3). This is in accordance with the only study on biodegradation of HMMM by activated sludge in the literature currently, where 77.4% of HMMM was degraded in 29 days (Alhelou et al., 2019). The significantly higher removal of HMMM in the activated sludge inoculated flasks in C-free medium compared to other test media and abiotic controls indicate that degradation occurs most likely through biotransformation (Figure 6.2). It is interesting to note that among four conditions tested, only C-free conditions promoted biotransformation of HMMM. A possible explanation could be that, when carbon sources are present (in full and N-free media), organisms prefer them over HMMM and no other organisms that can degrade it by metabolic or co-metabolic processes can selectively grow, since all organisms can consume simple sugars and thrive. On the other hand, in C/N-free conditions, absence of nitrogen possibly hinders metabolic activities that directly or indirectly result in HMMM degradation; therefore, no biotransformation occurs. As a result, the conditions that facilitate HMMM biotransformation by activated sludge seem to be met only in the C-free (carbon deficient, nitrogen provided) medium.

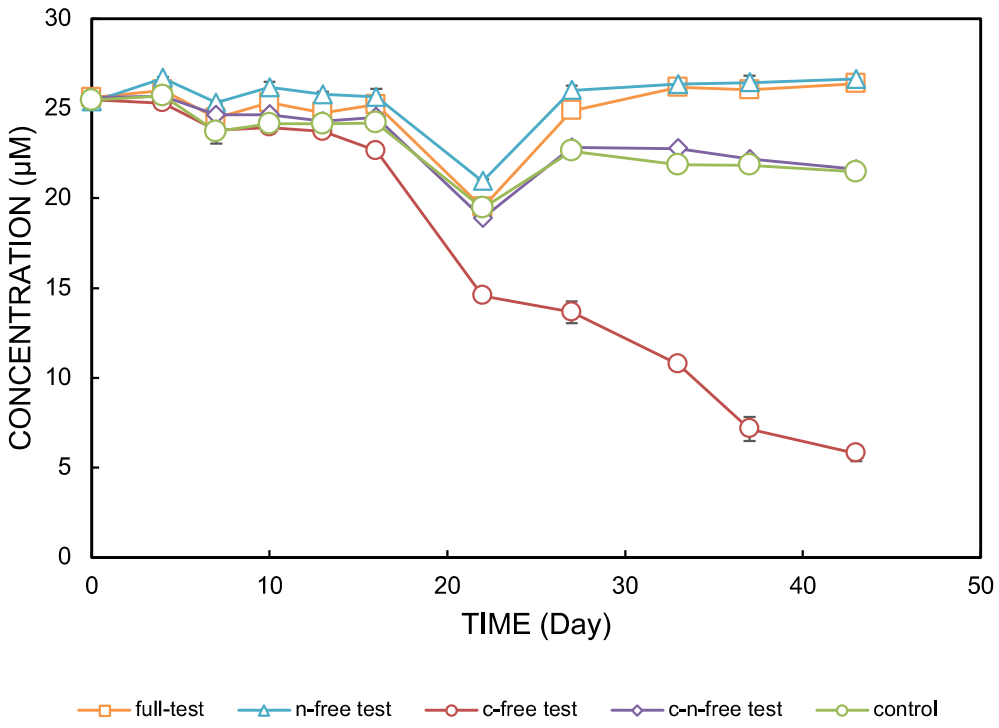


Figure 6.2. Concentration of HMMM in selective media inoculated by activated sludge during 43 days of incubation at 25°C (mean ±one STDV, *n*=2).

The faster degradation of HMMM with activated sludge compared to *Pseudomonas sp.* BIOMIG1^{BAC} might be attributed to the richer microorganism community present in an activated sludge sample as opposed to a single strain. However, biotransformation still takes much longer time compared to readily biodegradable xenobiotics in the literature. For instance diethyl phthalate was mineralized within 3 days by an activated sludge treatment (Chen, Zhang, et al., 2014). It is possible to make the same commentary on the current results of activated sludge process that was made for *Pseudomonas sp.* BIOMIG1^{BAC}: biological activity certainly plays a role in degradation of HMMM by activated sludge, but this is most likely governed by co-metabolic processes, rather than growth promoting ones. Indeed, slow and incomplete degradation is often encountered in the literature of biotransformation of persistent xenobiotics by activated sludge or native microcosms such as soil or river water (Chen, Zhang, et al., 2014). This is once again a reminder that HMMM is a recalcitrant pollutant.

6.3.2. Transformation Products of HMMM

The details about TP screening method development and semi-quantification process were explained in Section 3.5 and Section 5.3.2. TP screening was performed on duplicate samples from 5 time points (days 0, 22, 33, 43 and 55) for C-free biological treatments and from 3 time points (days 0, 33 and 55) for abiotic controls. A total of 18 TPs out of 27 were detected, excluding HMMM and melamine. TPs were separated into four column stack graphs for visualization (Figure 6.4, Figure 6.5, Figure 6.6 and Figure 6.7). The groups were selected arbitrarily, for the purpose of clearer visualization only.

Several outcomes of TP analysis results differ from the experiments with *Pseudomonas sp.* BIOMIG1^{BAC} described in Chapter 5 and studies of Alhelou et al. (Alhelou et al., 2019). One such result is that melamine did not seem to emerge as a dead-end transformation product as a result of biodegradation with activated sludge. In fact, its concentration by day-55 was even less than several other TPs at that day (Figure 6.3, Table 6.2). Its maximum concentration was on day-55 at 0.15 ± 0.03 µM (Table 6.2). This suggests that an effective conversion to melamine did not occur as it did with *Pseudomonas sp.* BIOMIG1^{BAC}. Another interesting finding was that although mass balance of abiotic controls was conserved (100% is based on sum of HMMM, melamine and all TPs at day-0),

it is decreased to 48% in C-free biological treatments (Table 6.2). This result deviates from the findings of Alhelou et al., where they observed preservation of mass balance throughout the experiment (Alhelou et al., 2019).

This can be interpreted in several ways. First possible explanation is that HMMM degrades into many TPs that remained under limit of detection within the time frame of the experiment. This is a likely case since most of the lower molecular weight (<300 g/mol) TPs appear at lower concentrations than their final values in the treatments with BIOMIG1^{BAC}. Another explanation of mass balance loss may be the transformation of HMMM into TPs that were not in the targeted method employed. This a possibility since the target TP list is derived from the literature of three untargeted screening studies and current experimental conditions are different from those studies. However, the preservation of mass balance in the experiments with *Pseudomonas sp.* BIOMIG1^{BAC} renders this possibility rather unlikely, given the fact that it was also a novel experiment, and all possible TPs were detected with mass balance conservation.

Table 6.2. Concentrations of HMMM, melamine, all TPs (excluding melamine) and all analytes (HMMM, melamine, TPs) in flasks HMMM as the sole C source inoculated by activated sludge during 55 days of incubation at 25°C. Concentrations of TPs are reported as HMMM equivalents, melamine was quantified separately (mean ±one STDV, *n*=2). Mass balances as a percentage of sum of all analytes at day-0.

Treatment	Day	HMMM (µM)	Melamine (µM)	TPs (as HMMM µM)	HMMM lost (%)	HMMM+TPs+Melamine (as HMMM µM)	Mass Balance
Test	0	24.35	0.00	1.12	0.00	25.48	100.00
	33	12.32	0.03	8.54	49.41	20.88	81.98
	55	3.16	0.15	8.91	87.03	12.22	47.98
Control	0	25.35	0.00	1.14	0.00	26.49	100.00
	33	23.68	0.00	3.97	6.60	27.65	104.39
	55	20.28	0.00	5.04	20.01	25.32	95.58

A final interpretation of mass balance loss may be mineralization of HMMM, however, given the fact that melamine did not form to considerable extents, this seems like

the least likely case. It is conceivable that melamine degraders could be present in an activated sludge that might have consumed melamine as it formed, hence keeping its concentration low throughout the experiment. Similarly, it is previously reported in the work by Alhelou et al that HMMM degradation by activated sludge did not yield considerable amounts of melamine (Alhelou et al., 2019). Possibility of adsorption to biomass was not considered since HMMM removal was not observed in any other conditions (full, N-free, C/N-free) activated sludge treatment was employed. In future work, the reason for mass balance loss can be assessed by TOC analysis, which can also provide information about the extent of mineralization, if it took place.

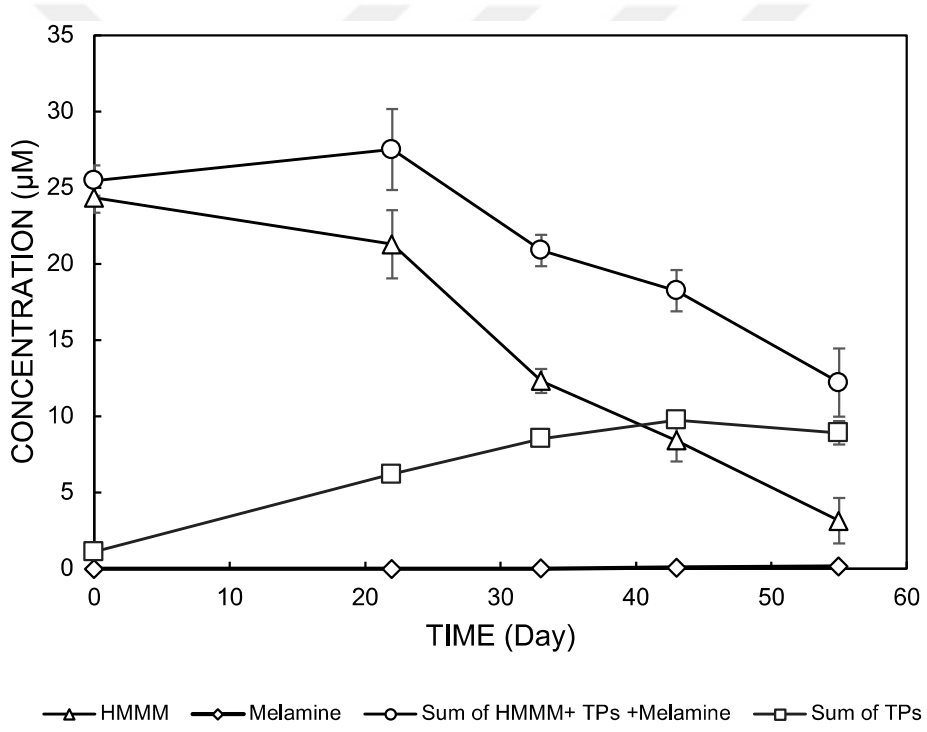


Figure 6.3. Concentrations of HMMM, melamine, all TPs (excluding melamine) and all analytes (HMMM, melamine, TPs) in flasks with HMMM as the sole C source inoculated by activated sludge during 55 days of incubation at 25°C. Concentrations of TPs are reported as HMMM equivalents, melamine was quantified separately (mean ±one STDV, *n*=2).

There are several differences between the TP profiles of single strain bacterial treatment and activated sludge treatment. As mentioned before, low molecular weight TPs generally exhibited lower concentrations in activated sludge treatments. For instance, TP214 concentration on 55th day of activated sludge treatment in C-free medium was 0.27 $\pm$ 0.07

μM (Figure 6.7), whereas its concentration of 100th day of *Pseudomonas sp.* BIOMIG1^{BAC} treatment in N-free medium was 0.61 ± 0.07 μM (Figure 5.11). Likewise, while TP200 was not observed at all during the activated sludge treatment, it had reached 0.17 ± 0.04 μM in the bacterial treatment (Figure 5.12).

On the other hand, some TPs that were prominent in the activated sludge treatments were either observed at much smaller concentration, such as TP330 and TP332, or not observed at all in the bacterial treatments, such as TP374. These observations exhibit the difference in biotransformation mechanisms between the bacterial treatment and activated sludge treatment.

In activated sludge treatments, although individual trends of TPs vary, the total concentration of TPs excluding melamine has an increasing-then-constant (logarithmic trend). For instance, TP314, TP362 and TP376 reach maximum concentration around day-33 then decrease, TP346, TP330, TP302, TP258 and TP214 have an increasing trend that slows down by the end. It is possible that if monitored for a longer time, more TPs could have become detectable, and degradation could have proceeded to melamine and other lower molecular weight TPs.

TPs that were present from day-0 were once again the known impurities of HMMM (TP376, TP346 and TP314). Their total concentration at day-0 didn't exceed 4% of HMMM initial concentration. Some TPs were observed in the abiotic controls as well, but by day-55, the total concentration of TPs in abiotic controls was nearly half of that was observed in activated sludge treatments. Furthermore, overall mass balance was preserved in abiotic controls, indicating that concentration of TPs formed correspond to the amount of HMMM lost (20% in abiotic controls).

Melamine and several TPs were exclusively observed in biological treatments and not in abiotic controls, such as TP170, TP214, TP258, TP286, TP332, TP346 and TP374; and the rest were observed in lower concentrations in controls than in biological treatments. This may be a highlight of how biological activity increases the extent of HMMM degradation.

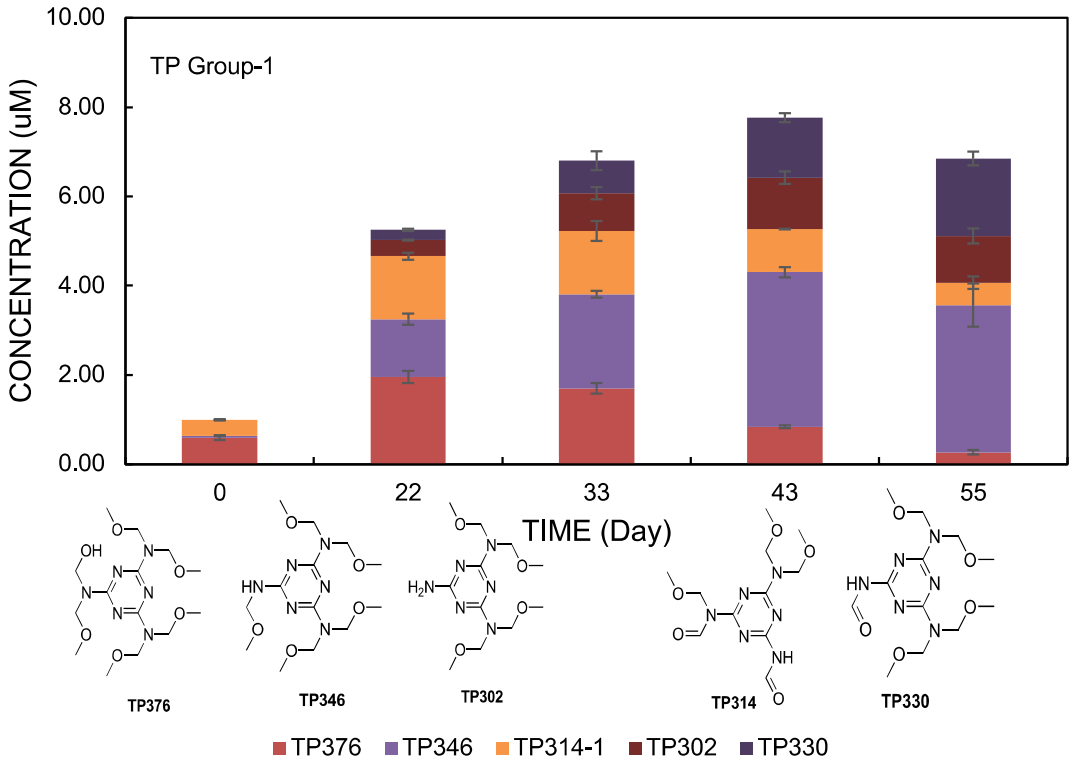


Figure 6.4. Concentration of Group-1 TPs in C-free flasks inoculated with activated sludge during 55 days of incubation at 25°C (mean ±one STDV, *n*=2).

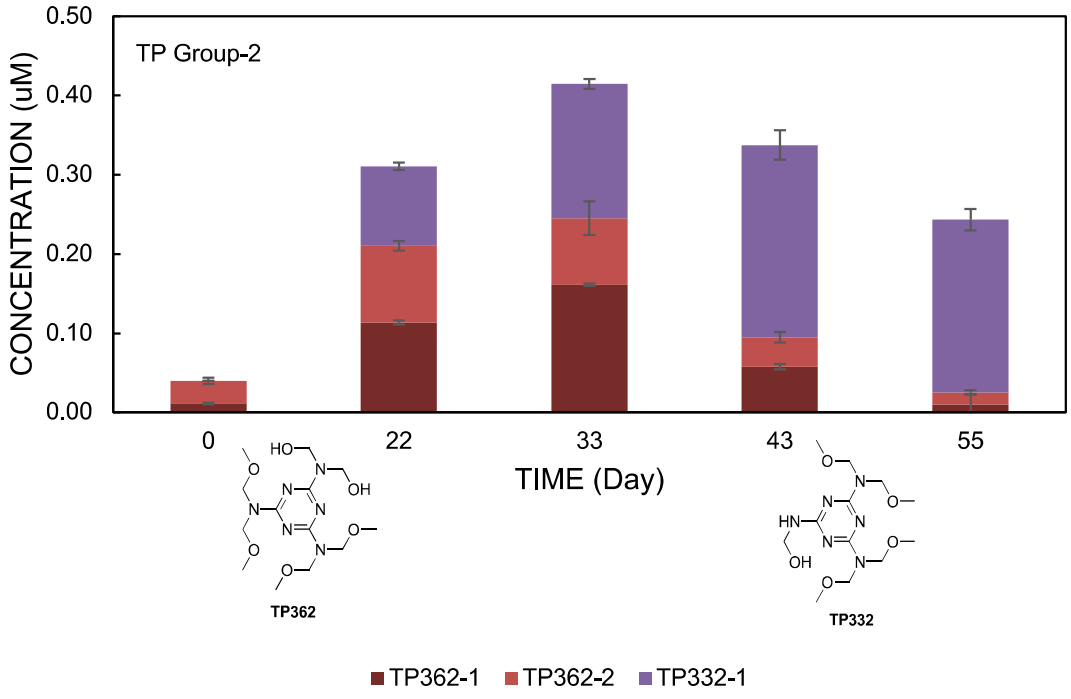


Figure 6.5. Concentration of Group-2 TPs in C-free flasks inoculated with activated sludge during 55 days of incubation at 25°C (mean ±one STDV, *n*=2).

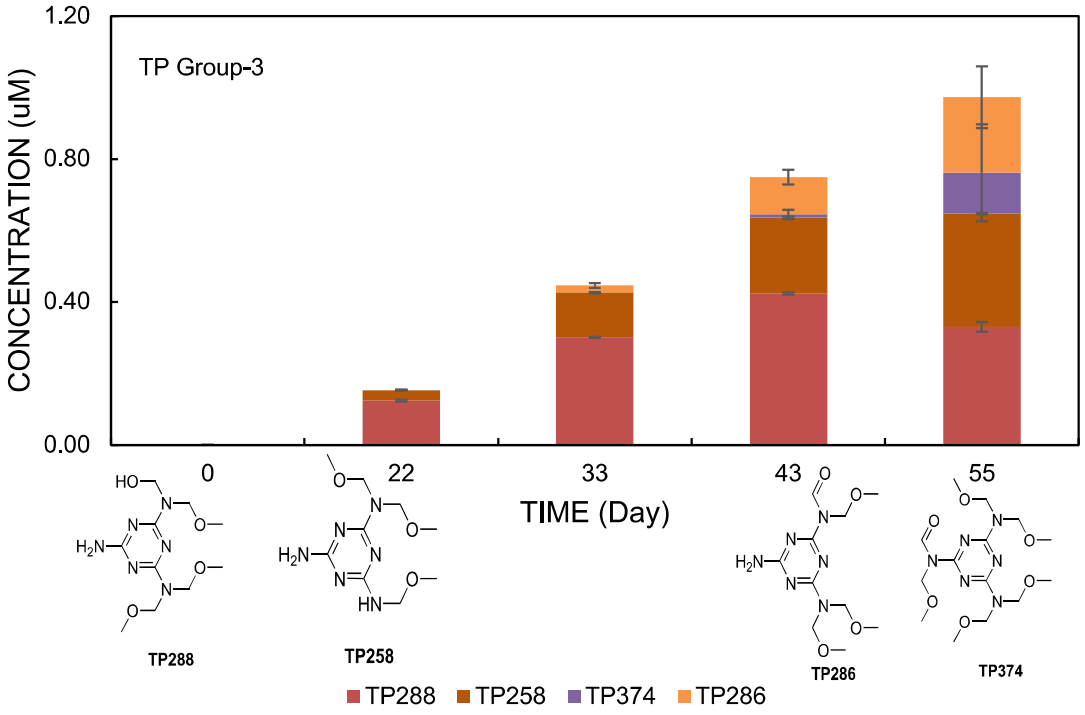


Figure 6.6. Concentration of Group-3 TPs in C-free flasks inoculated with activated sludge during 55 days of incubation at 25°C (mean ±one STDV, *n*=2).

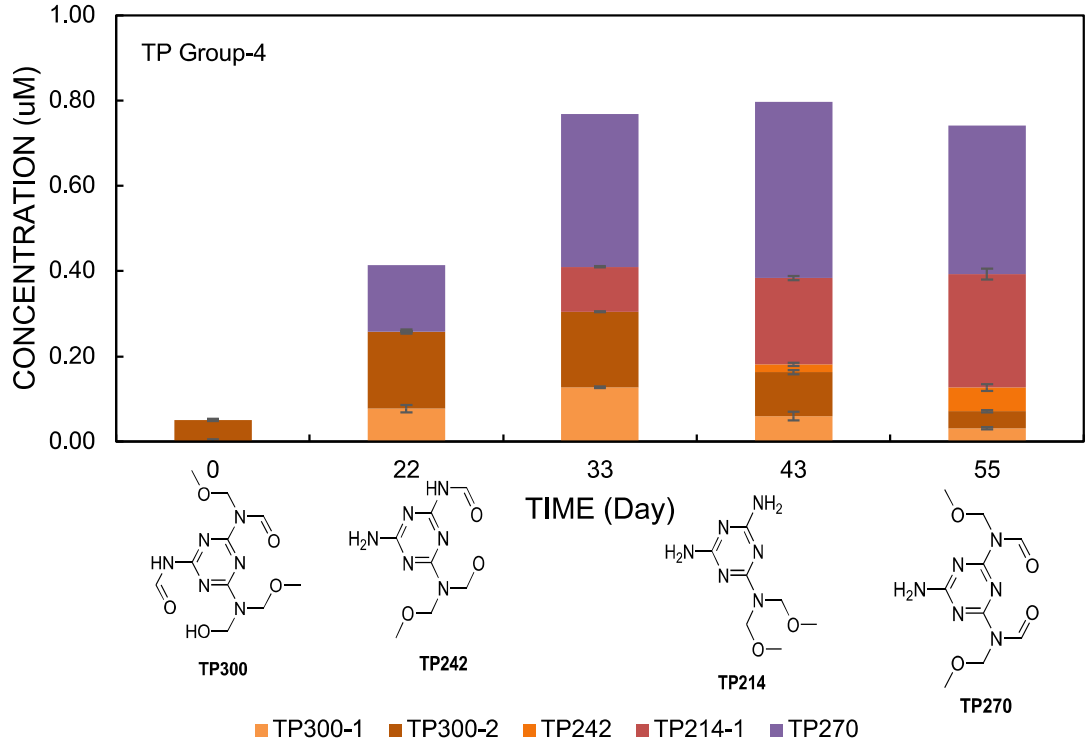


Figure 6.7. Concentration of Group-4 TPs in C-free flasks inoculated with activated sludge during 55 days of incubation at 25°C (mean ±one STDV, *n*=2).

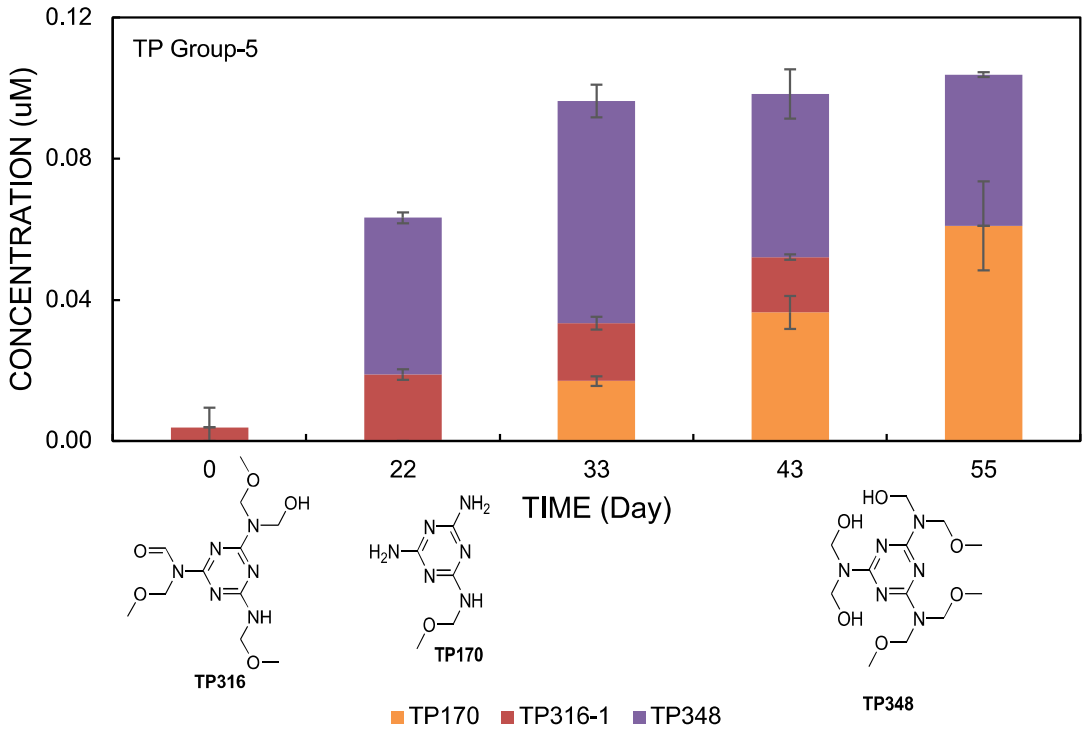


Figure 6.8. Concentration of Group-5 TPs in C-free flasks inoculated with activated sludge during 55 days of incubation at 25°C (mean ±one STDV, *n*=2).

6.3.3. Summary

As demonstrated by the results of these experiments, 87% of HMMM was removed by activated sludge when HMMM was present as the sole carbon source. The fact that this level of removal occurred only in C-free biological treatment conditions and not in any other biological treatments or abiotic controls hint that this is a biotransformation process and a selective one. Although a high removal was achieved in a shorter duration than the single strain biotransformation experiments conducted with *Pseudomonas sp.* BIOMIG1^{BAC} (55 days as opposed to 100), the degradation is found unlikely to result in either mineralization or a complete conversion to melamine. The most likely explanation for the loss of mass balance in biological treatments was that either concentration of some TPs that formed throughout the experiment fell below the limit of detection, or less likely, some TPs that formed as a result of degradation were not included in the targeted list of compounds. The slow biotransformation process indicates that degradation occurs possibly through co-metabolic processes. Just as demonstrated in the literature and the biotransformation with *Pseudomonas sp.* BIOMIG1^{BAC}, activated sludge biotransformation yielded a variety of

transformation products. Although complete removal is not achieved, this is the first study in literature to demonstrate that biotransformation of HMMM by activated sludge occurs selectively in a carbon deficient mineral medium, as opposed to carbon and nitrogen present, carbon-present nitrogen-absent, and carbon and nitrogen absent conditions. Further work may constitute of attempts to enrich and isolate species from activated sludge that are capable of HMMM biotransformation.

7. ENRICHMENT AND ISOLATION OF MELAMINE-DEGRADING SPECIES

7.1. Introduction

Melamine is a simple s-triazine compound that has a wide range of utilization in the industry. It is mass produced at a global volume of 500 mega tonnes per year (Bradley et al., 2011). It is used for various purposes, including manufacturing of plastic kitchen ware, adhesives and laminates for various applications in the form of melamine-urea or melamine-formaldehyde resins, cross-linkers in flame retardants, coating materials for textile and metal surfaces (such as beverage cans), and countless more examples can be listed (Bolden et al., 2017). In fact, melamine-formaldehyde resins are known to be used in seed coatings (Lütjens et al., 2023) and use of melamine and cyanuric acid as slow-releasing fertilizers have been tested in the past, due to their high N:C ratio (Wackett, M. Sadowsky, B. Martinez, 2002). Its structure is behind its versatility; since the triazine ring provides a stable core and the three amino branches are easily functionalizable, therefore, it has been used extensively in synthetic explorations. However, its use has not remained to be very innocent for long. Considering its high N:C ratio, it can be falsely identified as amino acids in routinely applied food analyses. Therefore, it was used for adulteration of various food products, including infant formula, pet foods and protein powders (Bolden et al., 2017). Between years of 2004 and 2010, there were several scandalous outbreaks of melamine related intoxications. Hundreds of children and house pets were harmed by renal failure or killed due to nephrotoxicity occurring as a result of melamine digestion (Bolden et al., 2017).

The mechanism by which melamine exerts toxicity in mammals lies in its catabolism. Once ingested, melamine is broken down to cyanuric acid, which has two tautomeric forms, the enol form being cyanuric acid and the keto form being isocyanuric acid. In the presence of non-metabolized melamine, a structure known as “melamine-cyanurate” gets formed (Figure 7.1) (Dalal and Goldfarb, 2011). This is not an ionic structure contrary to what the name implies. It is a complex formed by the strong hydrogen bonds between melamine and keto tautomer of cyanuric acid. Neither compound is highly toxic on its own, but when this insoluble complex is formed and it precipitates, it leads to generation of kidney stones and

consequentially renal failure (Takagi et al., 2012). Recently, studies harboring implications of neurological and reproductive damage in humans upon exposure to melamine have entered the literature (Bolden et al., 2017). Clearly, melamine and related derivatives are health hazards and the effects of exposure to them require further inquiry.

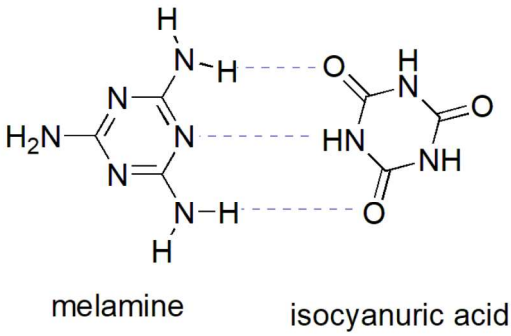


Figure 7.1. Structure of melamine-cyanurate complex.

There are several entrance routes for melamine and cyanuric acid into the environment and living systems. First and foremost, industrial wastewater is a major source. Since melamine is not included in many controlled substances lists (for instance, EPA Priority Pollutant List) regarding environmental discharge, there aren't strict regulations about its concentration in wastewater effluents released into environment. Hence wastewaters may contain melamine itself or its precursors that can break down into melamine, such as melamine-formaldehyde resins and even HMMM, which is essentially a melamine-formaldehyde compound. Regulations are only present for food ingredients, after the catastrophic events mentioned earlier (Zhu and Kannan, 2019). Therefore, melamine containing wastewater can be easily released into surface waters. Evidence suggests that conventional treatments with activated sludge do not effectively eliminate melamine and cyanuric acid due to their moderate biodegradability and low adsorption to activated sludge (Piai et al., 2021). Furthermore, it was found that melamine and its derivatives could cause toxicity towards certain species in activated sludge. In a recent study on regarding melamine induced toxicity and fate of the chemical, it was reported that even after long durations for sludge acclimation melamine removal did not exceed the range of 15-20% (S. Xu et al., 2013). There have been sightings of melamine in various surface waters, drinking water and groundwater, in concentrations ranging from 0.05-21 μg/L (Lütjens et al., 2023). Another pathway through which melamine ends up in the environment is through agricultural

activities. Some triazine herbicides such as cyromazine break down to melamine, which is an indirect input route. Cyromazine can break down to melamine when ingested by living beings, which can lead to nephrotoxicity as discussed before (Bolden et al., 2017). This ingestion is very likely through consumption of pesticide exposed crops. Another route is the direct use of melamine in the seed coatings and fertilizers, or melamine- contaminated irrigation water (Zhu and Kannan, 2019). Either way, melamine, its precursors, and derivatives can easily enter both the food chain and the environment.

When this extensive literature is taken into consideration, it is evident that studies regarding bioremediation and fate of melamine and its derivatives are relevant to environmental and public health, and this constitutes the motivation behind the work described in this chapter.

7.1.1. Melamine Biotransformation

Melamine biotransformation was studied extensively in the literature after infant formula and pet food adulteration misconducts over the past years (Zhu et al., 2019) (see Section 2.2), it is known to be poorly removed in conventional activated sludge processes (Piai et al., 2021), and it is shown to be a persistent transformation product of several triazine pesticides like cyromazine (Ge et al., 2014). Melamine is relevant to this study not only because it is a hazardous micropollutant itself, but also because it is a transformation product of HMMM.

Despite its poor removal in the environment and in activated sludge treatments, various degraders were isolated from range of sources in limited number of studies (Table 7.1). Aerobic biotransformation mechanism is therefore well established. Through consecutive removal of amine groups from melamine via deaminase enzymes, melamine is converted into ammeline, ammelide and finally cyanuric acid. In several melamine degradation reports, stochiometric amounts of cyanuric accumulation is observed since enzymes that enable its degradation are not abundant (Takagi et al., 2012). When these enzymes, particularly cyanuric acid amidohydrolase is present, cyanuric acid is mineralized via stepwise hydrolysis reactions into biuret, urea and finally CO_2 and ammonia (Wackett, M. Sadowsky, B. Martinez, 2002) (Figure 7.2).

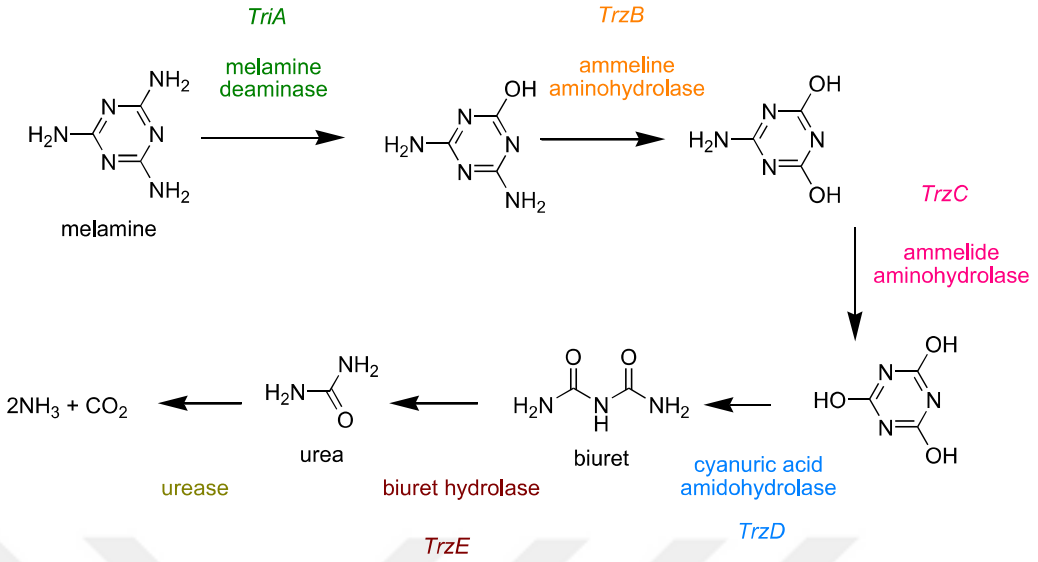


Figure 7.2. Biotransformation pathway of melamine.

Table 7.1. Biotransformation of melamine as observed in the literature.

Organism	Source	Degradation Conditions	Melamine	CYA Removal	References
Microbacterium esteramaticum	Soil	As sole N source	100% in 4 days	100% in 4 days	(Shiomi and Ako, 2012)
Nocardioides sp. ATD6	Farmland soil	As sole C and N source	100% in 10 days	Accumulated	(Takagi et al., 2012)
Acidovorax sp. relative- CY1	Industrial WWTP activated sludge	As sole C source	94% in 10 days	100% in 10 days	(Wang et al., 2014)
Arthrobacter sp. MCO, *Arthrobacter sp.* CSP	Soil	As sole C and N source	100% in 2 days	100% in 2 days	(Hatakeyama et al., 2015)

In most of these reports, the sources from which melamine degraders were isolated belonged to areas where direct and indirect melamine exposure occurred. For instance, soil samples were collected from agricultural lands where s-triazine herbicides were heavily employed, or activated sludge samples were collected from WWTPs of melamine manufacturing sites. In order to assess whether melamine degrading organisms could be

isolated from unexposed sources, in this study, samples taken from the biofilm reactors of the domestic WWTP of Bogazici University Saritepe Campus were used as inoculum for enrichment cultures.

7.1.2. Enrichment Culturing

Enrichment culturing is a commonly employed technique for the selection of organisms capable of degrading targeted chemicals or growing on specific conditions. The process is straightforward in essence (Figure 7.3). An initial inoculum composed of a mixed population of microorganisms are cultivated in a selective medium. The selection criteria depend on the desired outcome. For instance, the medium may contain a xenobiotic as the sole C and energy source, or as the sole N source, or both (Wackett and Douglas Hershberger, 2001).

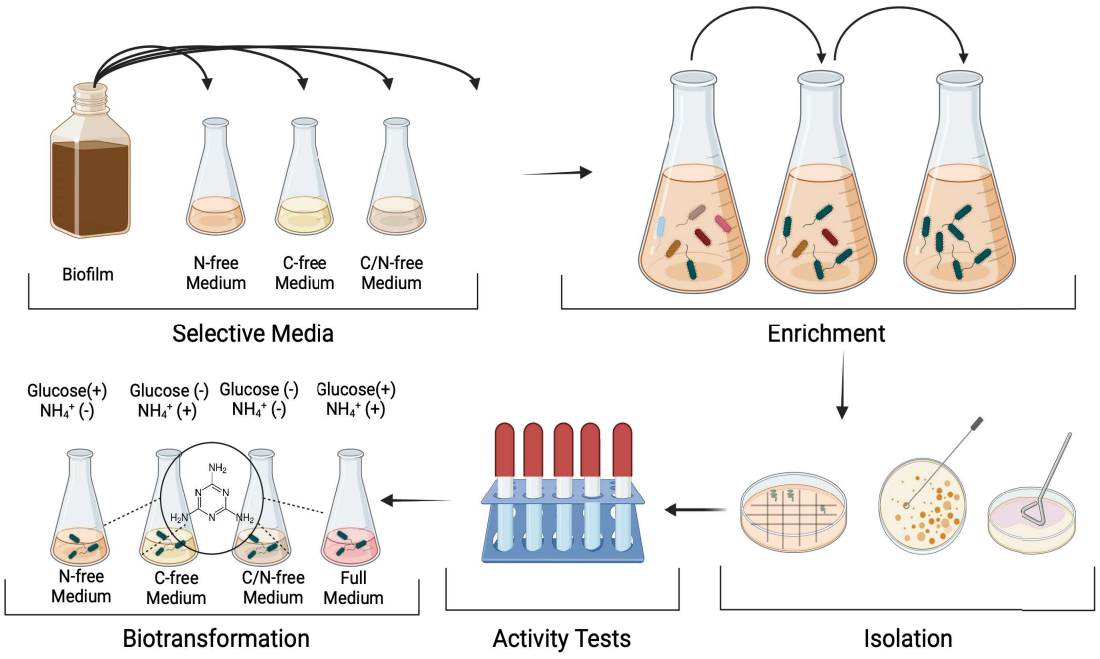


Figure 7.3. Illustration of enrichment culturing, isolation of the degrader and biotransformation experiments workflow.

The medium salinity, acidity, temperature and oxygenation can be altered to target different types of organisms, such as halophiles, acidophiles, thermophiles or anaerobes. Upon degradation of the target chemical in the selective conditions, a culture from the first

medium is used as an inoculum in a fresh medium and this process is continued for several cycles, while in each generation, the selective degraders are enriched, and the remaining populations are extinct (Pepper and Gerba, 2015). Then, the enriched cultures are isolated in the corresponding selective solid media and individual colonies are assessed for their activity. A selected isolate was used in the following biotransformation assays. Given the versatility of enrichment culturing technique, it was employed to selectively isolate melamine degraders from a mixed community in this study.

7.2. Materials and Methods

7.2.1. Enrichment and Biotransformation Media

The media used throughout enrichment and biotransformation assays were based on modifications on M63B1 medium. Four treatment conditions were tested similar to the experimental conditions explained in Section 6.2.2. N-free (nitrogen absent, carbon source present), C-free (nitrogen present, carbon source absent), full (both nitrogen and carbon source present) and C/N-free (both nitrogen and carbon source absent).

The full medium was not used during the enrichment process since it is not a selective medium towards melamine degraders. After the degrader was isolated, all four treatment types were applied, in order to assess the effect of presence/ absence of carbon and nitrogen sources in melamine biodegradation.

In preparation of N-free and C/N-free treatment media, M63B1 medium stock solution (see Section 3.3.1.) prepared without $(NH_4)_2SO_4$ was used. In preparation of C-free and full treatments, M63B1 medium stock solutions were prepared following the recipe in Section 3.3.1. without modifications. While preparing N-free and full treatments, the media were amended aseptically with appropriate amount of 5% glucose stock solution to set the final concentrations of carbon source in the media to 5 g/L. All treatment media and abiotic controls contained 10 mg/L melamine (79.4 μM). All treatment and control media were prepared in sterile 100 mL screw-capped Erlenmeyer flasks, the caps of which were kept loose in biological treatments to allow air entrance. The volume of enrichment cultures was 20 mL and that of biotransformation assays was 40 mL. These volumes included the M63B1/

N-free M63B1 medium, carbon source and melamine stock solutions, and inoculum, when present. Abiotic controls consisted of non-inoculated full and C/N-free media. All biological treatments and abiotic controls were in duplicate. All flasks were agitated on orbital shaker at 100 rpm and grown at 25°C. Table 7.2. summarizes contents of the media used in enrichment and biotransformation experiments.

Table 7.2. Contents of the media prepared for the enrichment culturing and biotransformation experiments involving isolated melamine degrader.

	N-free Medium	C-free Medium	Full Medium	C/N-free Medium
Inoculum (mL)	1	1	1	1
Glucose (5%) (mL)	4	-	4	-
Melamine (1g/L) (mL)	0.4	0.4	0.4	0.4
N-free M63B1 Stock (mL)	34.6	-	-	38.6
M63B1 Stock (mL)	-	38.6	35.6	-
Total Volume (mL)	40	40	40	40

7.2.2. Enrichment of Melamine Degrading Species

The initial inoculum for enrichment cultures was a biofilm sample obtained from the advanced biological wastewater treatment facility of Boğaziçi University Kilyos Sarıtepe Campus. The biofilm suspension was collected into a sterile 500 mL square-shaped polypropylene bottle with minimal headspace.

N-free, C-free and C/N-free media were prepared as described in Section 7.2.1. The inoculum size was 2 mL, which was added to 18 mL medium in each flask. Every day samples were taken from each flask, screened for melamine via LC-MS/MS (for sample preparation and analysis, see Section 7.2.5. and 3.4) and as soon as melamine was fully consumed, 2 mL sample from the flasks in which degradation occurred were used to inoculate 18 mL of fresh medium of composition, thus starting a new generation. This process was repeated until 10^{th} generation is reached. Throughout the enrichment culture experiments, melamine biodegradation was observed only in N-free treatment out of the three treatments conditions assessed.

7.2.3. Isolation of Melamine Degrading Species

In order to isolate the degrading species, agar plates of selective medium in which biodegradation activity was observed until 10^{th} generation were prepared according to the process described in Section 3.3.4.8. Using sterile 0.85% NaCl as diluent for the cell culture, 10^{-7}, 10^{-8} and 10^{-9} dilutions of 10^{th} generation flask were prepared and spread on these plates. After incubation at ambient conditions, single colonies from the spread plates were patched onto fresh plates. The patches that exhibited growth were tested for their biodegradation activity.

Activity tests were conducted in stoppered sterile glass tubes. Each tube contained 2 mL of the sterile selective media (in this case N-free M63B1 medium containing 5 g/L glucose and 10 mg/L melamine). Patches that exhibited growth were used to inoculate media in these tubes individually. After a period of three days samples were taken from the tubes and screened for melamine. Among the isolates that degraded melamine in the activity tests, one was selected to further assess the biotransformation characteristics of this strain.

7.2.4. Biotransformation Assay

Initially, a part of the selected degrader patch from the agar plate was taken via a sterile wooden stick and was used to inoculate 5 mL LB broth in a sterile 50 mL polypropylene centrifuge tube. After overnight growth on orbital shaker operated at 100 rpm, a sterile 100 mL screw-capped Erlenmeyer flask containing 40 mL LB broth was prepared. The broth was inoculated with 1 mL of the previously grown culture; thus, the seed was upscaled. This flask was agitated on the orbital shaker at 100 rpm and was cultivated for 36 hours. Upon reaching desired growth (approximately OD=2), the culture was transferred to a sterile 50 mL polypropylene centrifuge tube aseptically and centrifuged at 4500 rpm for 10 minutes. The supernatant was discarded, and the biomass was rinsed with 8 mL sterile 0.85% NaCl three times under aseptic conditions. After the final rinse, the biomass was suspended in 8 mL sterile 0.85% NaCl and each of the eight biological treatment flasks were inoculated with 1 mL of this dense culture.

For the biotransformation assay, N-free, C-free, full, and C/N-free media were prepared as explained in Section 7.2.1. From N-free and full treatment flasks, hourly samples were taken until 14 hours to monitor biodegradation of melamine. Follow-up samples were taken on 28th hour and 7th day to monitor remaining cyanuric acid. From C-free and C/N-free treatment flasks, daily samples were taken until 3rd day to monitor biodegradation of melamine. Follow-up samples were taken on 7th day to monitor remaining cyanuric acid.

7.2.5. Sampling, Sample Preparation and Analysis

For screening melamine and cyanuric acid, 0.75 mL samples were taken from the flasks aseptically and mixed with 0.75 mL MS grade methanol into 2 mL microcentrifuge tubes. The mixture was vortex mixed for 30 seconds, then centrifuged at 10000 rpm for 5 minutes. Supernatants were filtered through 0.22 µm hydrophilic PTFE filters into 2 mL amber chromatography vials. Prior to analysis, 100 µL of filtered samples were mixed with 100 µL 1 mg/L IS and 800 µL 1:1 MS grade methanol: MS grade water solution; thus, final sample composition included 20-fold diluted biotransformation sample and 100 µg/L IS. All samples were stored at 4˚C until analysis. Prepared samples were analyzed based on the procedure described in Section 3.4. For screening glucose in N-free and full treatments, 0.75 mL samples were taken from the flasks aseptically and combined with 0.75 mL 0.01 N H_2SO_4 in 2 mL microcentrifuge tubes. The mixture was agitated on vortex, centrifuged at 10000 rpm for 5 minutes and filtered through 0.22 µm hydrophilic PTFE filters into 2 mL amber chromatography vials. These were stored at 4˚C until analysis. Prepared samples were analyzed as explained in Section 3.7.

7.3. Results and Discussion

7.3.1. Enrichment and Isolation of Melamine Degrading Species

Among the tested conditions (N-free, C-free, C/N-free), melamine degradation was observed only in N-free media. All melamine was removed in less than 3 days in all generations up to the 10th. Concentrations of melamine on the 3rd day of activity tests are summarized in Table 7.3. The colony appearances were homogeneous for all patched colonies that yielded degradation. The colony “k” was selected for further study.

Table 7.3. Concentration of melamine in each flask on the 3rd day of the activity tests.

Colony ID	Melamine (mg/L)
CTRL	8.06
a	0.20
b	5.80
c	5.60
d	5.82
e	5.99
f	0.00
g	0.00
h	0.00
j	5.75
k	0.00
1	0.00
2	0.00
3	0.61
5	3.54
6	1.07
7	0.00
10	0.00
11	0.00
12	0.00
13	7.01

7.3.2. Biotransformation of Melamine by Isolated Degrader

As explained in Section 7.2.4, biotransformation assays were conducted in four conditions, N-free, full, C-free and C/N-free. It was found that in N-free and full media where glucose was present, melamine was completely removed within 30 hours (Figure 7.4). The complete removal occurred between 2 and 3 days in case of C-free and C/N-free media (Figure 7.5). The reason why these media were less frequently sampled was because melamine degradation was not observed in these conditions throughout enrichment culturing, therefore, a fast removal was not expected. Contrary to expectations, melamine was removed rapidly in all media, while no removal was observed in the abiotic controls.

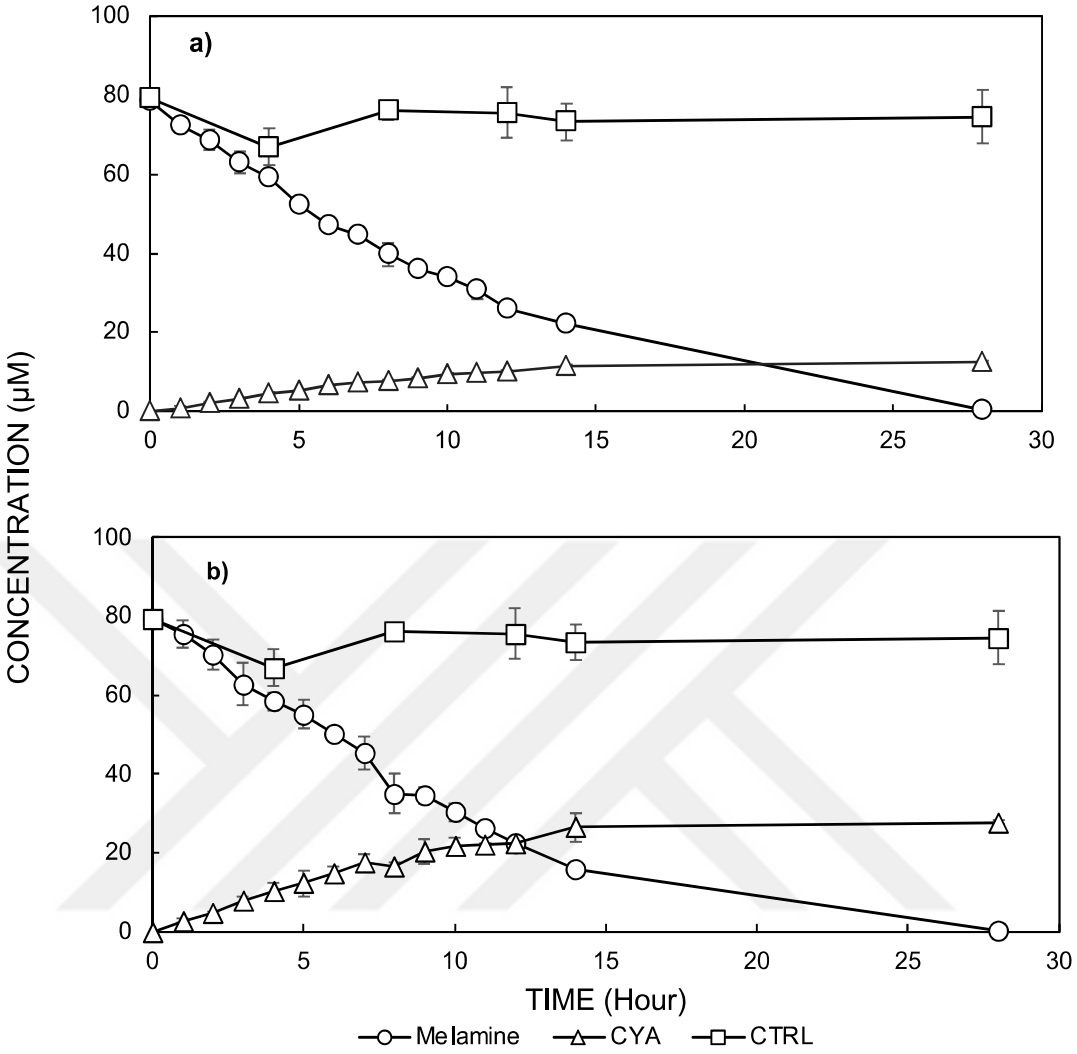


Figure 7.4. Concentrations of melamine and cyanuric acid in, flasks amended with a) glucose and nitrogen (full), and b) only glucose without nitrogen (N-free) inoculated with the isolated degrader during 28 hours of incubation at 25°C (mean ±one STDV, *n*=2).

As discussed earlier, cyanuric acid is a known transformation product of melamine and many other triazines, and it can accumulate as a dead-end metabolite since its degraders aren't prevalent (Wackett, M. Sadowsky, B. Martinez, 2002). In all tested conditions, cyanuric acid was detected throughout biotransformation of melamine (Figure 7.5). The concentration of formed cyanuric acid was always less than melamine loss, which can be explained either by biotransformation of melamine to other two known transformation products, namely, ammeline and ammelide, or mineralization of melamine to some degree. The fate of cyanuric acid was monitored by follow-up analyses (Figure 7.5).

It was found that only in the N-free medium complete removal of cyanuric acid was achieved. Remaining concentrations of cyanuric acid corresponded to 13.1%, 44.3% and 14.4% of initial melamine concentration in C-free, C/N-free and full media, respectively.

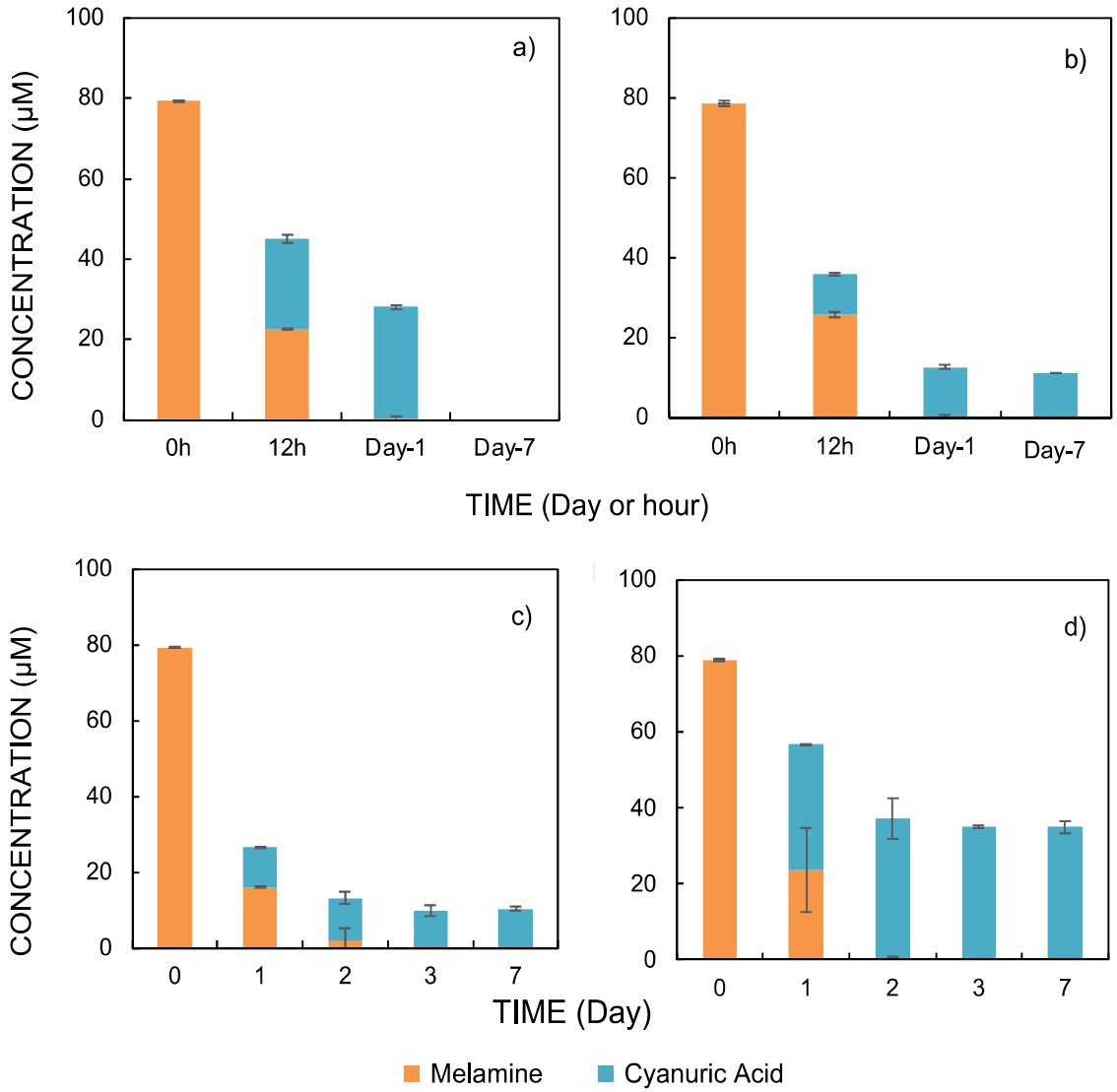


Figure 7.5. Concentrations of melamine and cyanuric acid in a) N-free, b) full, c) C-free and d) C/N-free selective media inoculated with the isolated degrader during 7 days of incubation at 25°C (mean ±one STDV, *n*=2).

The enhanced removal of cyanuric acid in N-free treatments suggests that nitrogen absence might have promoted its utilization as a nitrogen source, which is seen in various instances in the literature (Govantes et al., 2010). In recent studies, it was discovered that nitrogen presence in the medium hindered atrazine degradation by *Pseudomonas* sp. ADP,

however, when it was the sole N source in the medium, both degradation and cell growth was observed (García-González et al., 2003). This interpretation can be applicable to the findings of the current study and be supported by the fact that only N-free and full treatment conditions resulted in an increase in OD (Figure 7.6). In the full treatment, increase in growth was expected since both nitrogen and carbon are supplied in the medium. It is possible that growth in N-free medium could have been promoted by presence of both glucose as a carbon source and melamine as a nitrogen source. As evident by the slightly decreasing OD of C-free and C/N-free treatments where melamine degradation did not promote growth (Figure 7.6).

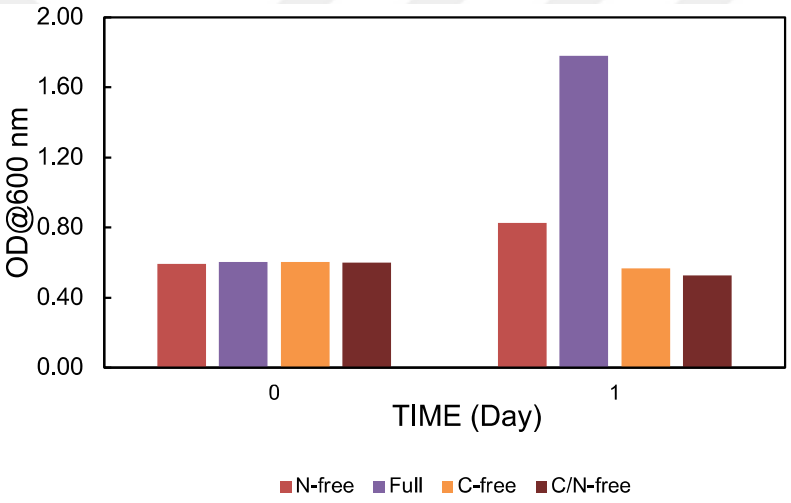


Figure 7.6. Optical density values of all biological treatments during biotransformation experiments with the isolated melamine degrader.

7.3.4. Summary

In this part of the study, a specie that can degrade melamine under four conditions (N-free, C-free, full, and C/N-free) was isolated via enrichment culturing technique. The cultures consisting of the isolate was able to biodegrade more than 90% of melamine within a day when glucose was provided (in N-free and full media), regardless of nitrogen presence. When melamine was the sole carbon source or sole carbon and nitrogen source in the medium, complete removal was still achieved in two days. Cyanuric acid was detected in all treatments; however, it was always less than stochiometric ratio. Only in N-free treatment complete removal of cyanuric acid was observed as well. This work contributes to the

existing literature regarding melamine biotransformation. Given the rapid action of the isolated species in various nitrogen and carbon deficient conditions, the results may be promising for real-life melamine and cyanuric acid bioremediation applications. Further work could focus on the regulation of melamine and cyanuric acid degradation mechanisms in this organism, and utilization of co-cultures of candidate HMMM degraders along with melamine degraders for complete removal of HMMM.

8. PHOTOCATALYTIC OXIDATION OF HMMM VIA UV/TiO_2

8.1. Introduction

In addition to biological treatment, there is a variety of well-established advanced oxidation treatment methods for removal of micropollutants. UV-TiO_2 photocatalysis is one of the various oxidation methods available. There are several aspects that render UV-TiO_2 photocatalysis an attractive advanced oxidation process, including the inexpensiveness, stability, well-documented photoactivity and availability of the photocatalyst TiO_2. While it can easily be synthesized, it can also be purchased for reasonable prices. The entire illumination and oxidation process does not require intricate equipment such as vacuum or ozone generators, nor does it require use of hazardous oxidants such as peroxides. The photocatalytic activity stems from the semi-conductor nature of TiO_2. When TiO_2 is exposed to photons with greater energy than its band gap (3.2 eV), electrons in its valence band, that is the highest occupied energy band, are excited to its conduction band, which refers to the lowest unoccupied energy band (Tuncel, 2014). This is achieved in UV range illumination typically at wavelengths less than 390 nm (Wong and Chu, 2003). With the generations of electron and hole charge carriers, a cascade of interesting redox reactions follows (Figure 8.1).

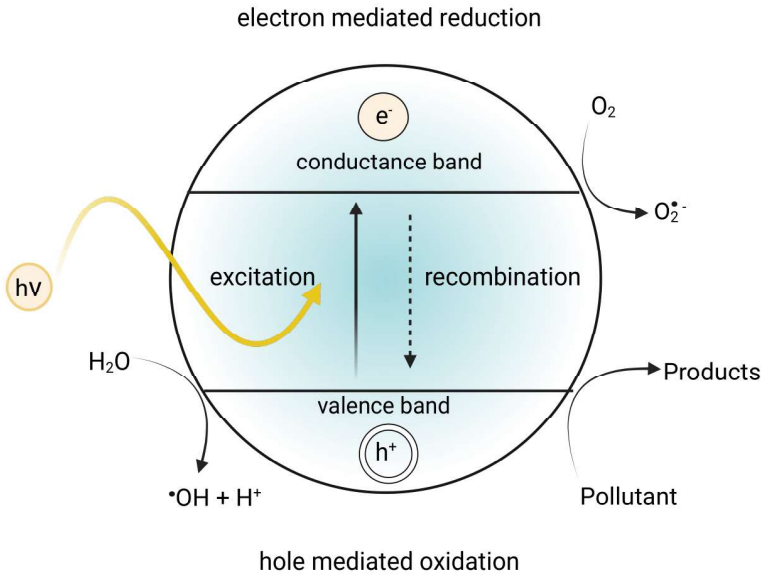


Figure 8.1. Illustration of TiO_2 photocatalysis mechanism.

Initially, the only reductants are the excited electrons, and the only oxidants are the generated positive holes. These can react with the target chemicals themselves, while they can also react with chemicals present in their vicinity, and other reactive intermediate species that can oxidize the target chemical. The matrix of such reactions is often water, where H_2O and O_2 molecules and OH^- and H_3O^+ ions that are in equilibrium with water are easily adsorbed on the surface of photocatalyst. The presence of oxidizable molecules like water also help prevent immediate recombination of the holes and electrons of the semiconductor, which would quench the photocatalytic activity (Ziylan Yavaş, 2017). A cascade of chemical reactions start when the ultraviolet light reaches TiO_2,

$$TiO_2 + h\nu\ (<390\ nm) \rightarrow e^- + h^+ \text{ (generation of electron-hole pairs)} \quad (8.1)$$

$$R + h^+ \rightarrow R^{+\bullet} \text{ (further degradation of target reactant, R)} \quad (8.2)$$

$$h^+ + H_2O \rightarrow OH^\bullet + H^+ \text{ (generation of hydroxyl radical)} \quad (8.3)$$

$$e^- + O_2 \rightarrow O_2^{\bullet-} \text{ (generation of superoxide radical)} \quad (8.4)$$

and resulting electrons and holes proceed to react with surrounding molecules, yielding reaction intermediates such as radicals. The generated superoxide and hydroxyl radicals are also highly reactive which enhance degradation of the target compound. The cascade of reactions described in Equation (8.1), (8.2), (8.3) and (8.4) stops when all the radicals and separate electrons and holes are paired eventually.

The efficiency of photocatalytic reaction depends on many factors, including the crystal form of TiO_2 used, the pH of the matrix, the amount of photocatalyst, the irradiation wavelength, the physicochemical properties of the target pollutant, etc. (Ziylan Yavaş, 2017) Over the years, UV-TiO_2 photocatalytic degradation of many micropollutants have been tested. Depending on the pollutant, a wide range of removal performances have been observed, from rapid 100% mineralization to slow incomplete removals.

Since there are no advanced oxidation studies employed on HMMM in the literature, a survey on chemicals sharing similar structures with HMMM would provide insight into its oxidative removal potential. For instance, in one study TiO_2 and H_2O_2 assisted solar light simulated photocatalytic degradation of several s-triazine pesticides was assessed and 100% disappearance within 2 hours was achieved for tested chemicals (Konstantinou et al., 2001). However, various transformation products were identified, suggesting complete mineralization was not achieved (Konstantinou et al., 2001). In another study, removal of

atrazine was assessed by a variety of oxidation processes including UV-TiO_2 photocatalysis, where 100% removal was achieved in 5 hours. Once again mineralization was not observed, and a range of transformation products formed (Bianchi et al., 2006).

The difficulty in complete mineralization of s-triazines is attributed to persistence of cyanuric acid, which is an inevitable transformation product (Zahraa et al., 2003), (Pelizzetti et al., 1992). Since cyanuric acid does not have oxidizable C-H bonds, its oxidation likely requires a high amount of activation energy. Considering the fact that in the literature higher transformation products of atrazine are reported to accumulate as a result of oxidation (for instance, de-ethyl isopropyl atrazine, DEIAT) (Bianchi et al., 2006), it is evident that those are persistent as well. In this chapter, the objective is to assess the performance of UV-TiO_2 photocatalysis on removal of HMMM and to identify the transformation products generated as a result of oxidation. The results are intended to provide a better comprehension of the reaction pathway and fate of the HMMM in advanced oxidation processes.

8.2. Materials and Methods

8.2.1. Chemicals and Experimental Setup

TiO_2 powder (Degussa P-25, Evonik) was used as the photocatalyst. All irradiation experiments were conducted in a Class IIA- C Series Biosafety Cabinet (Metisafe), using a germicidal UV-C lamp (Osram HNS 30W G13) which emits light at 254 nm, with 2.08 mW/cm^2 average irradiance (Corrêa et al., 2021). The reaction vessels were glass petri dishes in order to provide large surface area for effective light penetration. All petri dishes were placed on magnetic stirrers at a 50 cm distance to the UV lamp. All surfaces in the chamber were covered with aluminum foil to minimize UV light absorbance. The temperature of the cabinet was kept at ambient temperature (22-25°C) and did not elevate upon irradiation, since constant laminar flow was present in the biosafety cabinet.

For every condition tested, dark adsorption experiments were conducted in parallel. The dark adsorption experiments were conducted outside of the biosafety cabinet, using glass petri dishes covered with aluminum foil on magnetic stirrers. The HMMM initial concentration in all experiments was 10 mg/L. The volume of solution in all experiments

was 20 mL. The solvent was ultrapure water, and the pH was not adjusted except for the pH effect experiments. The non-adjusted pH of the solutions was in 7.5-8 range. For the experiments assessing the effect of pH on photocatalytic degradation, stock solutions of pure water the pH of which is adjusted to either 4 or 11 via dropwise addition of 1 N H_2SO_4 and 1 M NaOH were used. All conditions were tested at least in duplicate conditions.

The experiments conducted can be separated into four groups, based on the parameter tested: photocatalytic activity, synthetic wastewater, TiO_2 dose and pH. In experiments assessing the photocatalytic activity, three conditions were tested; UV-C treatment of HMMM without TiO_2 to test the extent of photodegradation alone, dark treatment of HMMM by TiO_2 to test the extent of adsorption of HMMM onto the photocatalyst and UV-C irradiated TiO_2 treatment on HMMM to test the extent of photocatalytic activity. Experiments conducted with synthetic wastewater tested the effect of ions and oxidizable chemicals present in wastewaters on photocatalytic degradation of HMMM, in comparison to the ultrapure water medium.

The ingredients of the synthetic wastewater that are presented in Table 8.1 and Table 8.2 were adopted from a literature example (Yaseen and Scholz, 2019). Additionally, effects of TiO_2 dose and pH were assessed. The experimental conditions that are used to examine the photocatalytic degradation of HMMM are summarized in the Table 8.3.

Table 8.1. Recipe used to prepare synthetic textile wastewater effluent.

Synthetic Wastewater Recipe	
Compounds	**Concentration (mg/L)**
C_6H_5COONa	107.1
CH_3COONa	204.9
NH_4NO_3	27.1
NaCl	7
$MgCl_2 \cdot 6H_2O$	3.4
$CaCl_2 \cdot 2H_2O$	4
K_2HPO_4	27.5
Trace Element Stock Solution	1 mL/L

Table 8.2. Trace metal stock solution recipe that is used in preparation of synthetic textile wastewater effluent.

Trace Element Stock Solution	
Compounds	**Concentration (mg/L)**
H_3BO_3	150
$FeSO_4.7H_2O$	3290
$ZnCl_2$	120
$MnCl_2 \cdot 4H_2O$	120
$CuCl_2 \cdot 2H_2O$	30
$CoCl_2 \cdot 6H_2O$	150
$Na_2MoO_4.2H_2O$	70.5

Table 8.3. Summary of the experimental conditions tested in the study.

Exp. No	TiO_2 Dose (mg/L)	Irradiation	pH	Medium	Condition Tested
1	1000	UV-C	7.5	UPW	Extent of photocatalysis
2	1000	Dark	7.5	UPW	Extent of dark adsorption, parallel control of #1
3	0	UV-C	7.5	UPW	Extent of photolysis
4	100	UV-C	7.5	UPW	Effect of TiO_2 dose
5	100	Dark	7.5	UPW	Dark adsorption parallel control of #4
6	50	UV-C	7.5	UPW	Effect of TiO_2 dose
7	50	Dark	7.5	UPW	Dark adsorption parallel control of #6
8	10	UV-C	7.5	UPW	Effect of TiO_2 dose
9	10	Dark	7.5	UPW	Dark adsorption parallel control of #8
10	1000	UV-C	7.5	S-WW	Effect of interfering ions/chemicals
11	1000	Dark	7.5	S-WW	Dark adsorption parallel control of #10
12	1000	UV-C	4	UPW	Effect of pH
13	1000	Dark	4	UPW	Dark adsorption parallel control of #12
14	1000	UV-C	11	UPW	Effect of pH
15	1000	Dark	11	UPW	Dark adsorption parallel control of #14

8.2.2. Kinetic Model

Pseudo first order kinetic model was applied on all tested conditions to obtain rate constants, which is expressed as

$$ln\frac{C_0}{C_t} = kt, \quad (8.1)$$

where t is a given time point, C_0 is the initial concentration of HMMM, C_t is its concentration at given time t, and k is pseudo first order rate constant.

8.2.3. Sampling and Analysis

All experiments were completed at most in 120 minutes. Sampling frequency was either 5 or 10 minutes. At each sampling, 1.5 mL sample was collected from the glass petri dishes into 2 mL microcentrifuge tubes, immediately centrifuged at 12000 rpm for 2.5 minutes and immediately filtered through 0.22 µm hydrophilic PTFE filters into 2 mL amber chromatography vials. The samples were screened for HMMM based on the procedure described in Section 3.6. Selected samples from the experiment where HMMM was treated with both UV-C and 1 g/L TiO_2 were screened for HMMM TPs. Samples were 10- fold diluted in 1:1 MS grade methanol: MS grade water solution and IS was added at a concentration of 100 µg/L prior to analysis. TP screening was conducted based on the procedure elaborated in Section 3.5.

8.3. Results and Discussion

8.3.1. Photocatalytic Activity

In initial experiments, three sets of conditions were compared to assess whether HMMM could be removed by only dark adsorption to TiO_2, only photolysis or photocatalysis as a result of combined UV-TiO_2 action. Initial concentration of HMMM was 10 mg/L in all experiments and TiO_2 was added in 1 g/L concentration when used. It was found that HMMM was only degraded in combined application of UV-TiO_2, which occurred quite rapidly. 98.3% of 10 mg/L initial concentration of HMMM was removed in one hour, whereas less than 4% disappearance was observed in dark adsorption (only TiO_2). In photolysis (only UV) degradation was not detected at all (Figure 8.2).

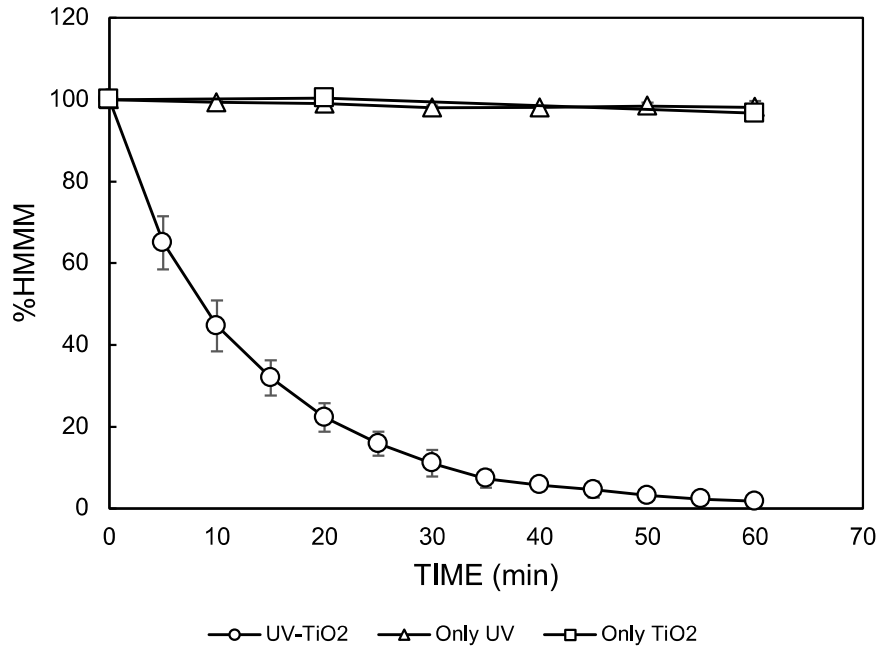


Figure 8.2. HMMM concentrations displayed as percentage of initial concentration in only TiO_2, only UV and UV-TiO_2 combined treatments. HMMM initial concentration =10 mg/L, TiO_2 dose (when used) =1 g/L, pH= 7.5, duration= 60 minutes, 25°C (mean ±one STDV, *n*=2).

8.3.2. Effect of TiO_2 Dose in Photocatalytic Degradation of HMMM

In order to better understand the photocatalytic activity at play, effect of TiO_2 dose on degradation performance was assessed. Four doses of TiO_2 were tested: 1 g/L, 100 mg/L, 50 mg/L and 10 mg/L. By the end of 90 minutes, greater than 98% HMMM removal was observed in 1 g/L, 100 mg/L and 50 mg/L TiO_2 treated solutions and 70% removal was achieved with 10 mg/L TiO_2 concentration (Figure 8.3). This is an interesting result, considering high rates of degradation could be achieved in TiO_2 doses as low as 10 mg/L. No degradation was observed in dark adsorption experiments. The degradation trends were all fit to pseudo-first order kinetic models with R^2>0.95 (Figure 8.4, Table 8.4). The lowest rate constant is observed in 10 mg/L TiO_2 dose with 0.018 min^{-1}, and the highest rate constant seen is 0.083 min^{-1} with 50 mg/L TiO_2 application. This shows that within that range, as the photocatalyst dose increases, so does the degradation rate. The rate constants of 100 mg/L and 1 g/L are slightly lower than that of 50 mg/L TiO_2, suggesting that although photocatalytic activity is still very close to that of 50 mg/L dose, the rate slightly decreases above 50 mg/L of TiO_2, possibly due to hindered light attenuation or aggregation.

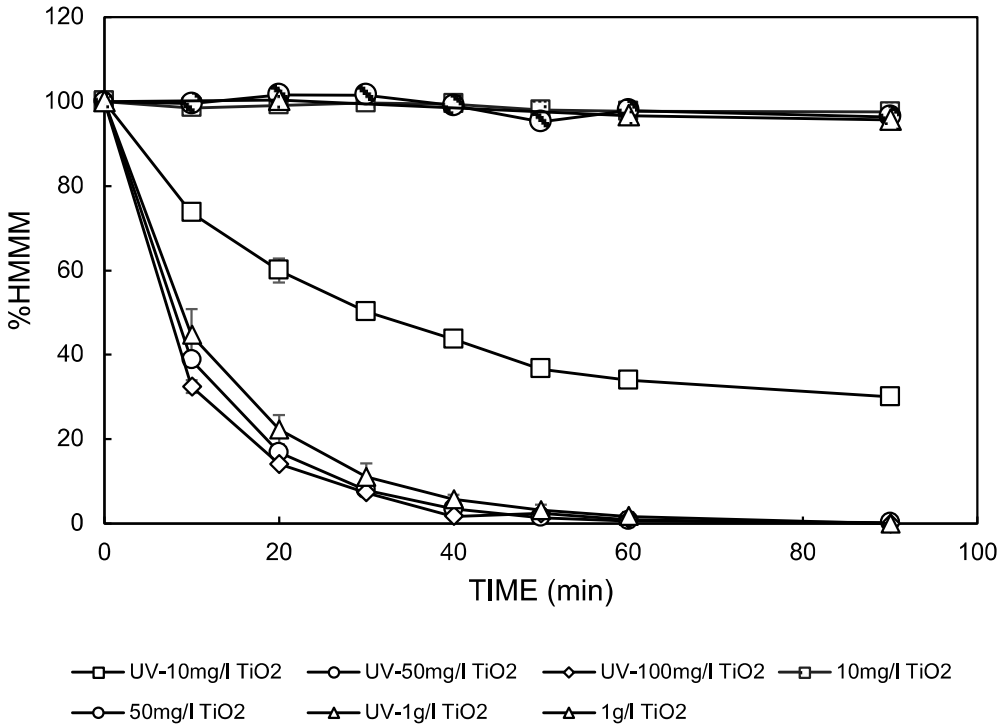


Figure 8.3. Effect of TiO_2 dose on HMMM degradation in dark adsorption and UV irradiation treatments. HMMM initial concentration =10 mg/L, TiO_2 dose =10-1000 mg/L , pH= 7.5, duration= 90 minutes, 25°C (mean ±one STDV, *n*=2).

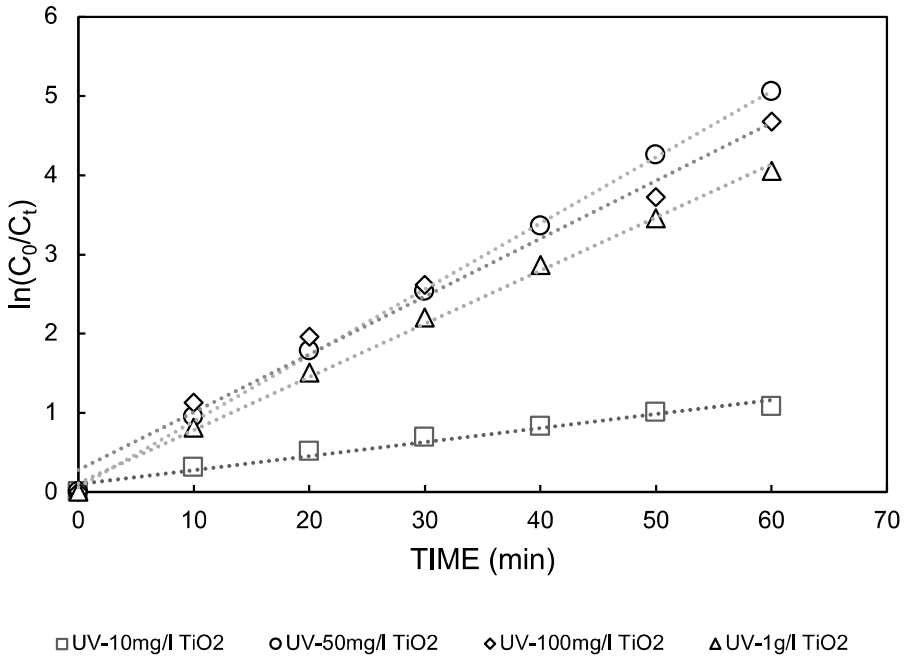


Figure 8.4. Pseudo-first order kinetic model fitting of the HMMM degradation profiles at various TiO_2 doses (10-1000 mg/L).

Table 8.4. R^2 values for the kinetic model linear regression lines and calculated rate constants (k) for the TiO_2 doses assessed (10-1000 mg/L).

TiO_2 (mg/l)	R^2	k (min^{-1})
10	0.972	0.018
50	0.999	0.083
100	0.986	0.073
1000	0.997	0.067

8.3.3. Effect of pH

In this set of experiments, effect of pH on photocatalytic activity was studied. The unmodified pH of 1 g/L TiO_2 solution with 10 mg/L HMMM was 7.5. Additionally, two experiments were conducted at pH= 4 and pH= 11, with the same TiO_2 dose and HMMM initial concentration. Within 60 minutes, 96%, 98% and 89% of HMMM was degraded in pH=4, pH=7.5 and pH=11 conditions, respectively (Figure 8.6). No significant loss was observed in dark adsorption parallels. Degradation trends were fit to pseudo-first order kinetics with R^2 values all greater than 0.996 (Figure 8.7, Table 8.5). Evidently, degradation rates are very close, indicating that pH did not have a major effect. The lowest rate constant belongs to pH=11 and highest belongs to pH=7.5, despite being considerably close to one another.

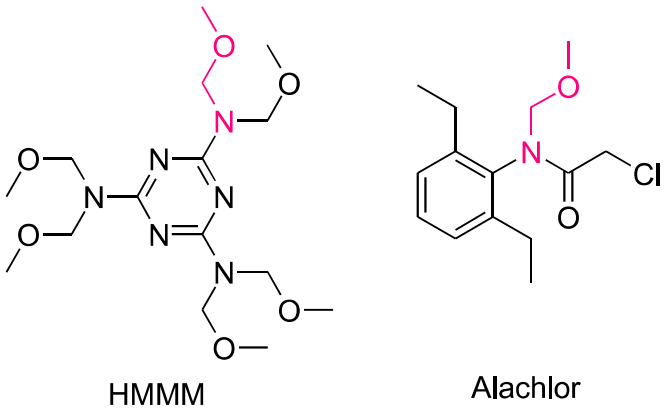


Figure 8.5. Structures of HMMM and alachlor depicting the shared methoxy-methyl moiety.

It was reported in a study on photocatalytic degradation of alachlor, a chloroacetanilide pesticide that shares a common N-methoxy-methyl moiety with HMMM (Figure 8.5), best removals were achieved in neutral pH (Wong and Chu, 2003). It is likely that oxidation of this moiety is an energy-intensive step in the overall course of reactions, and considering HMMM has six of these groups, it is not surprising that its degradation profile demonstrates similar pH trends with alachlor.

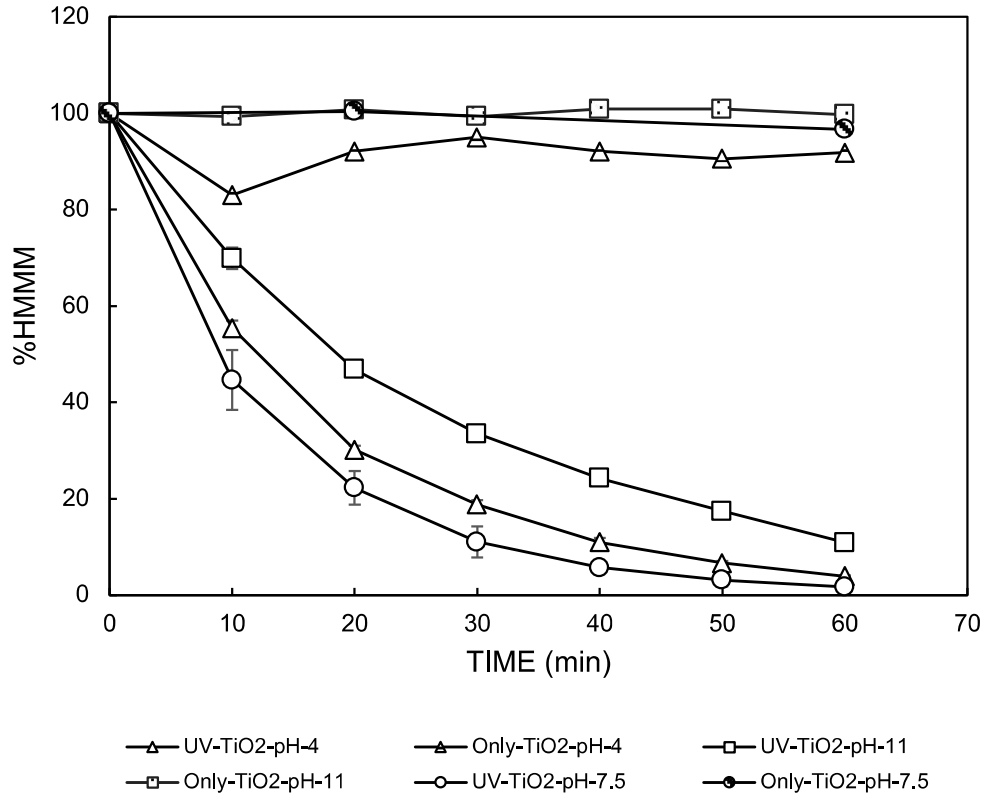


Figure 8.6. Effect of pH on HMMM degradation in dark adsorption and UV irradiation treatments. HMMM initial concentration =10 mg/L, TiO_2 dose =1 g/L, pH= 4, 7.5, 11, duration= 60 minutes, 25°C (mean ±one STDV, *n*=2).

Table 8.5. R^2 values for the kinetic model linear regression lines and calculated rate constants (k) for the pH values assessed (4, 7.5, 11).

pH	R^2	k (min^{-1})
4	0.999	0.053
7.5	0.997	0.067
11	0.998	0.036

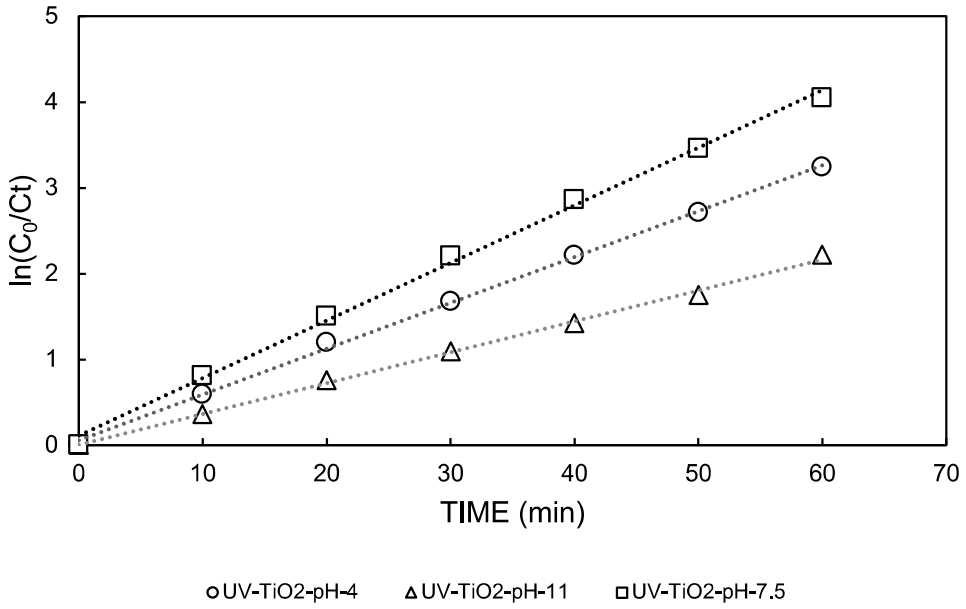


Figure 8.7. Pseudo-first order kinetic model fitting of the HMMM degradation profiles at various pH values (4, 7.5, 11).

8.3.4. Effect of Matrix: Synthetic Wastewater Effluent

Since in reality micropollutants are not alone in their matrices, it was essential to assess the photocatalytic performance of UV-TiO_2 application on HMMM in the presence of a mixture of ions and other oxidizable chemicals. In that respect, a recipe for textile wastewater effluents from literature (Yaseen and Scholz, 2019) was modified and used as a matrix in comparison to ultrapure water. The motivation behind the choice of a synthetic textile wastewater effluent (Table 8.1 and Table 8.2) instead of a municipal wastewater effluent was the fact that industrial wastewaters constitute a major point source for HMMM. It is also confirmed in our studies (Section 4) that industrial zones located around Ergene River are likely to be the main sources of HMMM in the river and textile manufacturing is one of the leading industrial activities in the area. In fact, analysis results of wastewater influent and effluent samples from Ergene-1 industrial zone WWTP, which is a textile dominated industrial zone, had clearly demonstrated that HMMM was not removed efficiently during the wastewater treatment processes. The synthetic wastewater was spiked with 10 mg/L HMMM and the experiment was conducted following the same procedure explained previously (Section 8.2.1) with 1 g/L TiO_2 dose. As expected, degradation rate was significantly lower in synthetic wastewater than in ultrapure water. While 98% of

HMMM was degraded in ultrapure water within 1 hour, by the end of 2 hours, only 53% was removed in synthetic wastewater (Figure 8.8). This is an expected outcome since other constituents of the synthetic wastewater are likely to interfere. The recipe contained sodium benzoate and sodium acetate, which had several applications in textile manufacturing (sizing and pH adjustment agents) and are often used as model contaminants to produce COD in simulated wastewater effluents (Yaseen and Scholz, 2019). It is highly probable that these were oxidized as well, which occupied a portion of the catalyst surface area. Similarly, presence of ions is expected to interfere with the catalytic activity, both in the sense that TiO_2 surface area would be less available and that electron excitation-hole generation-radical formation processes would be altered (Schneider et al., 2014). In fact, in a literature study it was demonstrated that removal efficiency significantly decreased when the reaction matrix was tap water instead of ultrapure water during UV-TiO2 photocatalytic degradation of atrazine (Hustert et al., 1991). Both degradation trend lines were fit to pseudo-first order decay with R^2 values greater than 0.99 (Figure 8.9 and Table 8.6). As expected, rate constant of HMMM degradation in synthetic wastewater was much less than in ultrapure water.

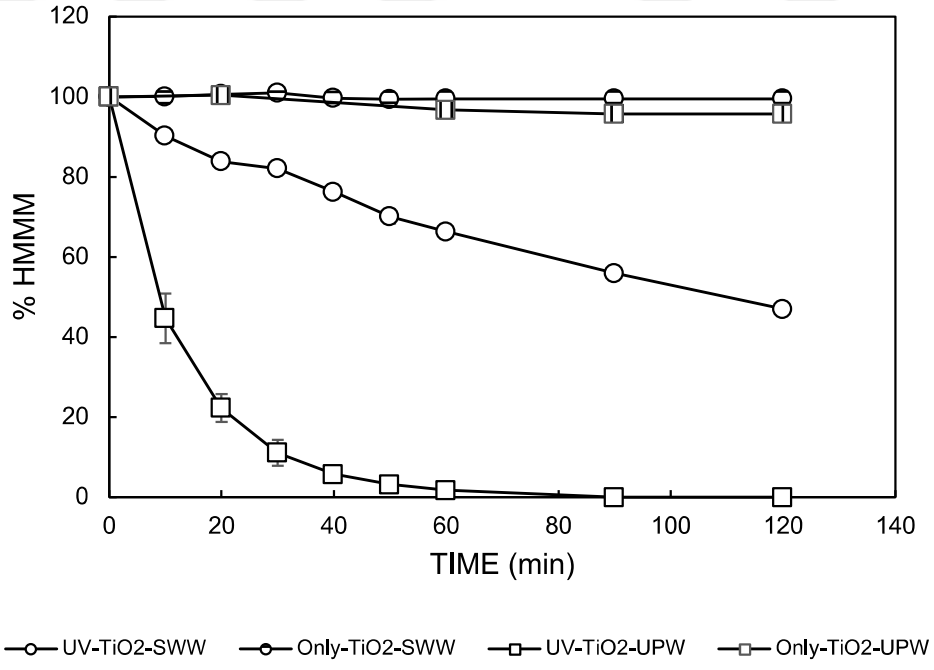


Figure 8.8. HMMM degradation via dark adsorption and UV irradiation treatments in ultrapure water and synthetic wastewater effluent matrices. HMMM initial concentration =10 mg/L, TiO_2 dose =1 g/L , pH= 7.5, duration= 120 minutes, 25°C (mean ±one STDV, *n*=2).

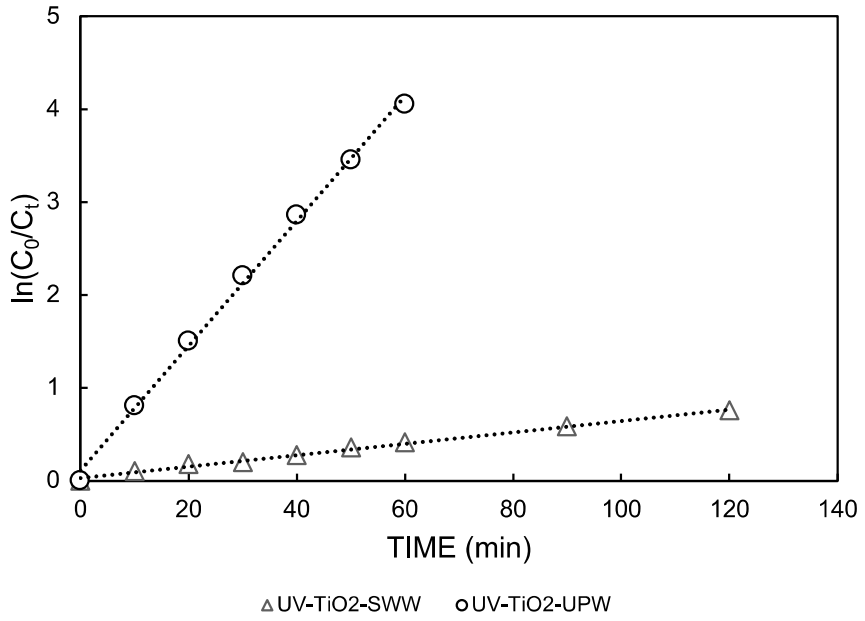


Figure 8.9. Pseudo-first order kinetic model fitting of the HMMM degradation profiles in synthetic wastewater and ultrapure water matrices.

Table 8.6. R^2 values for the kinetic model linear regression lines and calculated rate constants (k) for photocatalysis experiments in synthetic wastewater and ultrapure water.

Medium	R^2	k (min^{-1})
S-WW	0.994	0.006
UPW	0.997	0.067

8.3.5. Transformation Products of Photocatalytic Degradation of HMMM

Although degradation of HMMM through UV-TiO_2 appears to have promising results, it is critically important to understand its fate during this process. In order to shed light on the oxidation mechanism, the targeted LC-MS/MS method (Section 3.5) applied to biotransformation samples was used to screen for known TPs of HMMM in oxidation samples. Duplicate samples from six time points were selected (0, 5, 10, 20, 30 and 60 minutes). Samples were from the experiment in which UV irradiation and 1 g/L TiO_2 was applied to 10 mg/L HMMM in pH=7.5 ultrapure water (Section 8.3.1).

Out of 27 TPs screened, 22 were detected. TPs were visualized in stack column graphs in five arbitrary groups in order to observe trends more clearly (Figures 8.10, 8.11, 8.12,

8.13 and 8.14). As seen previously, a few TPs were there as impurities of HMMM from day-0 (TP346, TP362, TP314). Overall, both the sum of TPs and their individual concentrations had an increasing trend (Figure 8.15). Only some higher molecular weight TPs had decreasing trend, such as TP314 and TP362.

It was noteworthy that concentration of low molecular weight TPs remained generally lower and increased only towards the end of the experiment, suggesting their ongoing formation (Figure 8.13, 8.14). These groups are dominated by 2MM-, 1MM- and 0MM-Mel families of TPs that are M-OH or M=O derivatized. Melamine was only observed in minor amounts and only at the 60-minute samples (0.056 μM). On the other hand, TP186 and TP156, low molecular weight TPs that were not observed in biotransformation assays, were detected in the oxidation samples. It is safe to state that oxidation experiment samples had the highest variety of TPs.

However, mass balance was not preserved. Overall mass balance decreased to 55% by the end of 60 minutes, in comparison to 100% value assigned to sum of HMMM, TPs and melamine concentration at the beginning of the experiment (Table 8.7 and Figure 8.15). Three possible causes for this outcome can be proposed, as discussed in Section 6.3.2: some TPs might have formed at lower concentrations than limit of detection, some unknown TPs might have formed that weren't detected by the targeted method or a portion of HMMM might have been mineralized. Since the UV-TiO_2 photocatalysis involves hydroxyl radical formation and a cascade of oxidation reactions, all three cases seem equally possible. Since radicals involved oxidation reactions are highly reactive, they can yield highly unpredictable byproducts, which may be best surveyed by untargeted screening methods involving LC- or GC- HRMS.

Although a comprehensive unknown screening method development was not within the scope of this study, it is a noteworthy starting point for prospective work following these results. It is also equally possible that at least a partial mineralization of HMMM could have taken place, which can be tested conveniently by a TOC analysis, however, the device and equipment for such an analysis was beyond our reach at the time of the study. Nevertheless, these remaining questions will be the basis of our future work.

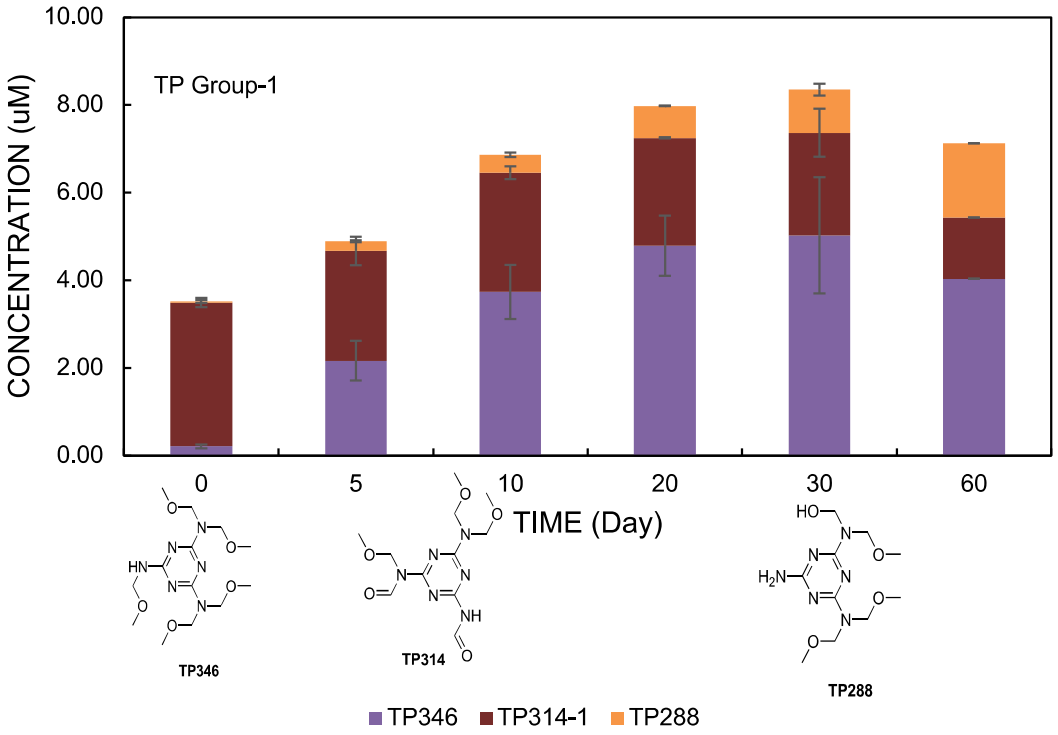


Figure 8.10. Concentrations of Group-1 TPs during 60 minutes of UV-TiO_2 treatment (initial HMMM=25.6 µM, TiO_2=1 g/L, pH= 7.5, 25°C, mean ±one STDV, *n*=2).

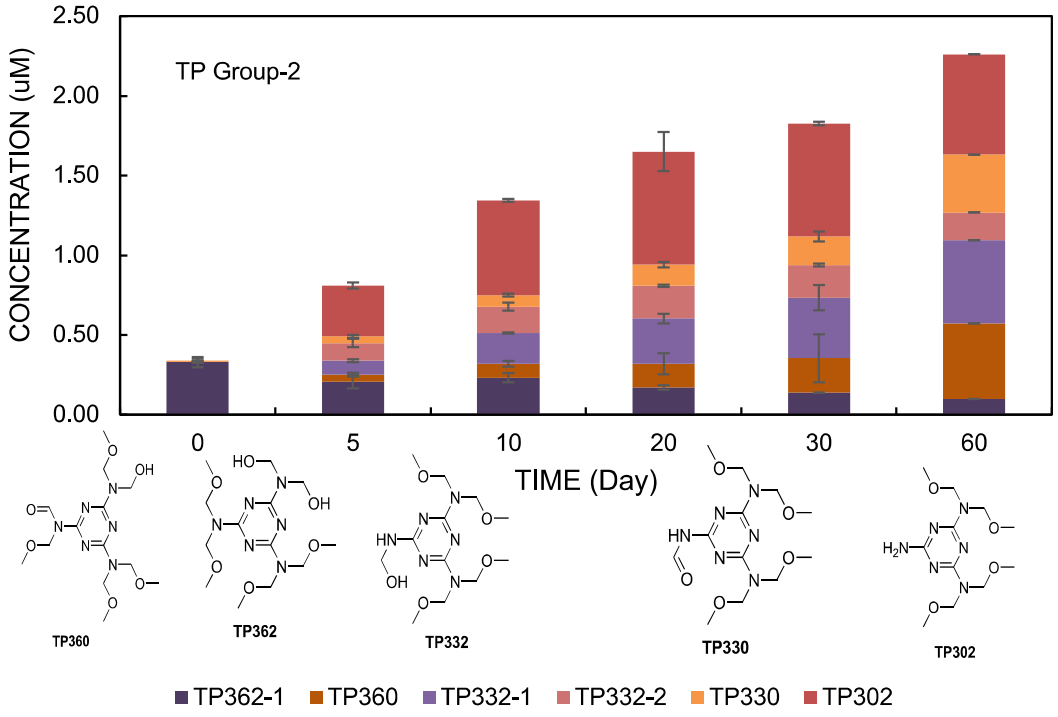


Figure 8.11. Concentrations of Group-2 TPs during 60 minutes of UV-TiO_2 treatment (initial HMMM=25.6 µM, TiO_2=1 g/L, pH= 7.5, 25°C, mean ±one STDV, *n*=2).

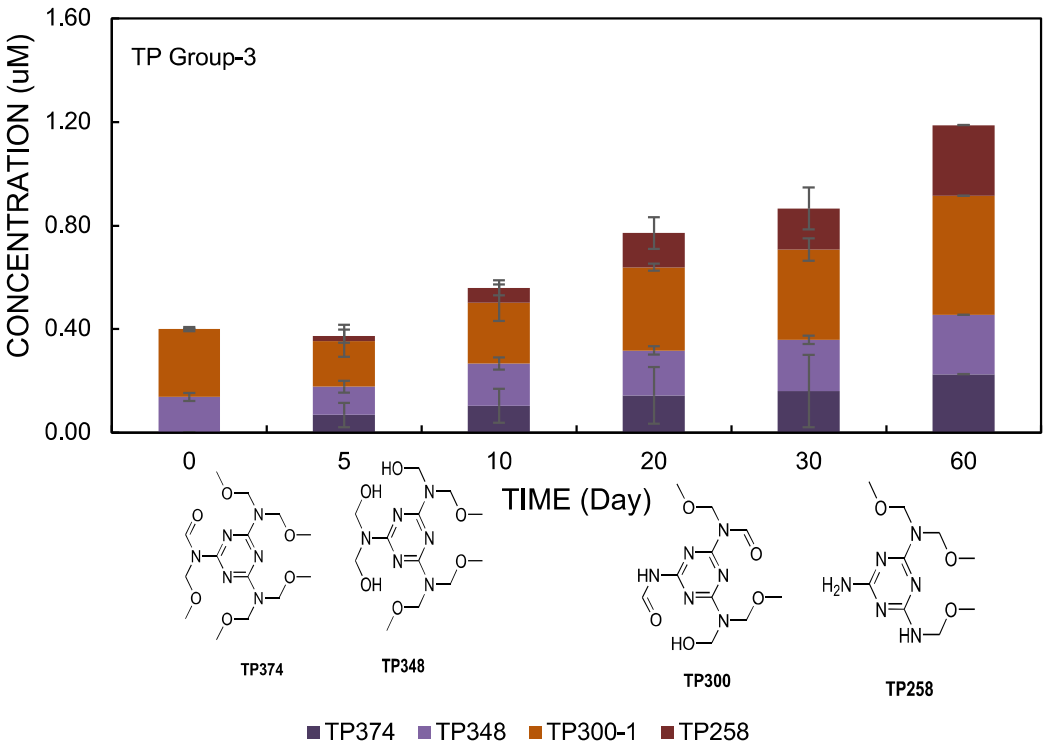


Figure 8.12. Concentrations of Group-3 TPs during 60 minutes of UV-TiO_2 treatment (initial HMMM=25.6 µM, TiO_2=1 g/L, pH= 7.5, 25°C, mean ±one STDV, *n*=2).

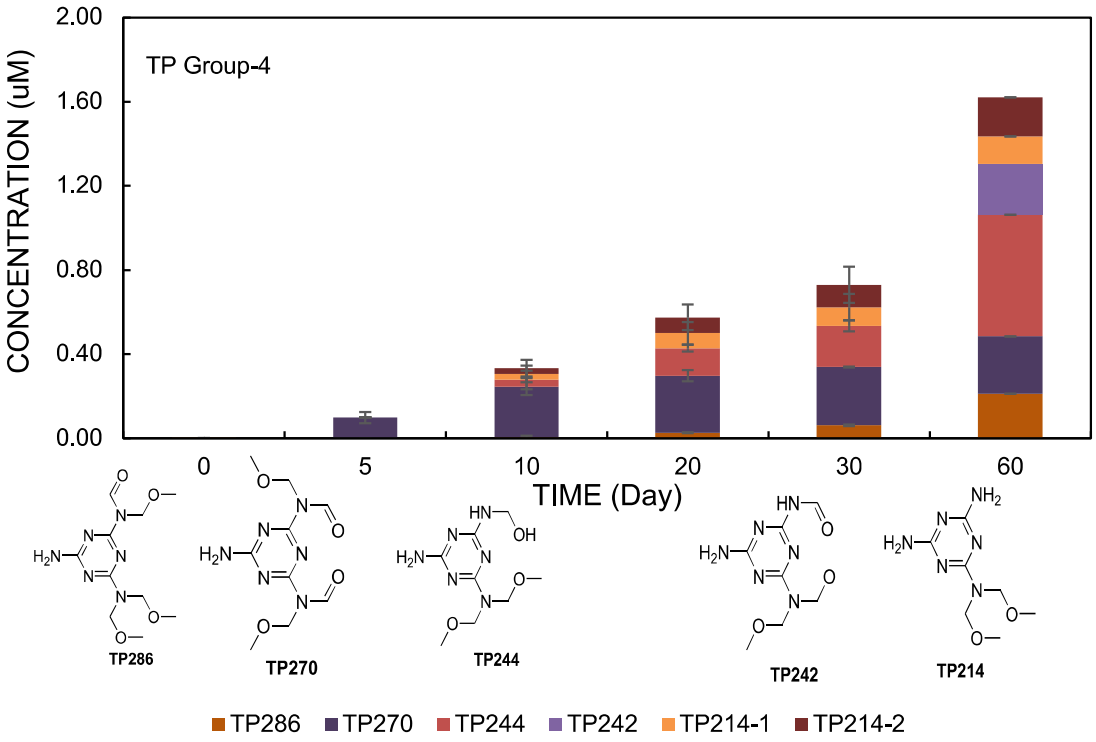


Figure 8.13. Concentrations of Group-4 TPs during 60 minutes of UV-TiO_2 treatment (initial HMMM=25.6 µM, TiO_2=1 g/L, pH= 7.5, 25°C, mean ±one STDV, *n*=2).

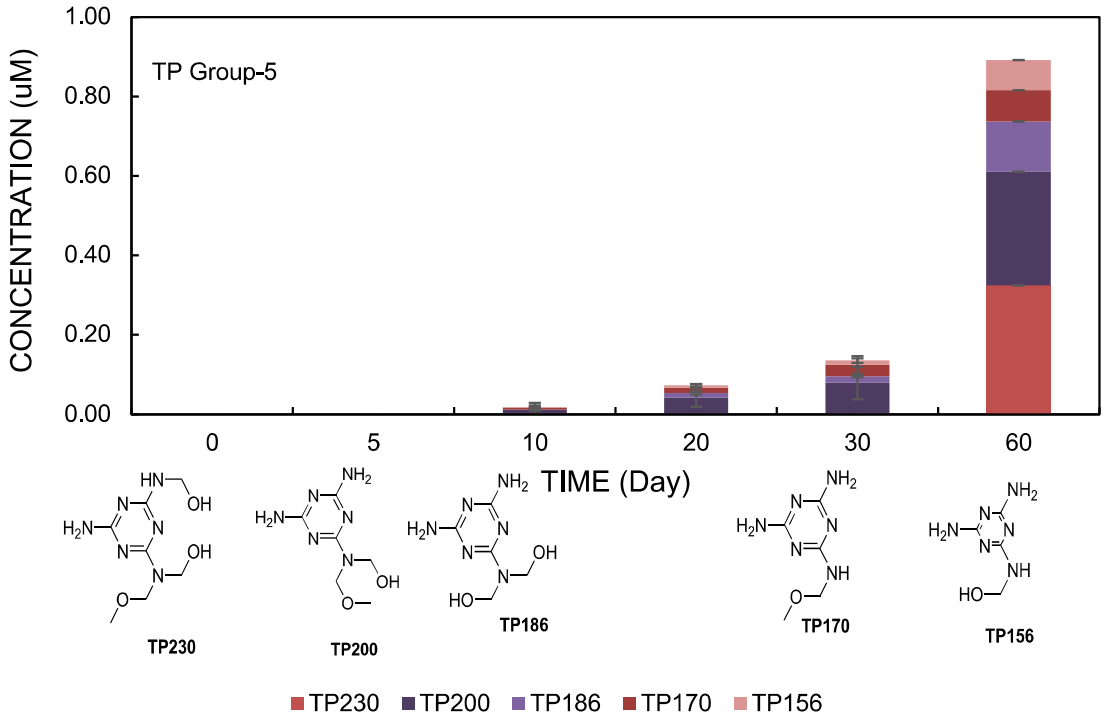


Figure 8.14. Concentrations of Group-5 TPs during 60 minutes of UV-TiO_2 treatment (initial HMMM=25.6 µM, TiO_2=1 g/L, pH= 7.5, 25°C, mean ±one STDV, *n*=2).

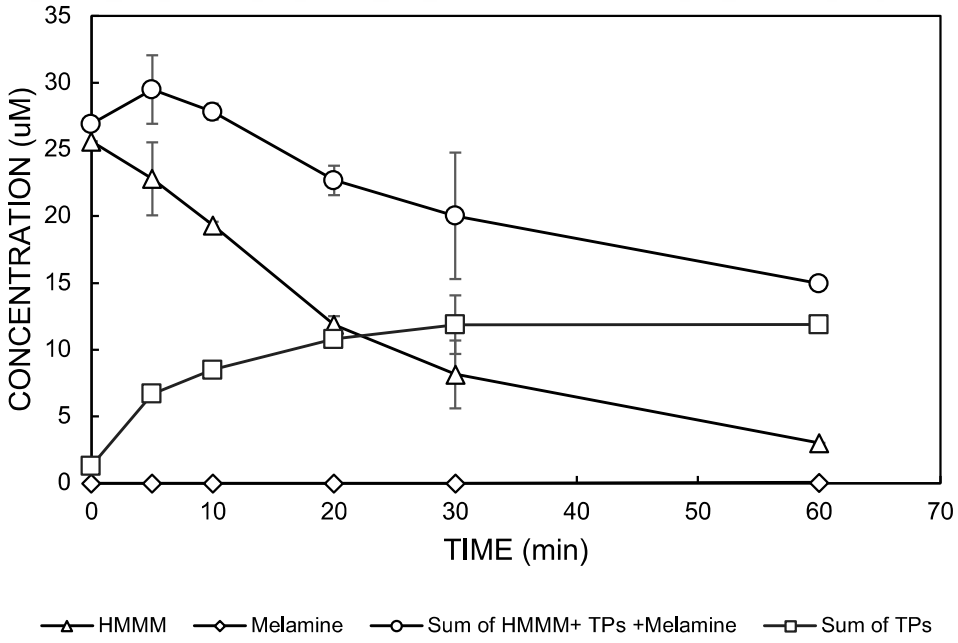


Figure 8.15. Concentrations of HMMM, melamine, all TPs (excluding melamine) and all analytes (HMMM, melamine, TPs) in UV-TiO_2 treatments (initial HMMM=25.6 µM, TiO_2=1 g/L, pH= 7.5, 25°C, 60 minutes, ultrapure water). Concentrations of TPs are reported as HMMM equivalents. Melamine was quantified separately.

Table 8.7. Concentrations of HMMM, melamine, all TPs (excluding melamine) and all analytes (HMMM, melamine, TPs) in UV-TiO_2 treatments (initial HMMM=25.6 µM, TiO_2=1 g/L, pH= 7.5, 25°C, 60 minutes, ultrapure water). Mass balances as a percentage of sum of all analytes at t=0. Concentrations of TPs are reported as HMMM equivalents. Melamine was quantified separately.

Time (min)	HMMM (µM)	Melamine (µM)	TPs (as HMMM µM)	HMMM lost (%)	HMMM+TPs+Melamine (as HMMM µM)	Mass Balance
0	25.602	0.000	1.598	0.000	27.201	100.00
5	22.801	0.000	3.846	10.943	26.647	97.96
10	19.335	0.000	6.640	24.482	25.975	95.49
20	11.887	0.000	8.766	53.571	20.653	75.93
30	8.155	0.000	9.734	68.147	17.889	65.77
60	3.028	0.056	11.874	88.173	14.958	54.99

8.3.6. Summary

This study demonstrated that with HMMM could be degraded rapidly by UV-TiO_2 photocatalysis under various conditions. The degradation efficiency remained higher than 90% with TiO_2 doses as low as 50 mg/L and 70% degradation was observed even at the lowest TiO_2 concentration tested (10 mg/L). Photocatalytic activity was slightly decreased with increased acidity and basicity, and best degradation was demonstrated at neutral pH. Degradation was drastically hindered, but still occurred (53% in 2 hours, 1 g/L TiO_2, 10 mg/L HMMM), in synthetic wastewater matrix where interfering ions and oxidizable chemicals were present. Furthermore, targeted transformation product screening suggests that HMMM is degraded into several TPs, which might implicate incomplete mineralization. Further work is needed to assess the extent of HMMM mineralization in this process. Despite the detection of TPs which might indicate formation of oxidation byproducts instead of complete mineralization, and the adverse effect of synthetic wastewater matrix on the removal, this work constitutes the first promising study regarding the treatment of HMMM by an advanced oxidation process and the oxidation byproducts it yields. This work was conducted as a proof of concept, to assess whether UV-TiO_2 photocatalysis had any promise at all as to removal of this emerging persistent micropollutant. To that end, the experimental

setup was not a standard photocatalytic reactor, it was a biosafety cabinet re-purposed as a photocatalytic reactor. By employment of standard equipment and wider options of analytical techniques like TOC analyzer or HRMS, the extent of photocatalytic degradation and fate of HMMM could be determined further. Despite the lower degradation rate that was observed in synthetic wastewater matrix, the fact that more than 50% removal was achieved in 2 hours may also have promising implications for real-life applications.

9. CONCLUSIONS

In the work described in this thesis, an emerging micropollutant, HMMM, was studied by a holistic approach to shed light upon its biological and UV-TiO_2 catalyzed degradation, its fate in these processes, and its presence in the environment.

Work conducted within the scope of Chapter 4 demonstrated that HMMM is still a persistent micropollutant in Ergene River at concentrations ranging between 0.21 $\pm$ 0.02 µg/L and 32.0 $\pm$ 0.22 µg/L. Furthermore, it was shown that it is not removed efficiently in conventional wastewater treatment operations, since HMMM was found to reach concentrations as high as 14.7 $\pm$ 0.27 µg/L in an industrial zone WWTP effluent.

In Chapter 5, biotransformation of HMMM with *Pseudomonas sp*. BIOMIG1^{BAC}, a single strain of bacterium capable of mineralizing benzalkonium chlorides, was assessed in two conditions: N-free (nitrogen absent, additional carbon present) and C-free (nitrogen present, additional carbon absent). By day-100, 86% of initial HMMM concentration was depleted in N-free biological treatments, as opposed to 50% and 34% losses in C-free biological treatments and in abiotic controls, respectively. However, only in the N-free biological treatments HMMM was transformed to melamine to a large extent. The considerably higher loss of HMMM and higher formation of melamine in N-free treatments are strong indicators that degradation of HMMM is likely promoted by biological activity in these conditions. Overall mass balance was conserved during biodegradation, and the amount of depleted HMMM corresponded to the amount of melamine and other TPs generated. The results clearly indicate that biotransformation of HMMM by this strain does not occur fully and does not proceed to mineralization, rather, it results in accumulation of melamine and several other transformation products. Although complete mineralization was not achieved and degradation duration well exceeded ready biodegradability standards, this is the first work in the literature that includes assessment HMMM biotransformation by a single strain of bacterium and detection of its TPs. The results provide insight about its bacterial metabolism and future work may be conducted on other genetically well-characterized single strains of bacteria that are known to degrade xenobiotics bearing similar chemical features as HMMM, such as chloroacetanilide and s-triazine pesticides that were

mentioned earlier. These studies could shed light upon enzymatic mechanisms at play in degradation of persistent functionalities, such as ether groups or triazine rings, and can further be employed on bioremediation of pollutants that possess them.

In Chapter 6, biotransformation of HMMM with activated sludge was assessed in different four conditions: N-free (nitrogen absent, additional carbon present), C-free (nitrogen present), C/N-free (nitrogen and carbon absent) and full (nitrogen and additional carbon present). In 55 days, 87% of HMMM was depleted in C-free treatments, while no significant decrease was observed in other biological treatments or abiotic controls. These findings imply presence of selective biological activity in the conditions where HMMM was the sole carbon source. Many transformation products were detected and semi-quantified, however, melamine is not found to accumulate in stochiometric amount as it did in treatments with *Pseudomonas sp.* BIOMIG1^{BAC}. It was observed that in C-free biological treatment, overall mass balance was not conserved, which was attributed to two possible explanations: either some target TPs that formed as a result of degradation remained below the limit of detection or some TPs that appeared were not in the targeted list of compounds. Mineralization was not thought to be a highly probable reason for loss of mass balance since HMMM degradation was slow, however, it is still a possibility considering the diverse microbial population of activated sludge samples, which may harbor variety of s-triazine degraders. The overall results demonstrate that HMMM is not readily biodegradable by activated sludge and degradation yields various polar TPs which also persist. In the future studies, HMMM degrading species can be enriched and isolated, and the reason for loss of mass balance can be further assessed via TOC analyses. This work also contributes to the limited literature regarding fate of HMMM in activated sludge treatments and is the first to assess effects of carbon and nitrogen on its biodegradation. Given that wastewater almost always contains additional carbon sources and HMMM is degraded by activated sludge only when it was the sole carbon source, it can be commented that in real activated sludge treatments, its biodegradation is not promoted. This is also confirmed by the occurrences of HMMM in wastewaters (Section 2.1.2) and the observations explained in Chapter 4.

The work in Chapter 7 is motivated by the fact that melamine is a hazardous micropollutant and is a dead-end transformation product of HMMM (demonstrated by the work in Chapter 5) and many other hazardous s-triazine pesticides such as atrazine

(discussed in Section 7.1). Melamine degraders were enriched and isolated using inocula obtained from an advanced biological wastewater treatment facility. Melamine degrader was isolated in the condition where it was used as the sole nitrogen source, in a medium amended with glucose (N-free). Biotransformation assays were conducted in four test conditions (N-free, C-free, C/N free, full) using the isolated species, which exhibited rapid degradation of melamine in all tested conditions (100% degradation achieved within 2 days). In all treatment conditions except N-free treatments, cyanuric acid accumulation was observed. In N-free treatments, cyanuric acid was depleted while OD increased, indicating a growth-promoting metabolism. The work in this chapter contributes to the growing literature on melamine biotransformation. In the future studies, the isolated degrader can be phylogenetically characterized via 16S rRNA sequencing, the nitrogen and carbon regulation of melamine and cyanuric acid metabolism by this species could be examined in deeper detail. Additionally, co-culturing experiments with the melamine degrader and (if isolated) HMMM degraders might yield promising results in the complete mineralization of HMMM.

In Chapter 8, it was demonstrated that HMMM was photocatalytically degraded upon UV-TiO_2 treatment. HMMMM loss did not occur in dark adsorption experiments with TiO_2 alone and photolysis experiments with UV alone. In most conditions tested, over 90% HMMM degradation was achieved within an hour. Degradation rate exhibited an increasing trend when TiO_2 dose was within the range of 10-50 mg/L, then it showed a slightly decreasing trend, likely due to hindrance of light attenuation or aggregation of the photocatalyst. However, except for 70% degradation observed in 10 mg/L TiO_2 treatment, all higher TiO_2 doses yielded 100% degradation within an hour. The effect of pH was also slight, in all three pH conditions tested (4, 7.5 and 11) at least 89% of HMMM was degraded within an hour. The optimum pH was found to be 7.5, with 98% degradation. The matrix of the reaction, however, seems to have a strong impact on photocatalytic activity. When HMMM was treated in a matrix of synthetic wastewater effluent instead of ultrapure water, only 53% degradation was observed within two hours. This indicates that in a real-life advanced oxidation treatment where other ions and reductants are present, HMMM degradation may not proceed as efficiently. In addition to assessment of effects of parameters like pH, TiO_2 dose and matrix, targeted TP screening was conducted to examine the degradation mechanism. Just like in case of activated sludge treatment, melamine was found

to be a minor TP and overall mass balance was not conserved, suggesting that the total amount of detected TPs do not account for the amount of HMMM lost. This can be explained by formation of some TPs at very low concentrations that remain under detection limit, formation of unknown TPs as a result of unpredictable oxidation reactions and mineralization of some portion of HMMM. All three cases seem likely and require further study involving untargeted screening methods for detection of unknown TPs and TOC analyses for assessment of mineralization. With this work, it has been demonstrated for the first time that HMMM can undergo rapid photocatalytic degradation by UV-TiO_2 treatment.

It is evident from the studies conducted within the scope of this thesis that HMMM is a micropollutant that has an ongoing presence all along Ergene River and is not easy to degrade, through biological or chemical treatments. It was shown to biodegrade slowly and photocatalytically degrade rapidly, however, in both cases, it was found to yield a plethora of TPs, which are potentially even more persistent and mobile than it is. Although it appears that complete mineralization of HMMM is not achieved with the treatments tested, the studies provide significant insight regarding its fate during both biotransformation and advanced oxidation processes. The high percentages of HMMM degradation in most experiments suggest these processes may serve as a step in a series aimed at mineralizing HMMM and similar micropollutants. Future work should focus on assessment of stepwise processes like combination of biological and advanced oxidation treatments. Given its shared functional groups with s-triazine and chloroacetanilide pesticides, prioritizing the toxicity assessment of HMMM is crucial for prospective studies. Future studies on removal and fate of HMMM should be performed in a more holistic fashion, approaching the pollutants sharing similar structures as a family. For instance, co-degradation studies can be conducted on mixtures of HMMM and these pesticides via both biological and photocatalytic treatments. Further studies on biotransformation of HMMM and melamine by single strains of well-characterized bacteria can yield valuable information about mechanism and regulation of degradation. For instance, if spontaneous non-degrader mutants can be obtained from an otherwise degrader, comparative genomics can shed light on possible enzyme coding genes that promote HMMM or melamine degradation. In short, given the scarcity of literature on the removal and fate of this emerging pollutant, there seems to be abundant potential for further research on HMMM in the future.

REFERENCES

Alhelou, R., B. Seiwert, and T. Reemtsma, 2019, "Hexamethoxymethylmelamine – A precursor of Persistent and Mobile Contaminants in Municipal Wastewater and the Water Cycle", *Water Research*, Vol. 165, p. 114973.

Altinbag, R. C., E. Ertekin, and U. Tezel, 2020, "Complete Genome Sequence of *Pseudomonas* sp. Strain BIOMIG1 ^{BAC} which Mineralizes Benzalkonium Chloride Disinfectants", *Microbiology Resource Announcements*, Vol. 9, No. 20, pp. 00309-20.

Baird, R. B., A. D. Eaton, and E.W. Rice (Eds.), 2012, *Standard Methods for the Examination of Water and Wastewater,* Twenty-second Edition, American Public Health Association, Washington.

Baird, C., and M.C. Cann, 2012, *Environmental Chemistry*, Fifth Edition, W.H. Freeman, New York.

Bethsass, J., and A. Colangelo, 2006, "European Union Bans Atrazine, While the United States Negotiates Continued Use", *International Journal of Occupational and Environmental Health*, Vol. 12, No. 3, pp. 260–267.

Bianchi, C. L., C. Pirola, V. Ragaini, and E. Selli, 2006, "Mechanism and Efficiency of Atrazine Degradation Under Combined Oxidation Processes", *Applied Catalysis B: Environmental*, Vol. 64, No. 1–2, pp. 131–138.

Bobeldijk, I., P. G. M. Stoks, J. P. C. Vissers , E. Emke, J. A. Van Leerdam, B. Muilwijk, R. Berbee, and T. H. M. Noi, 2002, "Surface and Wastewater Quality Monitoring: Combination of Liquid Chromatography with (Geno)toxicity Detection, Diode Array Detection and Tandem Mass Spectrometry for Identification of Pollutants", *Journal of Chromatography A*, Vol. 970, No. 1–2, pp. 167–181.

Bolden, A. L., J. R. Rochester, and C. F. Kwiatkowski, 2017, “Melamine, Beyond the Kidney: A Ubiquitous Endocrine Disruptor and Neurotoxicant?”, *Toxicology Letters*, Vol. 280, pp. 181–189.

Bradley, E. L., L. Castle, J. S. Day, and J. Leak, 2011, “Migration of Melamine from Can Coatings Cross-linked with Melamine-based Resins, into Food Simulants and Foods”, *Food Additives and Contaminants: Part A*, Vol. 28, No. 2, pp. 243–250.

Castan, S., A. Sherman, R. Peng, M. T. Zumstein, W. Wanek, T. Hüffer, and T. Hofmann, 2023, “Uptake, Metabolism, and Accumulation of Tire Wear Particle-Derived Compounds in Lettuce”, *Environmental Science and Technology*, Vol. 57, No. 1, pp. 168–178.

Chauvaux, S., F. Chevalier, C. Le Dantec, F. Fayolle, I. Miras, F. Kunst, and P. Beguin, 2001, “Cloning of a Genetically Unstable Cytochrome P-450 Gene Cluster Involved in Degradation of the Pollutant Ethyl *tert* -Butyl Ether by *Rhodococcus ruber*”, *Journal of Bacteriology*, Vol. 183, No. 22, pp. 6551–6557.

Chen, Q., C. H. Wang, S. K. Deng, Y. D. Wu, Y. Li, L. Yao, J. D. Jiang, X. Yan, J. He, and S. P. Li, 2014, “Novel Three-Component Rieske Non-Heme Iron Oxygenase System Catalyzing the *N* -Dealkylation of Chloroacetanilide Herbicides in Sphingomonads DC-6 and DC-2”, *Applied and Environmental Microbiology*, Vol. 80, No. 16, pp. 5078–5085.

Chen, Q., J. Zhang, C. H. Wang, J. Jiang, S. W. Kwon, L. N. Sun, W. B. Shen, and J. He, 2014, “Novosphingobium chloroacetimidivorans sp. Nov., A Chloroacetamide Herbicide–degrading Bacterium Isolated from Activated Sludge”, *International Journal of Systematic and Evolutionary Microbiology*,Vol. 64, No. 8, pp. 2573–2578.

Corrêa, T. Q., K. C. Blanco, J. D. Vollet-Filho, V. S. Morais, W. R. Trevelin, S. Pratavieira, and V. S. Bagnato, 2021, “Efficiency of an Air Circulation Decontamination Device

for Microorganisms Using Ultraviolet Radiation", *Journal of Hospital Infection*, Vol. 115, pp. 32–43.

Dalal, R. P., and D. S. Goldfarb, 2011, "Melamine-related Kidney Stones and Renal Toxicity", *Nature Reviews Nephrology*, Vol. 7, No. 5, pp. 267–274.

De Hoogh, C. J., A. J. Wagenvoort, F. Jonker, J. A. Van Leerdam, and A. C. Hogenboom, 2006, "HPLC-DAD and Q-TOF MS Techniques Identify Cause of *Daphnia* Biomonitor Alarms in the River Meuse", *Environmental Science and Technology*, Vol. 40, No. 8, pp. 2678–2685.

Dsikowitzky, L., and J. Schwarzbauer, 2015, "Hexa(methoxymethyl)melamine: An Emerging Contaminant in German Rivers", *Water Environment Research*, Vol. 87, No. 5, pp. 461–469.

Du, B., Z. Tian, K. T. Peter, E. P. Kolodziej, and C. S. Wong, 2020, "Developing Unique Nontarget High-Resolution Mass Spectrometry Signatures to Track Contaminant Sources in Urban Waters", *Environmental Science and Technology Letters*, Vol. 7, No. 12, pp. 923–930.

Ekman, R., J. Silberring, A. Westman-Brinkmalm, A. Kraj (Ed.)., 2009, *Mass spectrometry: Instrumentation, Interpretation, and Applications*. John Wiley and Sons, New Jersey.

Emadian, S. M., F. O. Sefiloglu, I. Akmehmet Balcioglu, and U. Tezel, 2021, "Identification of Core Micropollutants of Ergene River and Their Categorization Based on Spatiotemporal Distribution", *Science of The Total Environment*, Vol. 758, p. 143656.

Fayolle, F., J. P. Vandecasteele, and F. Monot, 2001, "Microbial Degradation and Fate in the Environment of Methyl tert -butyl ether and Related Fuel Oxygenates", *Applied Microbiology and Biotechnology*, Vol. 56, No. 3–4, pp. 339–349.

Finckh, S., L. M. Beckers, W. Busch, E. Carmona, V. Dulio, L. Kramer, M. Krauss, L. Posthuma, T. Schulze, J. Slootweg, P. C. Von Der Ohe, and W. Brack, 2022, "A Risk Based Assessment Approach for Chemical Mixtures from Wastewater Treatment Plant Effluents", *Environment International*, Vol. 164, p. 107234.

Fink, J. K., 2013, *Reactive Polymers Fundamentals and Applications,* Second Edition, William Andrew Publishing, Waltham.

Fuchte, H. E., N. Beck, E. Bieg, V. J. Bayer, C. Achten, M. Krauss, A. Schäffer, and K. E. C. Smith, 2022, "A Look Down the Drain: Identification of Dissolved and Particle Bound Organic Pollutants in Urban Runoff Waters and Sediments", *Environmental Pollution*, Vol. 302, p. 119047.

Gao, Y., L. Jin, H. Shi, and Z. Chu, 2015, "Characterization of a Novel Butachlor Biodegradation Pathway and Cloning of the Debutoxylase (Dbo) Gene Responsible for Debutoxylation of Butachlor in *Bacillus* sp. Hys-1", *Journal of Agricultural and Food Chemistry*, Vol. 63, No. 38, pp. 8381–8390.

García-González, V., F. Govantes, L. J. Shaw, R. G. Burns, and E. Santero, 2003, "Nitrogen Control of Atrazine Utilization in *Pseudomonas* sp. StrainADP", *Applied and Environmental Microbiology*, Vol. 69, No. 12, pp. 6987–6993.

Ge, X., X. Wu, S. Liang, and H. Sun, 2014, "A Sensitive and Validated HPLC Method for the Determination of Cyromazine and Melamine in Herbal and Edible Plants Using Accelerated Solvent Extraction and Cleanup with SPE", *Journal of Chromatographic Science*, Vol. 52, No. 7, pp. 751–757.

Govantes, F., V. García-González, O. Porrúa, A. I. Platero, A. Jiménez-Fernández, and E. Santero, 2010, "Regulation of the Atrazine-degradative Genes in Pseudomonas sp. strain ADP: Regulation of Atrazine Biodegradation", *FEMS Microbiology Letters*, Vol. 310, No. 1, pp. 1–8.

Haandel, A. C. van, and J. G. van der Lubbe, 2012, *Handbook of Biological Wastewater Treatment*, Second Edition, IWA Publishing, London.

Hale, S. E., H. P. H. Arp, I. Schliebner, and M. Neumann, 2020, "Persistent, Mobile and Toxic (PMT) and Very Persistent and Very Mobile (vPvM) Substances Pose an Equivalent Level of Concern to Persistent, Bioaccumulative and Toxic (PBT) and Very Persistent and Very Bioaccumulative (vPvB) Substances Under REACH", *Environmental Sciences Europe*, Vol. 32, No. 1, pp. 155-157.

Hatakeyama, T., K. Takagi, K. Yamazaki, F. Sakakibara, K. Ito, E. Takasu, T. Naokawa, and K. Fujii, 2015, "Mineralization of Melamine and Cyanuric acid as Sole Nitrogen Source by Newly Isolated Arthrobacter spp. Using a Soil-charcoal Perfusion Method", *World Journal of Microbiology and Biotechnology*, Vol. 31, No. 5, pp. 785–793.

Hiki, K., K. Asahina, K. Kato, T. Yamagishi, R. Omagari, Y. Iwasaki, H. Watanabe, and H. Yamamoto, 2021, "Acute Toxicity of a Tire Rubber-Derived Chemical, 6PPD Quinone, to Freshwater Fish and Crustacean Species", *Environmental Science and Technology Letters*, Vol. 8, No. 9, pp. 779–784.

Hug, C., N. Ulrich, T. Schulze, W. Brack, and M. Krauss, 2014, "Identification of Novel Micropollutants in Wastewater by a Combination of Suspect and Nontarget Screening", *Environmental Pollution*, Vol. 184, pp. 25–32.

Hustert, K., P. N. Moza, and B. Pouyet, 1991, "Photocatalytic Degradation of s-triazine Herbicides", *Toxicological and Environmental Chemistry*, Vol. 31, No. 1, pp. 97–102.

Hyman, M. R., C. L. Page, and D. J. Arp, 1994, "Oxidation of Methyl Fluoride and Dimethyl Ether by Ammonia Monooxygenase in Nitrosomonas europaea", *Applied and Environmental Microbiology*, Vol. 60, No. 8, pp. 3033–3035.

Johannessen, C., P. Helm., and C. D. Metcalfe, 2021, “Detection of Selected Tire Wear Compounds in Urban Receiving Waters”, *Environmental Pollution*, Vol. 287, p. 117659.

Johannessen, C., P. Helm, and C. D. Metcalfe, 2022, “Runoff of the Tire-Wear Compound, Hexamethoxymethyl-Melamine into Urban Watersheds”, *Archives of Environmental Contamination and Toxicology*, Vol. 82, No. 2, pp. 162–170.

Johannessen, C., and C. D. Metcalfe, 2022, “The Occurrence of Tire Wear Compounds and Their Transformation Products in Municipal Wastewater and Drinking Water Treatment Plants”, *Environmental Monitoring and Assessment*, Vol. 194, No. 10, pp. 731.

Johannessen, C., and J. M. Parnis, 2021, “Environmental Modelling of Hexamethoxymethylmelamine, Its Transformation Products, and Precursor Compounds: An Emerging Family of Contaminants from Tire Wear”, *Chemosphere*, Vol. 280, p. 130914.

Karakaya, E., 2019, *Aerobic Biodegradation of Dominant Micropollutants in the Ergene River by River Microcosms and Pure Cultures of Bacteria*, MSc Thesis, Boğaziçi University.

Kim, Y. H., C. J. Cha, K. H. Engesser, and S. J. Kim, 2008, “Degradation of Various Alkyl Ethers by Alkyl Ether-degrading Actinobacteria Isolated from Activated Sludge of a Mixed Wastewater Treatment”, *Chemosphere*, Vol. 73, No. 9, pp. 1442–1447.

Konstantinou, I. K., T. M. Sakellarides, V. A. Sakkas, and T. A. Albanis, 2001, “Photocatalytic Degradation of Selected s-Triazine Herbicides and Organophosphorus Insecticides over Aqueous TiO_2 Suspensions”, *Environmental Science and Technology*, Vol. 35, No. 2, pp. 398–405.

Krauss, M., C. Hug, R. Bloch, T. Schulze, and W. Brack, 2019, "Prioritising Site-specific Micropollutants in Surface Water from LC-HRMS Non-target Screening Data Using a Rarity Score", *Environmental Sciences Europe*, Vol. 31, No. 1, p. 45.

Lütjens, L. H., S. Pawlowski, M. Silvani, U. Blumenstein, and I. Richter, 2023, "Melamine in the Environment: A Critical Review of Available Information", *Environmental Sciences Europe*, Vol. 35, No. 1, pp. 2-3.

Maurer, L., E. Carmona, O. Machate, T. Schulze, M. Krauss, and W. Brack, 2023, "Contamination Pattern and Risk Assessment of Polar Compounds in Snow Melt: An Integrative Proxy of Road Runoffs", *Environmental Science and Technology*, Vol. 57, No. 10, pp. 4143–4152.

McElroy, A., and M. Hyman, 2019, *Consequences of Microbial Interactions with Hydrocarbons, Oils, and Lipids: Biodegradation and Bioremediation*, Springer International Publishing, Cham.

Nagy, I., F. Compernolle, K. Ghys, J. Vanderleyden, and R. De Mot, 1995, "A Single Cytochrome P-450 System is Involved in Degradation of the Herbicides EPTC (S-ethyl dipropylthiocarbamate) and Atrazine by Rhodococcus sp. Strain NI86/21", *Applied and Environmental Microbiology*, Vol. 61, No. 5, pp. 2056–2060.

Organisation for Economic Cooperation and Development (OECD), 2006, *Revised Introduction to the OECD Guidelines for Testing of Chemicals, Section 3*. OECD Publishing, Paris.

Pelizzetti, E., V. Carlin, C. Minero, E. Pramauro, and M. Vincenti, 1992, "Degradation Pathways of Atrazine Under Solar Light and in the Presence of TiO_2 Colloidal Particles", *Science of The Total Environment*, Vol. 123–124, pp. 161–169.

Peng, Y., W. Fang, M. Krauss, W. Brack, Z. Wang, F. Li, and X. Zhang, 2018, "Screening Hundreds of Emerging Organic Pollutants (EOPs) in Surface Water from the

Yangtze River Delta (YRD): Occurrence, Distribution, Ecological Risk", *Environmental Pollution*, Vol. 241, pp. 484–493.

Pepper, I. L., and C. P. Gerba, 2015, *Environmental Microbiology*, Third Edition, Elsevier Academic Press, London.

Peter, K. T., Z. Tian, C. Wu, P. Lin, S. White, B. Du, J. K. McIntyre, N. L. Scholz, and E. P. Kolodziej, 2018, "Using High-Resolution Mass Spectrometry to Identify Organic Contaminants Linked to Urban Stormwater Mortality Syndrome in Coho Salmon", *Environmental Science and Technology*, Vol. 52, No. 18, pp. 10317–10327.

Petras, D., J. J. Minich, L. B. Cancelada, R. R. Torres, E. Kunselman, M. Wang, M. E. White, E. E. Allen, K. A. Prather, L. I. Aluwihare, and P. C. Dorrestein, 2021, "Non-targeted Tandem Mass Spectrometry Enables the Visualization of Organic Matter Chemotype Shifts in Coastal Seawater", *Chemosphere*, Vol. 271, p. 129450.

Piai, L., A. Van Der Wal, N. Boelee, and A. Langenhoff, 2021, "Melamine Degradation to Bioregenerate Granular Activated Carbon", *Journal of Hazardous Materials*, Vol. 414, p. 125503.

Pizzi, A., and C. C. Ibeh, 2014, *Handbook of Thermoset Plastics*, Third Edition, William Andrew, San Diego.

Rätzsch, M., H. Bucka, S. Ivanchev, V. Pavlyuchenko, P. Leitner, and O. N. Primachenko, 2004, "The Reaction Mechanism of the Transetherification and Crosslinking of Melamine Resins", *Macromolecular Symposia*, Vol. 217, No. 1, pp. 431–443.

Rauert, C., S. L. Kaserzon, C. Veal, R. Y. Yeh, J. F. Mueller, and K. V. Thomas, 2020, "The First Environmental Assessment of Hexa(methoxymethyl)melamine and Co-occurring Cyclic Amines in Australian Waterways", *Science of The Total Environment*, Vol. 743, p. 140834.

Rodgers, B. (Ed.)., 2004, *Rubber compounding: Chemistry and applications*., CRC Press, Boca Raton.

Roubeau Dumont, E., X. Gao, J. Zheng, J. Macairan, L. M. Hernandez, A. Baesu, S. Bayen, S. A. Robinson, S. Ghoshal, and N. Tufenkji, 2023, "Unraveling the Toxicity of Tire Wear Contamination in Three Freshwater Species: From Chemical Mixture to Nanoparticles", *Journal of Hazardous Materials*, Vol. 453, p. 131402.

Saifur, S., and C. M. Gardner, 2023, "Evaluation of Stormwater Microbiomes for the Potential Biodegradation of Tire Wear Particle Contaminants", *Journal of Applied Microbiology*, Vol. 134, No. 5, p. lxad086.

Schneider, J., M. Matsuoka, M. Takeuchi, J. Zhang, Y. Horiuchi, M. Anpo, and D.W. Bahnemann, 2014, "Understanding TiO_2 Photocatalysis: Mechanisms and Materials", *Chemical Reviews*, Vol. 114, No. 19, pp. 9919–9986.

Seitz, W., and R. Winzenbacher, 2017, "A Survey on Trace Organic Chemicals in a German Water Protection Area and the Proposal of Relevant Indicators for Anthropogenic Influences", *Environmental Monitoring and Assessment*, Vol. 189, No. 6, pp. 244.

Seiwert, B., P. Klöckner, S. Wagner, and T. Reemtsma., 2020, "Source-related Smart Suspect Screening in the Aqueous Environment: Search for Tire-derived Persistent and Mobile Trace Organic Contaminants in Surface Waters", *Analytical and Bioanalytical Chemistry*, Vol. 412, No. 20, pp. 4909–4919.

Shiomi, N., and M. Ako, 2012, "Biodegradation of Melamine and Cyanuric Acid by a Newly-Isolated Microbacterium Strain", *Advances in Microbiology*, Vol. 2, No. 3, pp. 303–309.

Słaba, M., R. Szewczyk, M. A. Piątek, and J. Długoński, 2013, "Alachlor Oxidation by the Filamentous Fungus Paecilomyces marquandii", *Journal of Hazardous Materials*, Vol. 261, pp. 443–450.

Smith, C. A., K. T. O'Reilly, and M. R. Hyman, 2003, "Cometabolism of Methyl *tertiary* Butyl Ether and Gaseous *n* -Alkanes by *Pseudomonas mendocina* KR-1 Grown on C $_5$ toC $_8$ *n* -Alkanes", *Applied and Environmental Microbiology*, Vol. 69, No. 12, pp. 7385–7394.

Smits, T. H. M., B. Witholt, and J. B. Van Beilen, 2003, "Functional Characterization of Genes Involved in Alkane Oxidation by Pseudomonas aeruginosa", *Antonie van Leeuwenhoek*, Vol. 84, No. 3, pp. 193–200.

Snyder, D. M., and T. J. Vuk, 1992, "Self-condensation of Aqueous Hexa(methoxymethyl) melamine: Effects of Concentration, pH, and Alcohol Content", *Journal of Applied Polymer Science*, Vol. 46, No. 7, pp. 1301–1306.

Steffan, R. J., K. McClay, S. Vainberg, C. W. Condee, and D. Zhang, 1997, "Biodegradation of the Gasoline Oxygenates Methyl tert-Butyl Ether, Ethyl tert-Butyl Ether, and tert-Amyl Methyl Ether by Propane-oxidizing Bacteria", *Applied and Environmental Microbiology*, Vol. 63, No. 11, pp. 4216–4222.

Takagi, K., K. Fujii, K. Yamazaki, N. Harada, and A. Iwasaki, 2012, "Biodegradation of Melamine and Its Hydroxy Derivatives by a Bacterial Consortium Containing a Novel Nocardioides Species", *Applied Microbiology and Biotechnology*, Vol. 94, No. 6, pp. 1647–1656.

Tan, A., S. Hussain, A. Musuku, and R. Massé, 2009, "Internal Standard Response Variations During Incurred Sample Analysis by LC–MS/MS: Case by Case Troubleshooting", *Journal of Chromatography B*, Vol. 877, No. 27, pp. 3201–3209.

Tekirdağ İli ÇED ve Çevre İzinleri Şube Müdürlüğü, Çevre Yönetimi ve Çevre Denetimi Şube Müdürlüğü, 2015, *Tekirdağ İli 2015 Yılı Çevre Durum Raporu*, T.C. Şehircilik ve Çevre Bakanlığı, Tekirdağ.

Thornton, S. F., H. C. G. Nicholls, S. A. Rolfe, H. E. H. Mallinson, and M. J. Spence, 2020, "Biodegradation and Fate of Ethyl tert-Butyl Ether (ETBE) in Soil and Groundwater: A Review", *Journal of Hazardous Materials*, Vol. 391, p. 122046.

Tian, Z., K. T. Peter, A. D. Gipe, H. Zhao, F. Hou, D. A. Wark, T. Khangaonkar, E. P. Kolodziej, and C. A. James, 2020, "Suspect and Nontarget Screening for Contaminants of Emerging Concern in an Urban Estuary", *Environmental Science and Technology*, Vol. 54, No. 2, pp. 889–901.

Tian, Z., H. Zhao, K. T. Peter, M. Gonzalez, J. Wetzel, C. Wu, X. Hu, J. Prat, E. Mudrock, R. Hettinger, A. E. Cortina, R. G. Biswas, F. V. C. Kock, R. Soong, A. Jenne, B. Du, F. Hou, H. He, R. Lundeen, and E. P. Kolodziej, 2021, "A Ubiquitous Tire Rubber–Derived Chemical Induces Acute Mortality in Coho Salmon", *Science*, Vol. 371, No. 6525, pp. 185–189.

Tirmenstein, M. A., and R. Mangipudy, 2014, *Encyclopedia of Toxicology*. Third Edition, Elsevier, London.

Tuncel, D., 2014, *TiO_2 and ZnO Loaded Fly Ash Catalysts*, Ph.D. Thesis, Boğaziçi University.

Wackett, L. P., and C. Douglas Hershberger, 2001, *Biocatalysis and Biodegradation: Microbial Transformation of Organic Compounds*. ASM Press, Washington DC.

Wackett, M., B. Sadowsky, L. Martinez, 2002, "Biodegradation of Atrazine and Related s - triazine Compounds: From Enzymes to Field Studies", *Applied Microbiology and Biotechnology*, Vol. 58, No. 1, pp. 39–45.

Wang, H., C. Geng, J. Li, A. Hu, and C. P. Yu, 2014, "Characterization of a Novel Melamine-degrading Bacterium Isolated from a Melamine-manufacturing Factory in China", *Applied Microbiology and Biotechnology*, Vol. 98, No. 7, pp. 3287–3293.

Wiener, E. A., and G. H. LeFevre, 2022, “White Rot Fungi Produce Novel Tire Wear Compound Metabolites and Reveal Underappreciated Amino Acid Conjugation Pathways”, *Environmental Science and Technology Letters*, Vol. 9, No. 5, pp. 391–399.

Wong, C. C., and W. Chu, 2003, “The Hydrogen Peroxide-Assisted Photocatalytic Degradation of Alachlor in TiO_2 Suspensions”, *Environmental Science and Technology*, Vol. 37, No. 10, pp. 2310–2316.

Wu, X., J. Ren, Q. Xu, Y. Xiao, X. Li, and Y. Peng, 2023, “Priority Screening of Contaminant of Emerging Concern (CECs) in Surface Water from Drinking Water Sources in the Lower Reaches of the Yangtze River Based on Exposure-Activity Ratios (EARs)”, *Science of The Total Environment*, Vol. 856, p. 159016.

Xu, E. G., N. Lin, R. S. Cheong, C. Ridsdale, R. Tahara, T. Y. Du, D. Das, J. Zhu, L. Peña Silva, A. Azimzada, H. C. E. Larsson, and N. Tufenkji, 2019, “Artificial Turf Infill Associated with Systematic Toxicity in an Amniote Vertebrate. *Proceedings of the National Academy of Sciences*”, Vol. 116, No. 50, pp. 25156–25161.

Xu, S., Y. Zhang, A. Sims, M. Bernards, and Z. Hu, 2013, “Fate and Toxicity of Melamine in Activated Sludge Treatment Systems After a Long-term Sludge Adaptation” *Water Research*, Vol. 47, No. 7, pp. 2307–2314.

Yaseen, D. A., and M. Scholz, 2019, “Textile Dye Wastewater Characteristics and Constituents of Synthetic Effluents: A Critical Review”, *International Journal of Environmental Science and Technology*, Vol. 16, No. 2, pp. 1193–1226.

Zahraa, O., L. Sauvanaud, G. Hamard, and M. Bouchy, 2003, “Kinetics of Atrazine Degradation by Photocatalytic Process in Aqueous Solution”, *International Journal of Photoenergy*, Vol. 5, No. 2, pp. 87–93.

Zhu, H., R. U. Halden, and K. Kannan, 2019, “A Nationwide Survey of the Occurrence of Melamine and Its Derivatives in Archived Sewage Sludge from the United States”, *Environmental Pollution*, Vol. 245, pp. 994–999.

Zhu, H., and K. Kannan, 2019, “Melamine and Cyanuric Acid in Foodstuffs from the United States and Their Implications for Human Exposure”, *Environment International*, Vol. 130, p. 104950.

Ziylan Yavaş, A. 2017, *Destruction of Analgesic and Anti-Inflammatory Pharmaceuticals in Water by Catalytic and Advanced Oxidation Processes*, Ph.D. Thesis, Boğaziçi University.

APPENDIX A: HMMM DEGRADATION PATHWAY

In this section, a degradation pathway for HMMM is proposed by considering the observed transformation products throughout biotransformation and oxidation experiments.

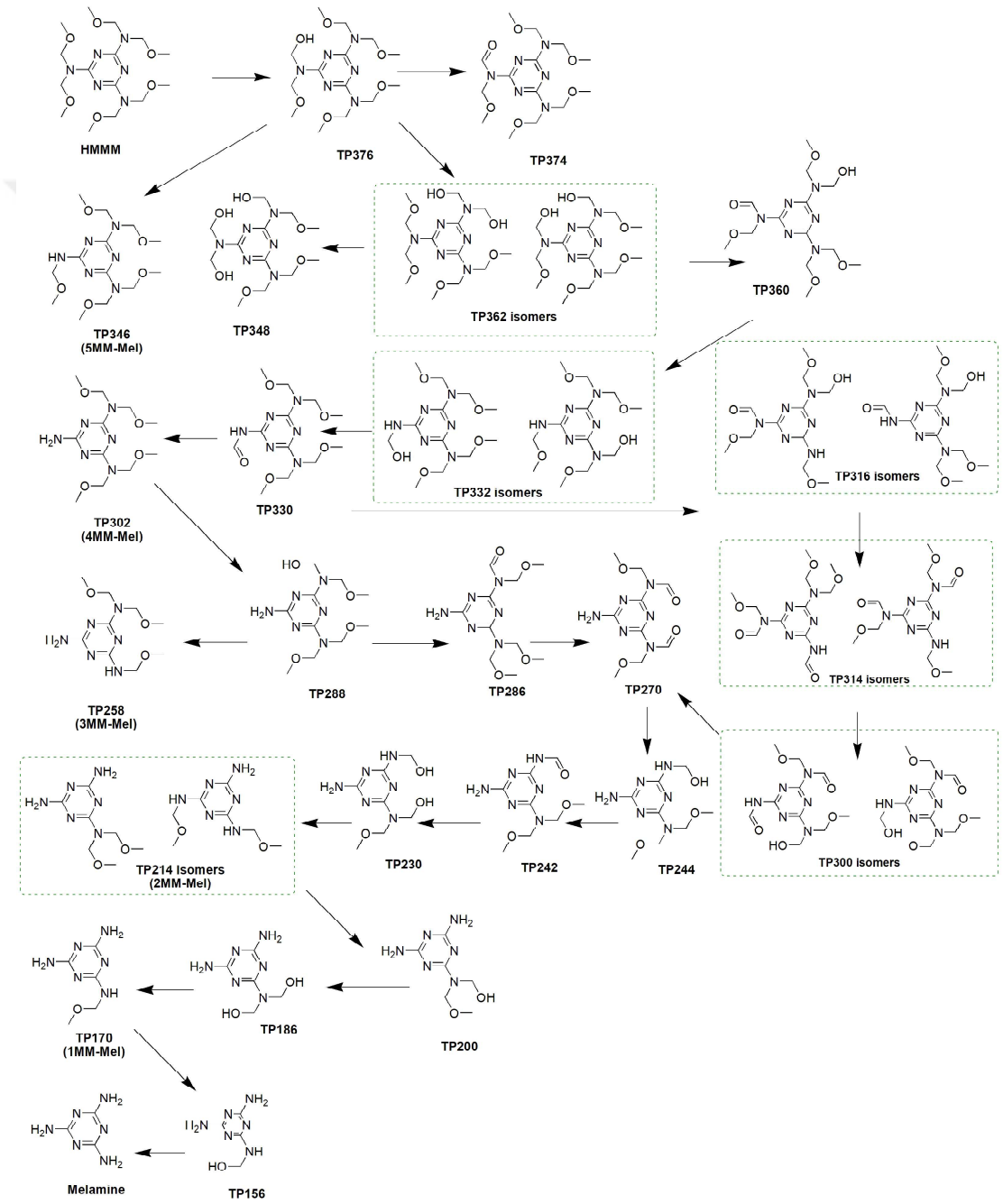


Figure A. 1. Proposed degradation pathway of HMMM.

APPENDIX B: PARENT AND FRAGMENT IONS OF TRANSFORMATION PRODUCTS

In this section, detailed information regarding the employed MRM method during analysis of transformation products is presented (Table B.1). Additionally, the proposed structures of detected transformation products are shown along with detected fragment ions (Table B.2).

Table B.1. MRM method parameters for the targeted screening of TPs with LC-MS-MS.

Q1 (m/z)	Q3 (m/z)	Time (msec)	ID	DP (V)	EP (V)	CE (V)	CXP (V)
391.000	177.100	5.0	HMMM-1	26.000	10.000	39.000	6.000
391.000	283.100	5.0	HMMM-2	26.000	10.000	19.000	8.000
126.988	84.900	5.0	Melamine-1	56.000	10.000	25.000	8.000
126.988	67.900	5.0	Melamine-2	56.000	10.000	41.000	6.000
280.100	183.000	5.0	IS-1	96.000	10.000	61.000	10.000
280.100	152.000	5.0	IS-2	96.000	10.000	91.000	8.000
383.160	321.130	5.0	TP360-Na-1	40.000	10.000	25.000	8.000
377.220	283.150	5.0	TP376-1	40.000	10.000	25.000	8.000
377.220	269.140	5.0	TP376-2	40.000	10.000	25.000	8.000
377.220	239.230	5.0	TP376-3	40.000	10.000	25.000	8.000
377.220	207.100	5.0	TP376-4	40.000	10.000	25.000	8.000
377.220	177.100	5.0	TP376-51	40.000	10.000	25.000	8.000
377.220	163.100	5.0	TP376-6	40.000	10.000	25.000	8.000
375.200	299.150	5.0	TP374-1	40.000	10.000	25.000	8.000
375.200	267.120	5.0	TP374-2	40.000	10.000	25.000	8.000
375.200	223.100	5.0	TP374-3	40.000	10.000	25.000	8.000
375.200	163.100	5.0	TP374-4	40.000	10.000	25.000	8.000
361.200	283.150	5.0	TP360-1	40.000	10.000	25.000	8.000
361.200	239.130	5.0	TP360-2	40.000	10.000	25.000	8.000
361.200	207.100	5.0	TP360-3	40.000	10.000	25.000	8.000
361.200	177.100	5.0	TP360-4	40.000	10.000	25.000	8.000
361.200	163.100	5.0	TP360-5	40.000	10.000	25.000	8.000
363.200	255.120	5.0	TP362-1	40.000	10.000	25.000	8.000

Table B.1. MRM method parameters for the targeted screening of TPs with LC-MS-MS (cont.).

Q1 (m/z)	Q3 (m/z)	Time (msec)	ID	DP (V)	EP (V)	CE (V)	CXP (V)
363.200	239.130	5.0	TP362-2	40.000	10.000	25.000	8.000
363.200	207.100	5.0	TP362-3	40.000	10.000	25.000	8.000
363.200	193.100	5.0	TP362-4	40.000	10.000	25.000	8.000
363.200	177.100	5.0	TP362-5	40.000	10.000	25.000	8.000
363.200	163.100	5.0	TP362-6	40.000	10.000	25.000	8.000
353.150	193.100	5.0	TP330-Na-1	40.000	10.000	25.000	8.000
353.150	179.100	5.0	TP330-Na -2	40.000	10.000	25.000	8.000
353.150	165.100	5.0	TP330-Na -3	40.000	10.000	25.000	8.000
349.200	255.120	5.0	TP348-1	40.000	10.000	25.000	8.000
349.200	225.110	5.0	TP348-2	40.000	10.000	25.000	8.000
349.200	207.100	5.0	TP348-3	40.000	10.000	25.000	8.000
349.200	193.100	5.0	TP348-4	40.000	10.000	25.000	8.000
349.200	177.100	5.0	TP348-5	40.000	10.000	25.000	8.000
349.200	163.100	5.0	TP348-6	40.000	10.000	25.000	8.000
347.200	239.130	5.0	TP346-1	40.000	10.000	25.000	8.000
347.200	163.100	5.0	TP346-2	40.000	10.000	25.000	8.000
339.140	283.100	5.0	TP316-Na-1	40.000	10.000	25.000	8.000
339.140	177.100	5.0	TP316-Na 2	40.000	10.000	25.000	8.000
335.170	207.100	5.0	TP334-1	40.000	10.000	25.000	8.000
335.170	193.100	5.0	TP334-2	40.000	10.000	25.000	8.000
335.170	177.100	5.0	TP334-3	40.000	10.000	25.000	8.000
335.170	163.100	5.0	TP334-4	40.000	10.000	25.000	8.000
333.200	239.130	5.0	TP332-1	40.000	10.000	25.000	8.000
333.200	225.100	5.0	TP332-2	40.000	10.000	25.000	8.000
333.200	195.100	5.0	TP332-3	40.000	10.000	25.000	8.000
333.200	177.100	5.0	TP332-4	40.000	10.000	25.000	8.000
333.200	163.100	5.0	TP332-5	40.000	10.000	25.000	8.000
331.150	283.150	5.0	TP330-1	40.000	10.000	25.000	8.000
331.150	193.100	5.0	TP330-2	40.000	10.000	25.000	8.000
331.150	179.100	5.0	TP330-3	40.000	10.000	25.000	8.000
331.150	165.100	5.0	TP330-4	40.000	10.000	25.000	8.000
317.150	283.150	5.0	TP316-1	40.000	10.000	25.000	8.000
317.150	195.100	5.0	TP316-2	40.000	10.000	25.000	8.000
317.150	177.100	5.0	TP316-3	40.000	10.000	25.000	8.000
315.150	283.130	5.0	TP314-1	40.000	10.000	25.000	8.000
315.150	177.100	5.0	TP314-2	40.000	10.000	25.000	8.000
311.150	249.100	5.0	TP288-Na-1	40.000	10.000	25.000	8.000

Table B.1. MRM method parameters for the targeted screening of TPs with LC-MS-MS (cont.).

Q1 (m/z)	Q3 (m/z)	Time (msec)	ID	DP (V)	EP (V)	CE (V)	CXP (V)
303.200	195.100	5.0	TP302-1	40.000	10.000	25.000	8.000
303.200	165.200	5.0	TP302-2	40.000	10.000	25.000	8.000
301.150	225.100	5.0	TP300-1	40.000	10.000	25.000	8.000
301.150	207.100	5.0	TP300-2	40.000	10.000	25.000	8.000
301.150	195.100	5.0	TP300-3	40.000	10.000	25.000	8.000
301.150	177.100	5.0	TP300-4	40.000	10.000	25.000	8.000
301.150	165.100	5.0	TP300-5	40.000	10.000	25.000	8.000
301.150	163.100	5.0	TP300-6	40.000	10.000	25.000	8.000
289.160	195.100	5.0	TP288-1	40.000	10.000	25.000	8.000
289.160	165.100	5.0	TP288-2	40.000	10.000	25.000	8.000
289.160	151.100	5.0	TP288-3	40.000	10.000	25.000	8.000
287.150	255.120	5.0	TP286-1	40.000	10.000	25.000	8.000
287.150	211.100	5.0	TP286-2	40.000	10.000	25.000	8.000
287.150	193.100	5.0	TP286-3	40.000	10.000	25.000	8.000
287.150	151.100	5.0	TP286-4	40.000	10.000	25.000	8.000
271.150	241.140	5.0	TP270-1	40.000	10.000	25.000	8.000
271.150	195.100	5.0	TP270-2	40.000	10.000	25.000	8.000
271.150	165.100	5.0	TP270-3	40.000	10.000	25.000	8.000
259.150	195.100	5.0	TP258-1	40.000	10.000	25.000	8.000
259.150	165.100	5.0	TP258-2	40.000	10.000	25.000	8.000
245.140	165.100	5.0	TP244-1	40.000	10.000	25.000	8.000
245.140	151.100	5.0	TP244-2	40.000	10.000	25.000	8.000
243.120	181.100	5.0	TP242-1	40.000	10.000	25.000	8.000
243.120	153.100	5.0	TP242-2	40.000	10.000	25.000	8.000
243.120	151.100	5.0	TP242-3	40.000	10.000	25.000	8.000
243.120	139.100	5.0	TP242-4	40.000	10.000	25.000	8.000
231.120	165.100	5.0	TP230-1	40.000	10.000	25.000	8.000
231.120	151.100	5.0	TP230-2	40.000	10.000	25.000	8.000
215.130	151.100	5.0	TP214-1	40.000	10.000	25.000	8.000
215.130	139.100	5.0	TP214-2	40.000	10.000	25.000	8.000
213.110	165.100	5.0	TP212-1	40.000	10.000	25.000	8.000
213.110	151.100	5.0	TP212-2	40.000	10.000	25.000	8.000
201.110	151.100	5.0	TP200-1	40.000	10.000	25.000	8.000
201.110	139.100	5.0	TP200-2	40.000	10.000	25.000	8.000
187.100	151.100	5.0	TP186-1	40.000	10.000	25.000	8.000
187.100	139.100	5.0	TP186-2	40.000	10.000	25.000	8.000
171.100	151.100	5.0	TP170-1	40.000	10.000	25.000	8.000

Table B.1. MRM method parameters for the targeted screening of TPs with LC-MS-MS (cont.).

Q1 (m/z)	Q3 (m/z)	Time (msec)	ID	DP (V)	EP (V)	CE (V)	CXP (V)
171.100	139.100	5.0	TP170-2	40.000	10.000	25.000	8.000
157.080	139.100	5.0	TP156-1	40.000	10.000	25.000	8.000
157.080	127.070	5.0	TP156-2	40.000	10.000	25.000	8.000
157.080	110.040	5.0	TP156-3	40.000	10.000	25.000	8.000
157.080	97.050	5.0	TP156-4	40.000	10.000	25.000	8.000
155.070	127.070	5.0	TP156-1	40.000	10.000	25.000	8.000
155.070	85.000	5.0	TP154-3	40.000	10.000	25.000	8.000

Table B.2. Proposed structures and molecular formula of the detected transformation products and their fragment ions, their relative retention times with respect to HMMM and the type of treatments they were observed in.

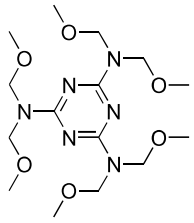
Name	**Proposed Structure**	**Proposed Molecular Formula $[MH]^+$**	**Parent Ion (m/z)**	**Relative Retention Time to HMMM**	**Selected Fragment Ions (m/z)**	**Proposed Fragment Molecular Formula $[MH]^+$**	**Biological Treatment**	**UV/TiO_2 Treatment**
HMMM		$C_{15}H_{31}N_6O_6^+$	391.2	1	283.10	$C_{11}H_{19}N_6O_3^+$	+	+
					177.10	$C_7H_9N_6^+$	+	+

Table B.2. Proposed structures and molecular formula of the detected transformation products and their fragment ions, their relative retention times with respect to HMMM and the type of treatments they were observed in (cont.).

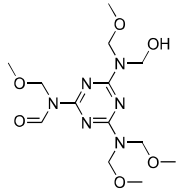
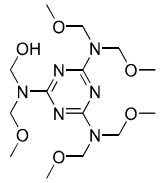
Name	**Proposed Structure**	**Proposed Molecular Formula $[MH]^+$**	**Parent Ion (m/z)**	**Relative Retention Time to HMMM**	**Selected Fragment Ions (m/z)**	**Proposed Fragment Molecular Formula $[MH]^+$**	**Biological Treatment**	**UV/TiO_2 Treatment**
TP360 Na-Adduct		$C_{13}H_{24}N_6O_6Na^+$	383.16	0.92	321.13	$C_{11}H_{18}N_6O_4Na^+$	-	+
TP376		$C_{14}H_{28}N_6O_6^+$	377.22	0.95	207.10	$C_8H_{11}N_6O^+$	+	+
					177.10	$C_7H_9N_6^+$		

Table B.2. Proposed structures and molecular formula of the detected transformation products and their fragment ions, their relative retention times with respect to HMMM and the type of treatments they were observed in (cont.).

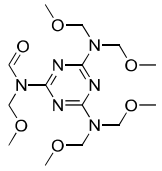
Name	Proposed Structure	Proposed Molecular Formula $[MH]^+$	Parent Ion (m/z)	Relative Retention Time to HMMM	Selected Fragment Ions (m/z)	Proposed Fragment Molecular Formula $[MH]^+$	Biological Treatment	UV/TiO_2 Treatment
TP374		$C_{14}H_{26}N_6O_6^+$	375.20	0.97	267.12	$C_{10}H_{15}N_6O_3^+$	+	+
					163.10	$C_6H_7N_6^+$		

Table B.2. Proposed structures and molecular formula of the detected transformation products and their fragment ions, their relative retention times with respect to HMMM and the type of treatments they were observed in (cont.).

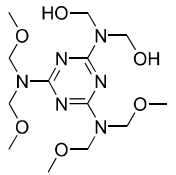
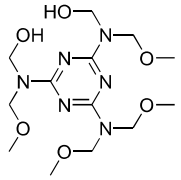
Name	Proposed Structure	Proposed Molecular Formula $[MH]^+$	Parent Ion (m/z)	Relative Retention Time to HMMM	Selected Fragment Ions (m/z)	Proposed Fragment Molecular Formula $[MH]^+$	Biological Treatment	UV/TiO_2 Treatment
TP362 isomers*		$C_{13}H_{27}N_6O_6^+$	363.20	1.00	177.10	$C_7H_9N_6^+$	+	+
				0.89	163.10	$C_6H_7N_6^+$		

Table B.2. Proposed structures and molecular formula of the detected transformation products and their fragment ions, their relative retention times with respect to HMMM and the type of treatments they were observed in (cont.).

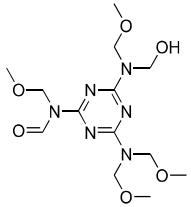
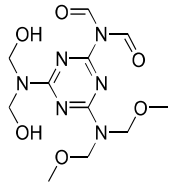
Name	**Proposed Structure**	**Proposed Molecular Formula $[MH]^+$**	**Parent Ion (m/z)**	**Relative Retention Time to HMMM**	**Selected Fragment Ions (m/z)**	**Proposed Fragment Molecular Formula $[MH]^+$**	**Biological Treatment**	**UV/TiO_2 Treatment**
TP360		$C_{13}H_{24}N_6O_6^+$	361.20	1.00	207.10	$C_8H_{11}N_6O^+$	+	+
					177.10	$C_7H_9N_6^+$		
TP330 Na-Adduct		$C_{12}H_{22}N_6O_5Na^+$	353.15	1.3	193.10	$C_7H_9N_6O^+$	+	-
					165.10	$C_6H_9N_6^+$		

Table B.2. Proposed structures and molecular formula of the detected transformation products and their fragment ions, their relative retention times with respect to HMMM and the type of treatments they were observed in (cont.).

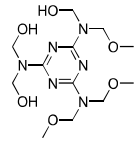
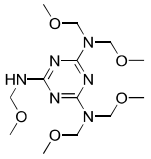
Name	**Proposed Structure**	**Proposed Molecular Formula $[MH]^+$**	**Parent Ion (m/z)**	**Relative Retention Time to HMMM**	**Selected Fragment Ions (m/z)**	**Proposed Fragment Molecular Formula $[MH]^+$**	**Biological Treatment**	**UV/TiO_2 Treatment**
TP348		$C_{12}H_{25}N_6O_6^+$	349.20	0.94	163.10	$C_6H_7N_6^+$	+	+
TP346		$C_{13}H_{27}N_6O_5^+$	347.20	0.94	239.13	$C_9H_{15}N_6O_2^+$	+	+
					163.10	$C_6H_7N_6^+$		

Table B.2. Proposed structures and molecular formula of the detected transformation products and their fragment ions, their relative retention times with respect to HMMM and the type of treatments they were observed in (cont.).

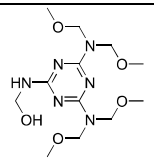
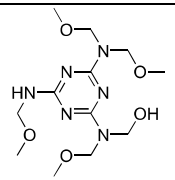
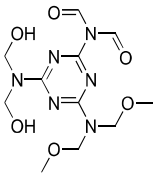
Name	Proposed Structure	Proposed Molecular Formula $[MH]^+$	Parent Ion (m/z)	Relative Retention Time to HMMM	Selected Fragment Ions (m/z)	Proposed Fragment Molecular Formula $[MH]^+$	Biological Treatment	UV/TiO_2 Treatment
TP332 isomers		$C_{12}H_{25}N_6O_5^+$	333.15	0.89	239.13	$C_9H_{15}N_6O_2^+$	+	+
				0.94	163.10	$C_6H_7N_6^+$		
TP330		$C_{12}H_{23}N_6O_5^+$	331.15	0.92	193.10	$C_7H_9N_6O^+$	+	+
					165.10	$C_6H_9N_6^+$		

Table B.2. Proposed structures and molecular formula of the detected transformation products and their fragment ions, their relative retention times with respect to HMMM and the type of treatments they were observed in (cont.).

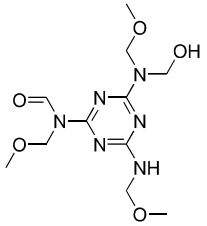
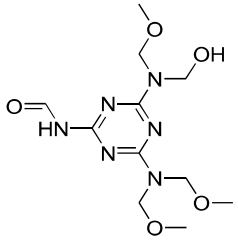
Name	Proposed Structure	Proposed Molecular Formula $[MH]^+$	Parent Ion (m/z)	Relative Retention Time to HMMM	Selected Fragment Ions (m/z)	Proposed Fragment Molecular Formula $[MH]^+$	Biological Treatment	UV/TiO_2 Treatment
TP316 isomers		$C_{11}H_{21}N_6O_5^+$	317.10	0.99	177.10	$C_7H_9N_6^+$	+	+
				0.95				

Table B.2. Proposed structures and molecular formula of the detected transformation products and their fragment ions, their relative retention times with respect to HMMM and the type of treatments they were observed in (cont.).

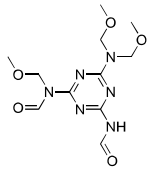
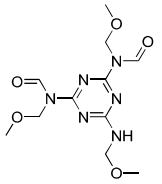
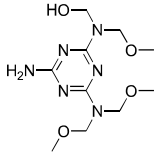
Name	Proposed Structure	Proposed Molecular Formula $[MH]^+$	Parent Ion (m/z)	Relative Retention Time to HMMM	Selected Fragment Ions (m/z)	Proposed Fragment Molecular Formula $[MH]^+$	Biological Treatment	UV/TiO_2 Treatment
TP314 isomers		$C_{11}H_{19}N_6O_5^+$	315.10	0.99	177.10	$C_7H_9N_6^+$	+	+
				0.95				
TP289 Na-Adduct		$C_{10}H_{20}N_6O_4Na^+$	311.15	0.77	249.10	$C_8H_{14}N_6O_2Na^+$	+	+

Table B.2. Proposed structures and molecular formula of the detected transformation products and their fragment ions, their relative retention times with respect to HMMM and the type of treatments they were observed in (cont.).

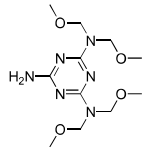
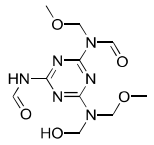
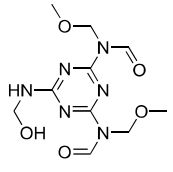
Name	Proposed Structure	Proposed Molecular Formula $[MH]^+$	Parent Ion (m/z)	Relative Retention Time to HMMM	Selected Fragment Ions (m/z)	Proposed Fragment Molecular Formula $[MH]^+$	Biological Treatment	UV/TiO_2 Treatment
TP302		$C_{11}H_{23}N_6O_4^+$	303.20	0.86	195.10	$C_7H_{11}N_6O^+$	+	+
					165.10	$C_6H_9N_6^+$		
TP300 isomers		$C_{10}H_{17}N_6O_5^+$	301.15	0.90	177.10	$C_7H_9N_6^+$	+	+
				0.95	163.10	$C_6H_7N_6^+$		

Table B.2. Proposed structures and molecular formula of the detected transformation products and their fragment ions, their relative retention times with respect to HMMM and the type of treatments they were observed in (cont.).

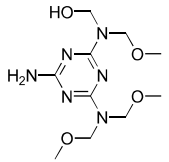
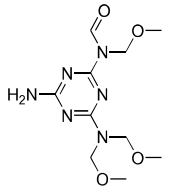
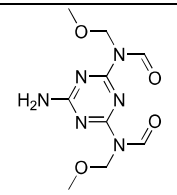
Name	**Proposed Structure**	**Proposed Molecular Formula $[MH]^+$**	**Parent Ion (m/z)**	**Relative Retention Time to HMMM**	**Selected Fragment Ions (m/z)**	**Proposed Fragment Molecular Formula $[MH]^+$**	**Biological Treatment**	**UV/TiO_2 Treatment**
TP288		$C_{10}H_{21}O_4N_6^+$	289.16	0.84	165.10	$C_6H_9N_6^+$	+	+
					151.10	$C_5H_7N_6^+$		
TP286		$C_{10}H_{19}N_6O_4^+$	287.15	0.85	193.10	$C_7H_9N_6O^+$	+	+
					151.10	$C_5H_7N_6^+$		
TP270		$C_9H_{15}N_6O_4^+$	271.15	0.85	195.10	$C_7H_{11}N_6O^+$	+	+
					165.10	$C_6H_9N_6^+$		

Table B.2. Proposed structures and molecular formula of the detected transformation products and their fragment ions, their relative retention times with respect to HMMM and the type of treatments they were observed in (cont.).

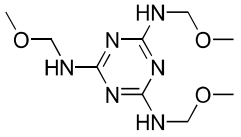
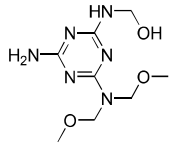
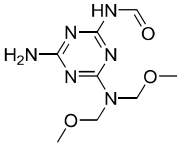
Name	Proposed Structure	Proposed Molecular Formula $[MH]^+$	Parent Ion (m/z)	Relative Retention Time to HMMM	Selected Fragment Ions (m/z)	Proposed Fragment Molecular Formula $[MH]^+$	Biological Treatment	UV/TiO_2 Treatment
TP258		$C_9H_{19}N_6O_3^+$	259.15	0.69	165.10	$C_6H_9N_6^+$	+	+
TP244		$C_8H_{17}N_6O_3^+$	245.14	0.42	165.10	$C_6H_9N_6^+$	-	+
TP242		$C_8H_{15}N_6O_3^+$	243.12	0.83	151.10	$C_5H_7N_6^+$	+	+

Table B.2. Proposed structures and molecular formula of the detected transformation products and their fragment ions, their relative retention times with respect to HMMM and the type of treatments they were observed in (cont.).

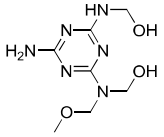
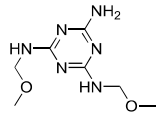
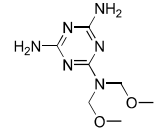
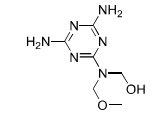
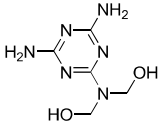
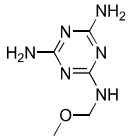
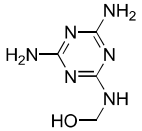
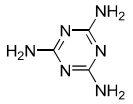
Name	Proposed Structure	Proposed Molecular Formula $[MH]^+$	Parent Ion (m/z)	Relative Retention Time to HMMM	Selected Fragment Ions (m/z)	Proposed Fragment Molecular Formula $[MH]^+$	Biological Treatment	UV/TiO_2 Treatment
TP230		$C_7H_{15}O_3N_6^+$	231.12	0.26	151.10	$C_5H_7N_6^+$	-	+
TP214 isomers		$C_7H_{15}N_6O_2^+$	215.13	0.28	139.10	$C_4H_7N_6^+$	+	+
				0.33				
TP200		$C_6H_{13}O_2N_6^+$	201.10	0.29	151.10	$C_5H_7N_6^+$	+	+
					139.10	$C_4H_7N_6^+$		

Table B.2. Proposed structures and molecular formula of the detected transformation products and their fragment ions, their relative retention times with respect to HMMM and the type of treatments they were observed in (cont.).

Name	Proposed Structure	Proposed Molecular Formula $[MH]^+$	Parent Ion (m/z)	Relative Retention Time to HMMM	Selected Fragment Ions (m/z)	Proposed Fragment Molecular Formula $[MH]^+$	Biological Treatment	UV/TiO_2 Treatment
TP186		$C_5H_{11}O_2N_6^+$	181.10	0.19	151.10	$C_5H_7N_6^+$	-	+
					139.10	$C_4H_7N_6^+$		
TP170		$C_5H_{11}N_6O^+$	171.10	0.21	139.10	$C_4H_7N_6^+$	+	+
TP156		$C_4H_9N_6O^+$	157.08	0.18	127.07	$C_3H_7N_6^+$	-	+
					139.10	$C_4H_7N_6^+$		
Melamine		$C_3H_7N_6^+$	126.99	0.19	67.90	$C_2H_2N^+$	+	+
					84.90	$C_2H_5N_4^+$		